Methanol Sprays in Marine Internal Combustion Engines

A Computational Fluid Dynamics Approach

Konstantinos Zoumpourlos

METHANOL SPRAYS IN MARINE INTERNAL COMBUSTION ENGINES

A COMPUTATIONAL FLUID DYNAMICS APPROACH

METHANOL SPRAYS IN MARINE INTERNAL COMBUSTION ENGINES

A COMPUTATIONAL FLUID DYNAMICS APPROACH

Dissertation

for the purpose of obtaining the degree of doctor
at Delft University of Technology
by the authority of the Rector Magnificus, Prof. Dr. Ir. H. Bijl,
chair of the Board for Doctorates
to be defended publicly
on Wednesday 29th, April 2026

by

Konstantinos ZOUMPOURLOS

This dissertation has been approved by the (co)promotors.

Composition of the doctoral committee:

Rector Magnificus,	chairperson
Dr. ing. A. Coraddu,	Delft University of Technology, promotor
Dr. ir. R.D. Geertsma,	Netherlands Defence Academy / Delft University of Technology, copromotor
Prof. dr. ir. R.G. van de Ketterij,	Netherlands Defence Academy, copromotor
Independent Members:	
Prof. dr. ir. B.J. Boersma,	Delft University of Technology
Prof. dr. ir. S. Verhelst,	Ghent University, Belgium / Lund University, Sweden
Dr. ir. R.J.M. Bastiaans,	Eindhoven University of Technology, The Netherlands
Dr. ir. W.P. Breugem,	Delft University of Technology
Other Member:	
Prof. G.D. Weymouth,	Delft University of Technology, reserve member

The present research is part of the MENENS project (Methanol als Energiestap Naar Emissieloze Nederlandse Scheepvaart). The project is funded by the Netherlands Enterprise Agency (RVO: Rijksdienst voor Ondernemend Nederland) under the grant number MOB21012.

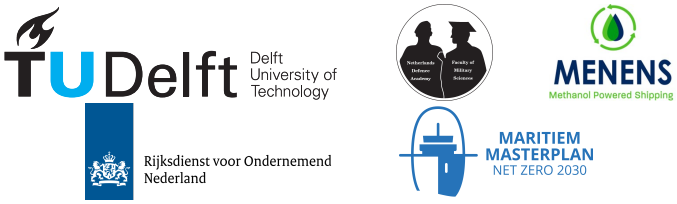

Keywords: Methanol, marine internal combustion engines, computational fluid dynamics, alternative fuels, sprays, port fuel injection, direct injection, engine combustion network, late-injection

Printed by: Ridderprint

Front & Back: Methanol fuel injection artwork by Dimitris Groke Mitsopoulos.

ISBN 978-94-6537-442-0

An electronic version of this dissertation is available at
`http://repository.tudelft.nl/`.

Γηράσκω ἀεὶ διδασκόμενος ὑπὸ χρηστῶν μόνον

Σόλων & Πλάτων

Contents

Summary

THE maritime industry is a significant contributor to global emissions, with carbon dioxide (CO_2) as a major greenhouse gas (GHG) and nitrogen oxides (NO_x) being harmful air pollutants. The International Maritime Organization (IMO) and the Paris Agreement have imposed stringent regulations to mitigate these emissions, driving the need for sustainable alternatives to fossil fuels in marine internal combustion engines (ICEs). Methanol has emerged as a promising candidate due to its renewable production potential, liquid state at atmospheric conditions, and ability to significantly reduce harmful emissions compared to conventional fuels like diesel. However, the integration of methanol in ICEs presents unique challenges, particularly during injection and mixture formation. These arise due to methanol's peculiar physical properties (i.e., increased latent heat of vaporization, higher vapour pressure, and decreased lower heating value compared to diesel and gasoline) hindering the adaptation in maritime engines. As current knowledge and modelling practices are predominantly validated using conventional fuels, significant knowledge gaps remain regarding the behaviour of methanol sprays. This PhD thesis aims to address these challenges by developing a computational fluid dynamics (CFD) framework in CONVERGE-CFD using the Reynolds-Averaged Navier–Stokes (RANS) and large eddy simulation (LES) turbulence approaches. The framework is used to analyse methanol spray behaviour under marine-relevant engine conditions, covering both port fuel injection (PFI) and direct injection (DI) configurations.

Initially, in Chapter 2, a literature review is conducted on the combustion pathways of methanol-fuelled heavy-duty ICEs. The thesis introduces a unified classification framework for methanol injection and ignition strategies, including both spark ignition (SI) and compression ignition (CI) concepts. By synthesizing diverse definitions from the literature, this framework provides clarity for future research and engine development. Additionally, by outlining the different injection methods, this chapter identifies the inherent knowledge gap in methanol sprays and establishes the necessary conditions for the subsequent numerical modelling.

Chapter 3 examines methanol sprays under PFI conditions reminiscent of small and medium-bore maritime engines. The CFD model is validated using methanol-specific experimental data from literature at both low and high injection pressures, utilizing light-duty engine injection quantities. Consequently, the validated PFI model is scaled up for marine engine injection quantities to analyse atomization and evaporation phenomena. The analysis demonstrates that using higher injection pressures accelerates the liquid jet breakup, improving atomization and evaporation prior to wall impingement. While at-

omization improves, methanol evaporation remains minimal for all the tested conditions, indicating that spray-wall interaction phenomena dominate PFI mixture formation.

Subsequently, in Chapter 4, the spray framework is further extended to DI conditions, using experimental data from the Engine Combustion Network (ECN) Spray M1 condition. Specifically, using computer tomography (CT) reconstruction methods, the ECN experiments yielded DI methanol spray results with a multi-hole injector under moderate ambient pressure and temperature conditions. The CFD model is successfully validated using state-of-the-art projected liquid volume (PLV) maps based on methanol spray liquid volume fraction (LVF). Due to methanol's high volatility and latent heat, the ECN methanol experiments exhibited unique spray phenomena, including plume collapse and sweeping. These phenomena are accurately captured by systematically calibrating the droplet breakup model using both RANS and LES turbulence approaches. This work establishes a validated methodology for simulating methanol DI sprays, bridging the gap between conventional fuel models and the specific requirements for methanol injection.

Chapter 5 investigates the charge cooling effect of methanol in dual-fuel methanol-diesel DI-CI engines. The non-reacting ECN spray D condition is used to validate the injection model, employing n-dodecane as a diesel surrogate. Consequently, the spray model is adapted for methanol injection and compared with n-dodecane under the same quantity and energy content injection cases. Methanol's high latent heat of vaporization and lower energy density result in slower evaporation rates and extended liquid penetration, which can induce wall wetting and influence combustion and emissions. In the dual-fuel CI engine environment, methanol's charge cooling effect locally reduces the mixture temperature by up to 100 K compared to n-dodecane, potentially creating cold spots that will hinder flame propagation and amplify cyclic variability. These insights highlight the need for tailored injection strategies, such as split injection, to optimise methanol combustion in marine engines.

The contributions of this work advance the understanding of methanol sprays by developing a predictive and computationally efficient spray modelling framework. Comparative analyses between methanol and conventional fuels such as diesel and iso-octane reveal critical differences in spray structure and mixture formation. The presented CFD models could serve as a valuable tool for engineers and researchers, enabling the optimisation of methanol-fuelled marine engines. As the maritime industry transitions toward sustainable energy solutions, this thesis provides critical guidance for overcoming the technical challenges of methanol adoption in marine ICEs.

Samenvatting

De maritieme sector levert een significante bijdrage aan de wereldwijde emissies, waarbij kooldioxide (CO_2) een belangrijk broeikasgas (GHG) is en stikstofoxiden (NO_x) luchtverontreiniging veroorzaken. De International Maritime Organization (IMO) en het Parijs akkoord hebben strenge regelgeving ingevoerd om deze emissies te beperken, waardoor er meer behoefte is aan duurzame alternatieven voor fossiele brandstoffen in maritieme verbrandingsmotoren (ICE's). Methanol is een veelbelovende brandstof omdat het hernieuwbaar geproduceerd kan worden; het vloeibaar is bij atmosferische druk en kamertemperatuur, en het schadelijke emissies aanzienlijk kan verminderen ten opzichte van conventionele brandstoffen zoals diesel. De integratie van methanol in ICE's brengt echter unieke uitdagingen met zich mee, met name tijdens de injectie en mengselvorming. Deze uitdagingen ontstaan door de specifieke fysische en chemische eigenschappen van methanol (d.w.z. een hogere latente verdampingswarmte, hogere dampdruk en lagere verbrandingswaarde in vergelijking met diesel en benzine), die de toepassing in maritieme motoren moeilijker maken. Aangezien bestaande kennis en modelleringspraktijken voornamelijk zijn gevalideerd met conventionele brandstoffen, is er een gebrek aan kennis over het gedrag van methanolverstuivingen. Dit proefschrift vult deze kennis aan door het ontwikkelen van een computational fluid dynamics (CFD)-raamwerk in CONVERGE-CFD, waarbij zowel Reynolds-Averaged Navier–Stokes (RANS)- als large eddy simulation (LES)-turbulentiebenaderingen gebruikt worden. Het raamwerk wordt toegepast om het verstuivingsgedrag van methanol te analyseren onder motorcondities die relevant zijn voor de maritieme sector, voor zowel poortinjectie (PFI) als directe injectie (DI).

In Hoofdstuk 2 wordt eerst een literatuurstudie uitgevoerd naar de verbrandingspaden van grote methanolgestookte ICE's. Het proefschrift introduceert een algemeen geldend classificatieraamwerk voor methanolinjectie- en ontstekingsstrategieën, met zowel vonkontsteking (SI) als compressieontsteking (CI). Door uiteenlopende definities uit de literatuur te combineren, biedt dit raamwerk helderheid voor toekomstig onderzoek en motorontwikkeling. Daarnaast identificeert dit hoofdstuk, door de verschillende injectiemethoden te beschrijven, het gebrek aan kennis rondom methanolverstuivingen en legt het de voorwaarden vast voor de daaropvolgende numerieke modellering.

Hoofdstuk 3 onderzoekt methanolverstuivingen onder PFI-condities die representatief zijn voor kleine en middelgrote maritieme motoren. Het CFD-model wordt gevalideerd met literatuurdata van methanol-ICE-experimenten met zowel lage als hoge injectiedrukken en brandstofhoeveelheden kenmerkend voor lichte motoren. Vervolgens wordt het gevalideerde PFI-model opgeschaald naar injectiehoeveelheden die typisch zijn

voor maritieme motoren om vernevelings- en verdampingsverschijnselen te analyseren. De analyse laat zien dat hogere injectiedrukken de vloeibare straal sneller laat opbreken, wat de verneveling en verdamping vóór het neerslaan op de wand verbetert. Hoewel de verneveling verbetert, blijft de methanolverdamping minimaal voor alle onderzochte scenario's, wat suggereert dat interactie tussen verstuiving en wandfilmvorming een dominante rol speelt in de PFI-mengselvorming.

Vervolgens wordt in Hoofdstuk 4 het verstuivingsraamwerk verder uitgebreid naar DI-condities, waarvoor experimentele data uit de Engine Combustion Network (ECN) Spray M1-conditie gebruikt is. Met name door gebruik te maken van computertomografie (CT)-reconstructiemethoden leverden de ECN-experimenten resultaten op van DI-methanolverstuiving met een injector met meerdere openingen onder gematigde omgevingsdruk en -temperatuur. Het CFD-model wordt succesvol gevalideerd met behulp van state-of-the-art 'projected liquid volume' (PLV)-kaarten, gebaseerd op de methanolverstuivingsfractie (LVF). Door methanols hoge vluchtigheid en latente verdampingswarmte vertoonden de ECN-methanolexperimenten unieke verstuivingsverschijnselen, waaronder 'plume collapse' en 'sweeping'. Deze verschijnselen worden nauwkeurig vastgelegd door een systematische kalibratie van het druppelverstuivingsmodel met zowel RANS- als LES. Dit werk vormt een gevalideerde methode voor het simuleren van methanol-DI-verstuivingen en overbrugt de kloof tussen modellen voor conventionele brandstoffen en de specifieke eisen voor methanolinjectie.

Hoofdstuk 5 onderzoekt het ladingskoelende effect van methanol in 'dual-fuel' methanol–diesel DI-CI-motoren. De niet-reactieve ECN Spray D-conditie wordt gebruikt om het injectiemodel te valideren, waarbij n-dodecaan wordt toegepast als diesel-surrogaat. Vervolgens wordt het verstuivingsmodel aangepast voor methanolinjectie en vergeleken met n-dodecaan onder identieke massa- en energie-injectiecondities. Methanols hoge latente verdampingswarmte en lagere energiedichtheid leiden tot tragere verdamingsprocessen en een langere vloeibare penetratie, wat wandfilmvorming kan veroorzaken en invloed kan hebben op de verbranding en emissies. In een 'dual-fuel' CI-motoromgeving vermindert methanol de temperatuur plaatselijk tot wel 100 K ten opzichte van n-dodecaan, wat koude zones kan creëren die vlamvoortplanting hinderen en cyclische variabiliteit kunnen versterken. Deze bevindingen benadrukken de noodzaak van aangepaste injectiestrategieën, zoals gesplitste injectie, om de methanolverbranding in maritieme motoren te optimaliseren.

De bijdragen van dit werk vergroten het inzicht in methanolverstuivingen door de ontwikkeling van een voorspellend en rekenefficiënt verstuivingsmodelleerraamwerk. Vergelijkende analyses tussen methanol en conventionele brandstoffen zoals diesel en iso-octaan tonen cruciale verschillen in verstuivingsstructuur en mengselvorming. De gepresenteerde CFD-modellen kunnen dienen als een waardevol instrumenten voor ingenieurs en onderzoekers, waarmee de optimalisatie van methanolgestookte maritieme motoren kan worden ondersteund. Terwijl de maritieme sector de transitie maakt naar duurzame energieoplossingen, biedt dit proefschrift essentiële richtlijnen voor het overwinnen van de technische uitdagingen rondom de toepassing van methanol in maritieme ICE's.

Nomenclature

Acronyms & Abbreviations

ICE	Internal combustion engine
GHG	Greenhouse gas
CFD	Computational fluid dynamics
ECN	Engine combustion network
PFI	Port fuel injection
DI	Direct injection
CI	Compression ignition
SI	Spark ignition
GDI	Gasoline direct-injection
DF	Dual-Fuel
PM	Particulate Matter
HD	Heavy-Duty
DISI	Direct-injection spark-ignition
DICI	Direct-injection compression-ignition
TDC	Top Dead Center
aSOI	After Start-of-Injection
LE	Lagrangian Eulerian
LPT	Lagrangian particle tracking
RANS	Reynolds averaged Navier Stokes
LES	Large Eddy Simulation
HP	High pressure
LP	Low pressure
LHV	Lower heating value
3D	Three-dimensional
CVC	Constant volume chamber
SV	Spray vessel
SMD	Sauter Mean Diameter
Re	Reynolds number
We	Weber number
Sc	Schmidt number
Sh	Sherwood number

Pr	Prandtl number
PISO	Pressure implicit with splitting of operators
CFL	Courant-Friedrichs-Lewy
AMR	Adaptive mesh refinement
TKE	Turbulent kinetic energy
KH-RT	Kelvin Helmholtz - Rayleigh Taylor
TAB	Taylor Analogy Breakup
NTC	No time counter
SOI	Start-of-injection
EOI	End-of-injection
VoF	Volume-of-Fluid
LVF	Liquid Volume Fraction
PLV	Projected Liquid Volume
DBI	Diffused Back Illumination
CT	Computer Tomography
HCCI	Homogeneous Charge Compression Ignition
ON	Octane Number
API	Air Path Injection
SPI	Single-Point Injection
MPI	Multipoint Injection
NG	Natural Gas
TJI	Turbulent Jet Ignition
LTC	Low Temperature Combustion
CDC	Conventional Diesel Combustion
DDFS	Direct Dual Fuel Stratification
DoF	Degrees of Freedom
MF	Mono-Fuel
CR	Compression Ratio
NO_x	Nitrogen Oxide
MCCI	Mixing-Controlled Compression Ignition
HP-DI	High-Pressure Direct Injection
ATAC	Active Thermo-Atmosphere Combustion
CIHC	Compression-Ignited Homogeneous Charge
PCCI	Premixed Charge Compression Ignition
UNIBUS	Uniform Bulky Combustion System
PPC	Partially Premixed Combustion
PPCI	Partially Premixed Compression Ignition
SACI	Spark Assisted Compression Ignition
CN	Cetane Number
RCCI	Reactivity Controlled Compression Ignition
PRDF	Premixed Dual-Fuel
CDF	Conventional Dual-Fuel
DMDF	Diesel Methanol Dual-Fuel
DMCC	Diesel Methanol Compound Combustion
DFDC	Dual-Fuel Diffusion Combustion

ICCI	Intelligent Charge Compression Ignition
PMPC	Premixed Micro Pilot Combustion
JCCI	Jet Controlled Compression Ignition
MPDF	Micro Pilot Dual Fuel
HRR	Heat Release Rate
LRF	Low Reactivity Fuel
HRF	High Reactivity Fuel
PREMIER	Premixed Mixture Ignition in the End-Gas Region
SWI	Spray Wall Interaction

Latin Symbols

k	Turbulent kinetic energy
k_0	Initial turbulent kinetic energy
u	velocity of the fluid
P	pressure of the fluid
e	specific energy
T	temperature of the fluid
K	thermal conductivity
D_m	species mass diffusion coefficient
Y_m	species mass fraction
h_m	species specific enthalpy
D	vapour mass diffusivity
u_r	relative velocity between the droplet and the gas
r_d	droplet radius
d	droplet diameter
r_c	child droplet radius
r_p	parent droplet radius
r_0	initial droplet radius
B_0	Kelvin Helmholtz model size constant
B_1	Kelvin Helmholtz breakup time constant
C_{RT}	Rayleigh Taylor model size constant
C_τ	Rayleigh Taylor breakup time constant
C_d	Discharge coefficient
C_v	Velocity coefficient
P_{inj}	Injection Pressure
P_{amb}	Ambient Pressure
u_{th}	Theoretical Bernoulli velocity
C_{ext}	Extinction Coefficient
C_p	specific heat capacity
h_{fg}	enthalpy of vaporization

Greek Symbols

ε	Turbulent kinetic energy dissipation rate
ε_0	Initial turbulent kinetic energy dissipation rate
α	droplet deceleration
ρ	fluid density
ρ_g	ambient air density
ρ_l	liquid density
δ	Kronecker delta
σ	droplet surface tension
μ	viscosity
μ_t	turbulent viscosity
μ_v	dilatational viscosity
τ_{ij}	Reynolds stress tensor
Ω_{KH}	growth rate of Kelvin Helmholtz waves
Λ_{KH}	wavelength of fastest growing unstable Kelvin Helmholtz surface wave
τ_{KH}	Kelvin Helmholtz breakup time
Λ_{RT}	wavelength of fastest growing unstable Rayleigh Taylor surface wave
τ_{RT}	Rayleigh Taylor breakup time
Ω_{RT}	growth rate of Rayleigh Taylor waves
α_{spray}	scaling mass transfer coefficient
τ	spray optical thickness

Chapter 1

Introduction

1

1.1 Background & Motivation

THE massive increase of anthropocentric greenhouse gas (GHG) emissions causes climate change. Carbon dioxide (CO_2) is one of the main GHGs and is mainly emitted during the combustion of hydrocarbon fuels [28, 9]. Environmental studies suggest that 3% of the annual global anthropogenic CO_2 emissions originate from the maritime industry, a percentage that is likely to increase in the coming years if the sector does not reduce its emissions quickly [16]. In addition to CO_2, nitrogen oxides (NO_x) are harmful combustion products formed at high temperatures [12]. Specifically, NO_x emissions cause respiratory and cardiovascular issues, and contribute to acid rain and ground-level ozone formation [26]. To mitigate the environmental and health impact of NO_x, the International Maritime Organization (IMO) regulates these emissions through strict limits [7]. Therefore, developing effective strategies and technologies to reduce both CO_2 and NO_x emissions is essential for a sustainable maritime sector [9, 21, 4, 18].

With the Paris Agreement in effect since 2016, a long-term joint policy agenda was imposed globally to reduce GHG emissions and attenuate global warming [25]. The agreement aims to limit the global temperature rise to well below 1.5°C, but current projections indicate that these targets may not be met without significant changes [28]. As a result, the maritime sector is under increasing pressure to adopt alternative energy solutions with a lower or zero-carbon footprint [14, 18]. However, sustainable energy technologies are not yet widely available, partly due to technical and operational constraints such as limited range and energy density [14, 15]. Battery-electric solutions, for example, currently do not meet the cost, weight, and range requirements required for long-haul or heavy-duty maritime applications [20]. Given the strong dependence on fossil fuels, internal combustion engines (ICEs) are expected to remain a key component in energy production and transportation [8].

1.1.1 Why Methanol?

The ongoing dependence on fossil fuels provides a short-term solution in alternative and synthetic fuels, which can power state-of-the-art ICEs [2, 27]. In this context, methanol has been identified as an adequate alternative option, especially for heavy-duty inland and maritime applications [30, 29, 19]. Methanol can be renewably produced using a wide range of feedstocks [19], and offers scalable production [29] and high technology readiness level (TRL) [14, 5]. Compared to other alternative fuels such as ammonia and hydrogen, methanol offers several practical advantages. It is in the liquid phase at atmospheric conditions, making it easy to store and handle, which allows for the use of marine fuel tanks [32]. Furthermore, several favourable properties (e.g., lower adiabatic flame temperature, knock resistance, simple molecular structure, etc.) allow significant reductions in hazardous NO_x, SO_x, and PM emissions compared to diesel and gasoline [24, 32, 29]. Lastly, for maritime transport, methanol is considered the most cost-effective alternative when accounting for total ownership costs [11]. These advantages make methanol an attractive energy carrier for reducing emissions and decarbonizing ICE-based transportation [23].

1.2 Problem Statement & Research Questions

METHANOL integration in ICE is realised through different injection methods, such as port fuel injection (PFI) and direct injection (DI) [23]. These injection methods significantly influence the in-cylinder combustion modes, their performance, and emissions [12], as illustrated in Figure 1.1. During injection, methanol is sprayed into the engine in liquid form, where it undergoes atomization, evaporation, and mixing with air. This process can be hindered by wall impingement and incomplete vaporization, potentially leading to wall wetting and inhomogeneous mixture. Wall wetting, in particular, may lead to the formation of unburned hydrocarbons (UHC) and formaldehyde [29]. Moreover, an inhomogeneous mixture is described by locally rich and lean regions of fuel-air mixture in the cylinder, which hinders flame propagation and contributes to unstable combustion [31]. Therefore, effective spray and mixture control is crucial for ensuring efficient and clean combustion [6, 3]. A comprehensive understanding of these phenomena—through both experimental and computational investigations—is essential for optimizing methanol-fuelled ICEs. Ultimately, improving our understanding of methanol spray and mixture formation can enable more efficient combustion and significantly lower emissions compared to conventional fuels [19, 29].

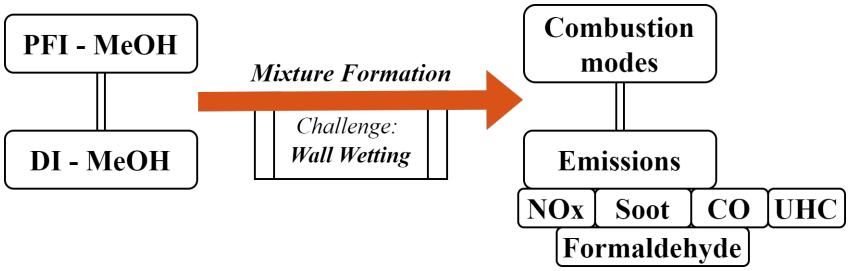

Figure 1.1: Schematic representation of the relationship between methanol injection methods (PFI and DI), mixture formation, and resulting combustion modes and emissions.

Compared to diesel, methanol has approximately four times higher latent heat of vaporization (Table 1.1). This also challenges the creation of a homogeneous mixture by requiring more heat and time for the evaporation of the fuel. Additionally, methanol's lower heating value (LHV) is approximately half of diesel's, thus demanding twice the fuel mass for the same power output [32, 23, 19]. This leads to longer injection duration or larger injector diameter to achieve the same power density as diesel operation. These two properties further complicate methanol retrofitting, often limiting the engine operating range [17].

Based on the motivation outlined above, the problem statement of the present thesis is formulated as follows:

> *How do methanol sprays influence evaporation and mixture formation in marine ICEs? Can we develop a predictive simulation framework to aid in optimizing various methanol-fuelled marine engine injection strategies?*

Table 1.1: Marine Fuel Properties [29, 22, 1, 13]

Property	Diesel	Methane	Methanol	Ammonia
Lower Heating Value (LHV) [MJ/kg]	42.7	50	20.1	18.8
Density (at STP) [kg/m^3]	840	0.65	790	0.718
Heat of Vaporization (at 1 bar) [kJ/kg]	250	510	1089	1370
Boiling Point (at 1 bar) [°C]	180-360	-161.5	65	-33.34
Surface Tension (at 20 °C) [mN/m]	27	-	23	18.1 (at 34.1 °C)
Dynamic Viscosity (at 20 °C) [mPa·s]	2.1 - 2.52	0.01	0.57	0.01

The research problem leads to the following research questions, which distinctively address PFI and DI methanol sprays associated with marine ICEs:

1. How do PFI and DI methanol injection strategies compare in marine engine applications?
2. What is the atomization quality of methanol under low injection pressure in PFI systems, and how can it be improved to enhance mixture formation?
3. To what extent does PFI of methanol lead to fuel wall film formation on the intake manifold?
4. Can existing state-of-the-art spray modelling practices reliably predict methanol spray behaviour, or do they require significant adaptation?
5. How does methanol spray formation in DI systems differ from conventional fuels such as diesel and gasoline, particularly in terms of morphology and vaporization behaviour?
6. How do methanol's distinct physical properties, such as high latent heat of vaporization and lower energy density, impact spray evolution and mixture preparation across injection strategies?
7. Is it feasible to develop a unified CFD-based spray modelling framework that accurately captures methanol behaviour in both PFI and DI configurations?
8. What are the implications of methanol DI spray characteristics on marine engine operation?

1.3 Research Approach

THE objective of the present thesis is to develop a modelling framework for methanol sprays relevant to marine ICEs. To achieve this, we use computational fluid dynamics (CFD) simulations to analyse the physical phenomena underlying the spray and mixture formation in both PFI and DI conditions. The CFD models employ the Lagrangian-Eulerian framework to simulate the interaction between liquid methanol droplets and the surrounding gas. Most of the thesis uses the Reynolds-Averaged Navier–Stokes (RANS)

approach for turbulence modelling, while high-fidelity simulations in Chapter 4 utilize a Large Eddy Simulation (LES) framework. Given methanol's distinct physical properties compared to conventional fuels, this thesis evaluates the applicability of existing spray models and aims to calibrate and validate them using experimental data specific to methanol. The validated CFD models are used to investigate mixture formation and its impact on pre-ignition in-cylinder conditions typical of marine engines.

Initially, we identify the various methanol injection strategies and combustion modes reported for marine internal combustion engines to answer the problem statement. After outlining the potential pathways for injecting methanol, the focus of the thesis shifts to spray modelling across different configurations: low- and high-pressure PFI, as well as single-hole DI using diesel-type and multi-hole DI using gasoline-type injectors. Recognizing the limited literature on methanol spray behaviour, the thesis conducts a dedicated investigation into methanol spray models, including droplet breakup, collision, and evaporation. To isolate spray dynamics from combustion effects, the study employs constant volume chamber (CVC) experiments for both PFI and DI configurations, allowing for targeted calibration of spray models under methanol-specific conditions. Comparisons with diesel and iso-octane highlight the distinct spray behaviour of methanol relative to conventional fuels. The calibrated spray framework developed in the present thesis enables accurate and computationally affordable engineering-level CFD simulations of full engine geometries. Ultimately, this work supports the analysis and optimization of mixture formation, enabling future studies on combustion and emission formation in marine engines, as illustrated in Figure 1.2.

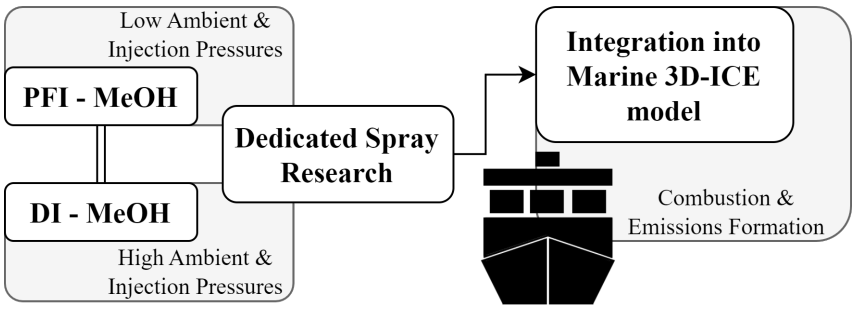

Figure 1.2: Schematic representation of the proposed research approach focusing on dedicated spray research using methanol experimental data.

1.4 Thesis Outline

THE thesis is organised into six chapters, as presented in Figure 1.3:

- Chapter 2 reviews methanol injection and ignition strategies specifically for heavy-duty and marine methanol engines. Due to inconsistent definitions found across the literature, a unified classification framework is introduced for spark ignition (SI)

and compression ignition (CI) engine concepts, including both mono-fuel and dual-fuel configurations. Lastly, by identifying the various port-fuel and direct injection methods, this chapter helps define the conditions and injection parameters relevant to the numerical modelling presented in the following chapters of the thesis.

- Chapter 3 investigates methanol spray behaviour under PFI conditions, which constitutes a low ambient pressure and temperature environment typical of intake port conditions in premixed CI marine engines. The validation is based on experimental data from the literature, using methanol at both low and high injection pressures, encompassing quantities relevant to light-duty engines. Subsequently, the validated PFI models are applied to scaled-up marine engine injection quantities to study atomization and evaporation phenomena. This marine engine investigation reveals the influence of injection pressure and intake ambient conditions on atomization and evaporation behaviour of methanol sprays.

- Chapter 4 extends the CFD approach of Chapter 3 to DI conditions by simulating the Engine Combustion Network (ECN) methanol Spray M1 using both RANS and LES turbulence models. The simulated conditions reflect high ambient pressure and temperature environments, representative of in-cylinder partially premixed marine engines[1] with moderate injection pressure from a multi-hole gasoline-style injector. Validation is performed using state-of-the-art projected liquid volume (PLV) maps, liquid penetration data, and spray morphology, aiming to capture complex physical phenomena such as spray collapsing and sweeping. Ultimately, by revealing these key insights into methanol sprays in multi-hole DI conditions, this chapter highlights a vastly different behaviour between methanol and gasoline sprays, due to the inherently distinct physical properties of methanol.

- Chapter 5 investigates the charge cooling effect of methanol in a heavy-duty dual-fuel DI-CI engine environment. This engine environment is characterised by extremely high ambient pressure and temperature conditions, where both methanol and diesel are injected close to top-dead-center (TDC) using ultra-high injection pressures. The computational framework is first validated against non-reacting ECN Spray D experimental data using n-dodecane[2] liquid and vapour penetration, as well as the spray morphology. Following validation, the diesel injection model is adapted for methanol injection and systematically compared with n-dodecane, which serves as a surrogate fuel for diesel. The analysis examines mixture formation characteristics and temperature distributions prior to ignition, providing insights into the thermal effects of methanol DI on marine dual-fuel engines.

- Chapter 6 summarises the main findings of the present thesis and recommends topics for future research directions.

[1] In the context of direct-injection spark-ignition engines, the simulated conditions are typically classified as late-injection for stratified operation. However, in larger marine engines, the same conditions align with partially premixed injection timings due to the higher in-cylinder pressures and temperatures characteristic of these engines.

[2] N-dodecane is widely used as a diesel surrogate in engine simulations.

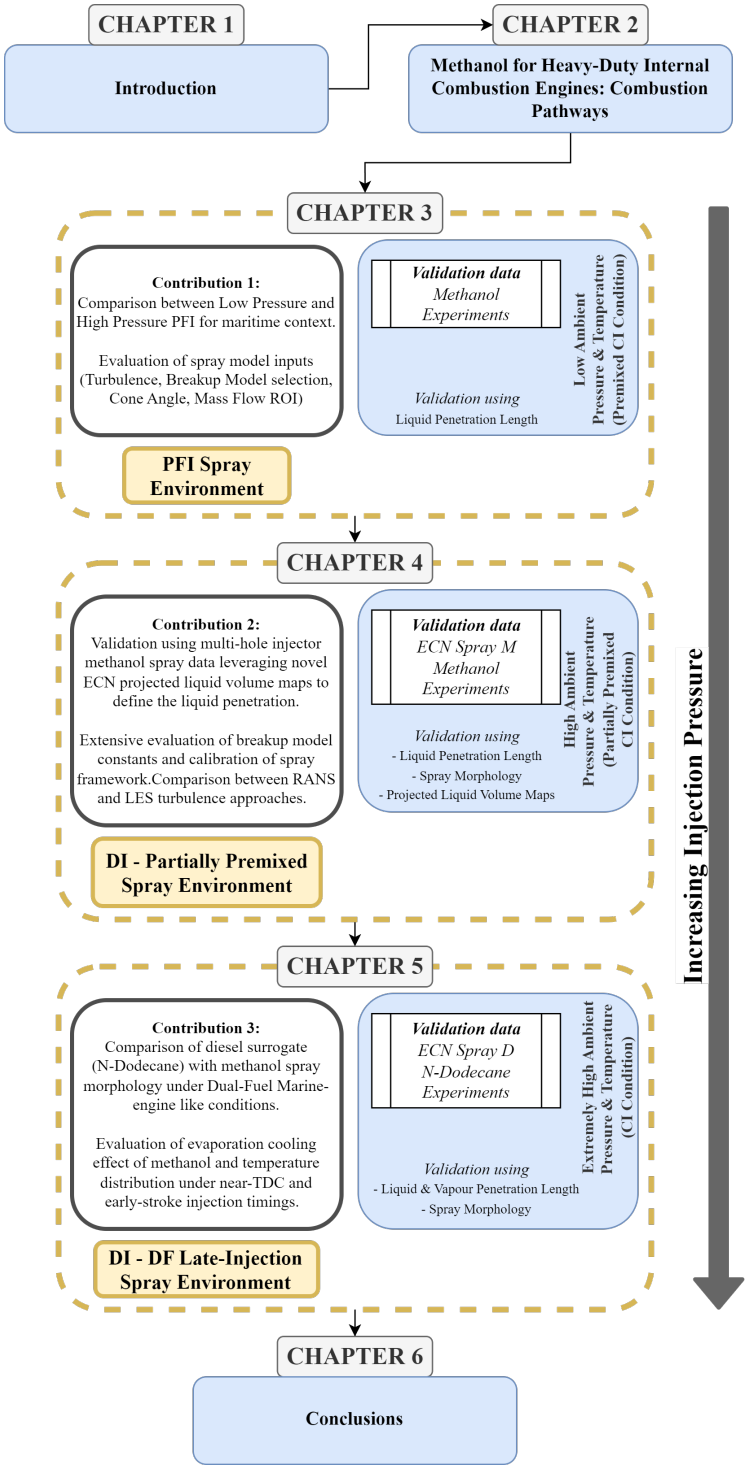

Figure 1.3: Outline of the present thesis, including the three chapters encompassing distinct ways of injection in PFI and DI conditions using increasing injection pressure.

1

1.5 Contributions

THE contributions of the present dissertation with respect to methanol spray CFD modelling are the following:

- A validated CFD model for methanol PFI sprays (both low and high injection pressures) under marine-relevant conditions using experimental data specifically for methanol, which fills the literature gap for marine applications.

  Exploration of marine-scale injection quantities, with the proposed approach, reveals that high injection pressures improve atomization and evaporation.

  Highlighting challenges in methanol retrofitting, such as wall wetting and delayed evaporation.

  Proposals for solutions, such as higher injection pressures to enhance mixture formation. This work is presented in Chapter 3 and published in Zoumpourlos et al. [33].

- Improved the state-of-the-art spray modelling using ECN Spray M data: expanded CFD validation by leveraging the ECN's Spray M1 dataset for late-injection DI conditions.

  Comparison of methanol spray morphology with iso-octane. Demonstration of the unique spray behaviour of methanol, which leads to plume collapsing due to high volatility. Capturing of the intrinsic flow phenomena by systematically tuning the droplet breakup model constants.

  A validated methodology for future methanol DI engine simulations, bridging the gap between conventional fuel models and methanol-specific requirements. This work is described in Chapter 4 and published in Zoumpourlos et al. [34].

- Comparison of the spray structure of methanol with n-dodecane in DI-CI engine environment, highlighting the increased liquid penetration of methanol due to slower evaporation rates.

  Validation of the n-dodecane model using liquid and vapour penetration data from the non-reacting ECN Spray D under heavy-duty conditions. This work is outlined in Chapter 5 and published in Zoumpourlos et al. [35] and Zoumpourlos et al. [36].

Additionally, the main contributions concerning methanol marine engine operation and mixture formation are as follows:

- Review of methanol injection and ignition strategies for heavy-duty and marine engines.

  Introduction of a unified classification framework for both SI and CI concepts. This work is presented in Chapter 2 and published in Kiouranakis et al. [10].

- Quantification of methanol's charge cooling effect.

  Demonstration of the influence of ambient temperature and injection timing on the charge cooling effect, and the resulting mixture temperature gradient.

  Highlighting the challenges in methanol adoption in marine engines, supporting the transition to sustainable maritime propulsion. This work is outlined in Chapter 5 and published in Zoumpourlos et al. [35] and Zoumpourlos et al. [36].

By addressing these aspects, this thesis aimed to advance the understanding of methanol sprays and support the development of efficient, low-emission marine engines.

Bibliography

[1] Avinash Kumar Agarwal et al. *Methanol and the alternate fuel economy*. Springer, 2019.

[2] A. Ait Allal et al. "Toward an evaluation of marine fuels for a clean and efficient autonomous ship propulsion energy". In: *Materials Today: Proceedings* 13 (2019), pp. 486–495. DOI: 10.1016/j.matpr.2019.04.005. (Visited on 05/23/2022).

[3] Carsten Baumgarten. *Mixture formation in internal combustion engines*. Springer Science & Business Media, 2006.

[4] Lindert van Biert et al. "A review of fuel cell systems for maritime applications". In: *Journal of Power Sources* 327 (2016), pp. 345–364.

[5] Kylee Harris et al. "A comparative techno-economic analysis of renewable methanol synthesis from biomass and CO2: Opportunities and barriers to commercialization". In: *Applied Energy* 303 (Dec. 2021). DOI: 10.1016/j.apenergy.2021.117637. (Visited on 08/23/2022).

[6] John B. Heywood. *Internal combustion engine fundamentals*. Second edition. McGraw-Hill Education, 2018. ISBN: 978-1-260-11610-6.

[7] *International Maritime Organization: Nitrogen Oxides (NOx) – Regulation 13*. 2011. URL: www.imo.org/en/OurWork/Environment/Pages/Nitrogen-oxides-(NOx)-%E2%80%93-Regulation-13.aspx.

[8] Gautam Kalghatgi. "Is it really the end of internal combustion engines and petroleum in transport?" In: *Applied energy* 225 (2018), pp. 965–974.

[9] Dagobert G Kessel. "Global warming—facts, assessment, countermeasures". In: *Journal of Petroleum Science and Engineering* 26.1-4 (2000), pp. 157–168.

[10] K. I. Kiouranakis et al. "Methanol for heavy-duty internal combustion engines: Review of experimental studies and combustion strategies." In: *Renewable and Sustainable Energy Reviews* (2025).

[11] A.D. Korberg et al. "Techno-economic assessment of advanced fuels and propulsion systems in future fossil-free ships". In: *Renewable and Sustainable Energy Reviews* 142 (May 2021), p. 110861. ISSN: 1364-0321. DOI: 10.1016/j.rser.2021.110861. URL: https://linkinghub.elsevier.com/retrieve/pii/S1364032121001556 (visited on 09/24/2023).

[12] Anand Krishnasamy et al. “Prospective fuels for diesel low temperature combustion engine applications: A critical review”. In: *International Journal of Engine Research* 22.7 (July 2021), pp. 2071–2106. DOI: 10.1177/1468087420960857. (Visited on 05/19/2022).

[13] Caneon Kurien et al. “Review on the production and utilization of green ammonia as an alternate fuel in dual-fuel compression ignition engines”. In: *Energy Conversion and Management* 251 (2022), p. 114990.

[14] Li Chin Law et al. “A comparison of alternative fuels for shipping in terms of lifecycle energy and cost”. In: *Energies* 14.24 (2021), p. 8502.

[15] Charles J McKinlay et al. “Route to zero emission shipping: Hydrogen, ammonia or methanol?” In: *International Journal of Hydrogen Energy* 46.55 (2021), pp. 28282–28297.

[16] International Maritime Organization. *International Maritime Organization: Fourth Greenhouse Gas Study 2020*. Tech. rep. Accessed: 2023-02-05. 2020. URL: https://www.imo.org/en/OurWork/Environment/Pages/Fourth-IMO-Greenhouse-Gas-Study-2020.aspx.

[17] Kasinath Panda et al. “HCCI combustion of methanol along with diesel through novel injection strategies and its potential over conventional dual fuel combustion”. In: *Fuel* 324 (Sept. 2022), p. 124766. DOI: 10.1016/j.fuel.2022.124766.

[18] Maja Perčić et al. “Life-cycle cost assessment of alternative marine fuels to reduce the carbon footprint in short-sea shipping: A case study of Croatia”. In: *Applied Energy* 279 (Dec. 2020). DOI: 10.1016/j.apenergy.2020.115848. (Visited on 05/23/2022).

[19] Michele Pipicelli et al. “Alcohol Fuels in Compression Ignition Engines”. In: *Energy, Environment, and Sustainability*. Springer Nature, 2022, pp. 9–31. DOI: 10.1007/978-981-16-8751-8_2.

[20] R D Reitz et al. “IJER Editorial: The future of the internal combustion engine”. In: *International Journal of Engine Research* (2020). DOI: 10.1177/1468087419877990.

[21] AP Roskilly et al. “Novel technologies and strategies for clean transport systems”. In: *Applied Energy* 100.157 (2015), pp. 563–566.

[22] American Bureau of Shipping (ABS). *Pathways to Sustainable Shipping*. Tech. rep. Accessed: 2022-07-07. 2020. URL: https://www.hernieuwbarebrandstoffen.nl/post/pathways-to-sustainable-shipping.

[23] Jaydeep Singh et al. “Methanol Fuel in Compression Ignition Engines”. In: *Application of Clean Fuels in Combustion Engines*. Springer Nature Singapore, 2022, pp. 71–101. ISBN: 9789811687501 9789811687518. DOI: 10.1007/978-981-16-8751-8_5.

[24] Dinesh Kumar Soni et al. “Optimization of methanol powered diesel engine: A CFD approach”. In: *Applied Thermal Engineering* 106 (Aug. 2016), pp. 390–398. DOI: 10.1016/j.applthermaleng.2016.06.026. (Visited on 05/24/2022).

[25] *The Paris Agreement*. 2015. URL: https://www.un.org/en/climatechange/paris-agreement.

[26] Margarita Theodorakidou et al. “Public health issues from the exposure to nitrogen oxides: a brief review”. In: *ARC J Public Health Community Med* 2 (2017), pp. 44–56.

[27] Martin Tuner. “Review and Benchmarking of Alternative Fuels in Conventional and Advanced Engine Concepts with Emphasis on Efficiency, CO2, and Regulated Emissions”. In: *SAE Technical Papers* (2016).

[28] UN. *Emissions Gap Report 2022*. Tech. rep. 2022. URL: www.unep.org/resources/emissions-gap-report-2022.

[29] Sebastian Verhelst et al. “Methanol as a fuel for internal combustion engines”. In: *Progress in Energy and Combustion Science* 70 (Jan. 2019), pp. 43–88. ISSN: 0360-1285. DOI: 10.1016/j.pecs.2018.10.001. URL: https://linkinghub.elsevier.com/retrieve/pii/S036012851830042X (visited on 09/16/2022).

[30] Xudong Zhen et al. “An overview of methanol as an internal combustion engine fuel”. In: *Renewable and Sustainable Energy Reviews* 52 (Dec. 2015), pp. 477–493. ISSN: 1364-0321. DOI: 10.1016/j.rser.2015.07.083.

[31] Zengqiang Zhu et al. “Investigation on mixture formation and combustion characteristics of a heavy-duty SI methanol engine”. en. In: *Applied Thermal Engineering* 196 (Sept. 2021), p. 117258. DOI: 10.1016/j.applthermaleng.2021.117258. (Visited on 09/20/2022).

[32] Burak Zincir et al. “Methanol as a Fuel for Marine Diesel Engines”. In: *Alcohol as an Alternative Fuel for Internal Combustion Engines*. Springer Singapore, 2021, pp. 45–85. ISBN: 9789811609305 9789811609312. DOI: 10.1007/978-981-16-0931-2_4. (Visited on 01/14/2023).

[33] K. Zoumpourlos et al. “Methanol sprays in marine engines: CFD modelling of port fuel injection systems.” In: *Journal of Marine Engineering Technology* (2025).

[34] Konstantinos Zoumpourlos et al. “CFD modeling approach for late-injection methanol sprays validated with ECN spray M”. In: *International Journal of Engine Research* (2025). DOI: 10.1177/14680874251323931.

[35] Konstantinos Zoumpourlos et al. “Methanol Operation in Heavy-Duty DICI Dual-Fuel Engines: Investigating Charge Cooling Effects Using ECN Spray D Data”. In: *Journal of Engineering for Gas Turbines and Power* (2025), pp. 1–10. DOI: 10.1115/1.4067862.

[36] Konstantinos Zoumpourlos et al. “Methanol Operation in Heavy-Duty DICI Dual-Fuel Engines: Investigating Charge Cooling Effects using ECN Spray D Data”. In: *ASME ICEF 2024*. 2024.

Chapter 2

Methanol for Heavy-Duty Internal Combustion Engines: Combustion Pathways

Konstantinos ZOUMPOURLOS, Konstantinos Ioannis KIOURANAKIS

The differences between various methanol injection and ignition strategies, as well as their corresponding combustion processes, remain inconsistently defined in the literature. In heavy-duty and marine engines, diffusion combustion is often favoured as it allows for higher methanol energy shares. However, this comes at the cost of higher nitrogen oxide (NO_x) and soot emissions, as well as an increasing impact on engine design compared to premixed strategies. To distinguish these differences, this chapter reviews the primary injection and ignition strategies employed in methanol engines. Moreover, to clarify the ambiguity found in the literature, we propose a structured classification framework covering heavy-duty spark ignition (SI) engines and mono-fuel and dual-fuel diesel-methanol compression ignition (CI) engines.

This chapter was partly reproduced from [40]:
Kiouranakis, K. I., de Vos, P., Zoumpourlos, K., Coraddu, A., & Geertsma, R. (2025). Methanol for heavy-duty internal combustion engines: Review of experimental studies and combustion strategies. Renewable and Sustainable Energy Reviews, 214, 115529.DOI: `https://doi.org/10.1016/j.rser.2025.115529`
The author of the present thesis contributed in the systematic literature review, the analysis and writing, and the conceptualisation of the classification framework. We include the parts of the published manuscript to which the author of this thesis contributed.

2

THIS chapter presents a review of the possible methods for the combustion of methanol in ICEs. For methanol implementation, different injection strategies can be utilized in the context of both spark ignition (SI) and compression ignition (CI) engines. The chapter reviews the primary combustion mechanisms and presents the application pathways for methanol. To accommodate these distinct combustion modes, relevant figures are provided to explain the different strategies of methanol utilization. Fundamentally, combustion in a piston engine can occur in three ways: Otto-type premixed flame propagation, HCCI-type premixed autoignition, and Diesel-type non-premixed diffusion combustion (Figure 2.1).

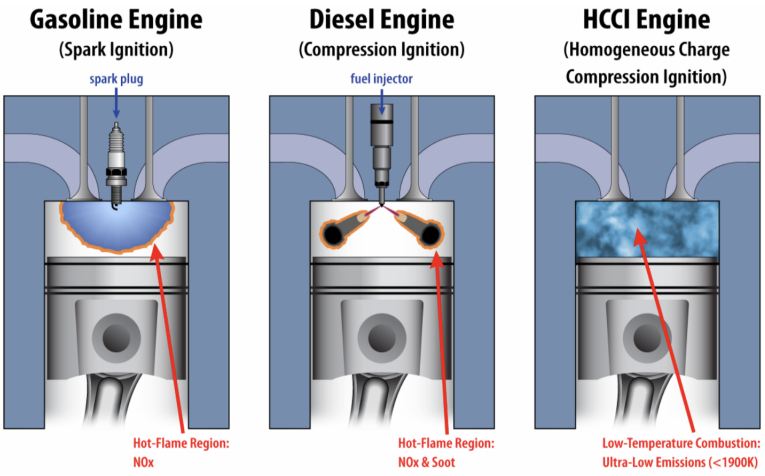

Figure 2.1: Fundamental combustion concepts in ICEs [56]

2.1 SI engines

ALCOHOL-based fuels with high octane number, such as methanol and ethanol, are well-suited for use in spark-ignition (SI) engines [81, 19]. In these engines, fuel is commonly introduced at low pressure into the intake port, a configuration known as port fuel injection (PFI), which promotes the formation of a homogeneous air-fuel mixture within the combustion chamber. Air path injection (API) can be achieved via single-point injection (SPI)—by means of carburation or spray injection upstream in the intake port—or through multipoint injection (MPI) using PFI [90, 12]. SPI is typically used in gaseous-fuelled engines, such as those powered by natural gas [73], whereas PFI is the preferred approach for liquid fuels, like methanol [44]. Figure 2.2 illustrates the injection strategies used in SI engine configurations.

Injection strategies in SI engines are fundamentally based on premixed flame propagation, with combustion duration being highly influenced by flame–turbulence interactions [31]. Increasing turbulence intensity accelerates flame speed [79], a principle central to the turbulent jet ignition (TJI) concept, which employs a pre-chamber to initiate

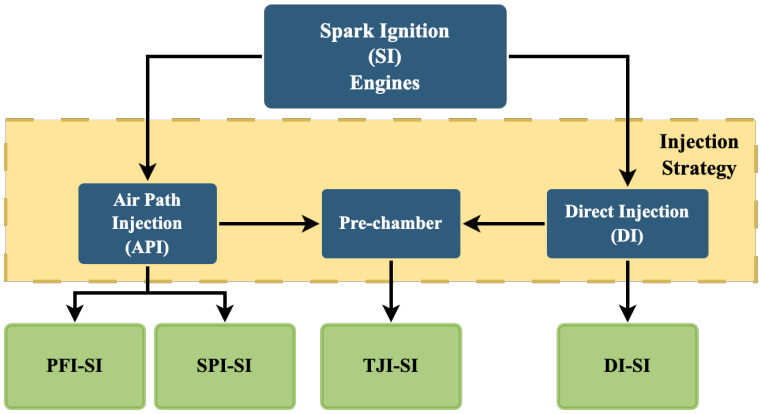

Figure 2.2: Engine strategies in SI engines [40]

combustion in lean mixtures [54, 66]. Beyond fully premixed approaches, efficiency gains can be achieved through in-cylinder DI or by combining API with pre-chamber ignition. These strategies allow charge stratification and operation under leaner conditions [46, 100], improving both thermal efficiency and emissions [45]. The TJI concept is a common strategy for implementing the SI engine technology in heavy-duty (HD) applications, such as marine [3, 34]. Although SI engines may employ a variety of injection configurations, their combustion mode is explicitly designed around premixed flame propagation [30], with autoignition intentionally avoided. Even in gasoline DI systems—often adopted to promote charge stratification for performance benefits—the primary combustion mechanism is flame-driven propagation [35].

2.2 CI engines

UNLIKE SI engines, CI engines operate under two primary combustion modes—low-temperature combustion (LTC) and conventional diesel combustion (CDC)—making the classification of combustion strategies more complex. Moreover, the development of dual-fuel (DF) engine concepts has further broadened this landscape by enabling a wide range of fuel combinations and injection strategies aimed at enhancing performance and integrating alternative fuels. These recent developments have also introduced inconsistencies in terminology, as overlapping and ambiguous definitions are often found across studies. This issue is particularly evident when discussing alternative fuels, such as methanol, where a lack of standardization can lead to confusion. For instance, the term direct dual-fuel stratification (DDFS), originally defined as a specific injection-based combustion strategy [88], has been applied with varying interpretations in methanol-related studies [50, 48]. Such inconsistencies in terminology are not unique to methanol and have also been noted in literature for other low-reactivity fuels (LRFs), such as natural gas [39].

Therefore, the primary goal of this review chapter is to introduce a practical classification framework that enables consistent categorization and interpretation of methanol

CI strategies. To achieve this, we identified four key degrees of freedom that shape methanol combustion behaviour: the fuel strategy (mono-fuel or dual-fuel), methanol injection location, ignition method, and the methanol to high-reactivity fuel (HRF) ratio in premixed DF engine concepts. These parameters collectively determine the dominant combustion mechanism. Figure 2.3 outlines the various pathways for methanol use in CI engines, showing that despite diverse configurations, combustion typically aligns with one of three primary combustion modes. These combustion modes can be either premixed flame propagation, premixed autoignition, or non-premixed diffusion. Although some approaches may involve hybrid combustion behaviour, the figure emphasizes the intended dominant mode in each scenario [9]. Additionally, the ignition approach is governed by the timing of fuel injection, which is further detailed in Figure 2.4, providing a complementary perspective to the strategy classification.

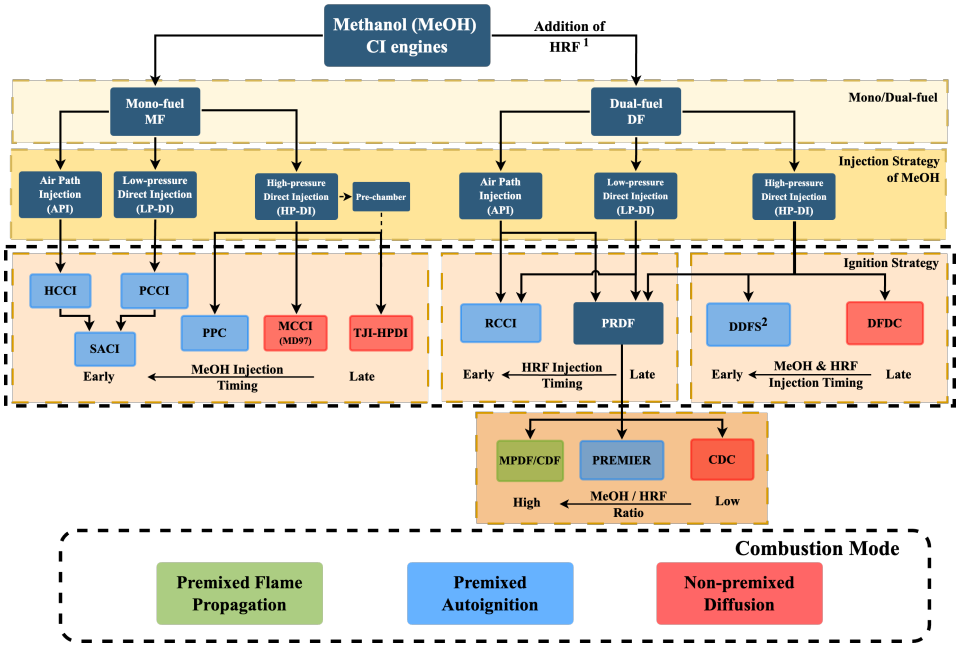

[1] High Reactivity Fuel (HRF) (e.g., Biodiesel)
[2] RCCI-type of combustion strategy

Figure 2.3: Classification framework for methanol CI engine strategies [40]

2.2.1 Mono-fuel strategies

Operating conventional diesel combustion (CDC) with neat methanol requires much higher compression ratios (CRs) than with diesel fuel [75]. In addition, higher intake air temperatures [70] or the use of hot recirculated exhaust gases [26] are needed to support ignition. These conditions can increase nitrogen oxide (NO_x) emissions and may compromise engine durability. To assist ignition under these demanding conditions—especially

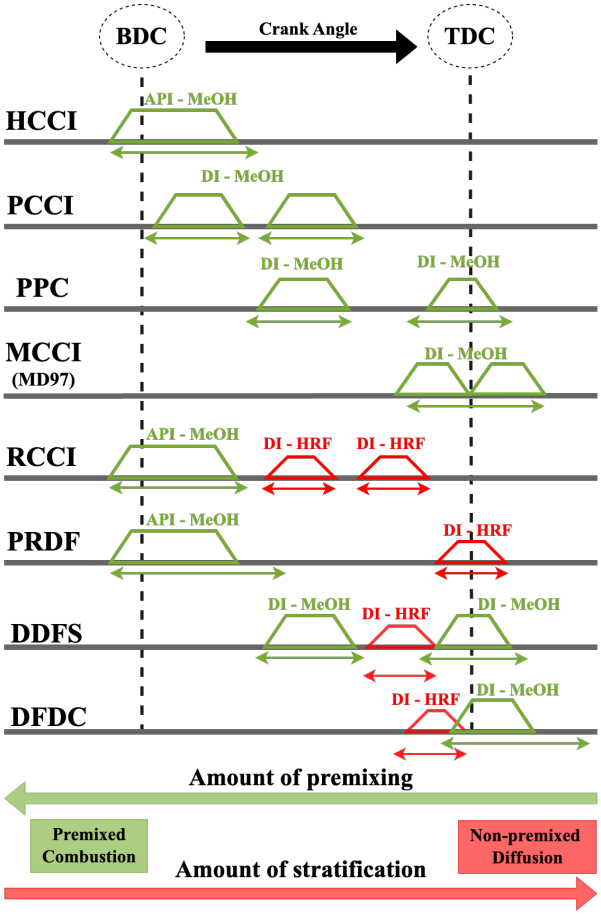

Figure 2.4: Fuel injection timing in different CI strategies [40]

during cold starts or at low loads—auxiliary ignition devices such as glow plugs are often used [69, 57]. For LRFs, a combustion strategy similar to CDC, where diffusive combustion is the primary mode, is typically referred to as mixing-controlled compression ignition (MCCI) [97]. This mode is generally achieved through two-stage high-pressure direct injection (HP-DI) of the LRF, such as methanol, close to top dead center (TDC) [24].

Due to the demanding conditions required for MCCI operation with neat methanol (such as the need for high CRs), most studies have instead concentrated on using methanol blended with ignition improvers for HD applications, including marine engines. Previous studies have examined the influence of various ignition and lubricity additives, as well as their blending ratios, on methanol diffusion combustion [72, 14]. These findings indicate that stable combustion could not be achieved with additive concentrations below 5%. However, a more recent study demonstrated stable combustion with a lower additive content of just 3% [77]. This approach, known as MD97 [77], can be classified as a mono-fuel

strategy [2].

To overcome methanol's low reactivity in CI engines without relying on ignition improvers or HRFs, recent studies explored the pre-chamber technology, a concept traditionally used in SI engines [66]. The pre-chamber strategy employs the TJI concept, utilizing HP-DI [84] in an MCCI-style approach. The goal of this strategy is to avoid end-gas auto-ignition (i.e., knocking) [86], a key challenge in premixed combustion in heavy-duty engines operating in a flame propagation mode. In this configuration, a small amount of methanol is injected and ignited in a pre-chamber, producing hot jets that shoot through narrow orifices into the main chamber. The bulk of the methanol is then injected via HP-DI into these jets, facilitating robust ignition and combustion. Due to the novelty and complexity of this approach, current investigations have been conducted primarily using computational simulations [36].

Alternative mono-fuel strategies—particularly LTC concepts-have attracted attention for their ability to lower NO_x and PM emissions without compromising, and potentially enhancing thermal efficiency [31]. LTC approaches aim to separate the fuel injection and combustion events in CI engines, thereby avoiding the typical diffusion-controlled combustion phase [43]. Among these, homogeneous charge compression ignition (HCCI) is considered the foundational LTC strategy, featuring a fundamentally different combustion mode from conventional gasoline SI and diesel CI engines. This concept first emerged under names such as active thermo-atmosphere combustion (ATAC) in 1979 [62] and compression-ignited homogeneous charge (CIHC) in 1983 [58], both emphasizing spontaneous chemical kinetics-driven autoignition. Furthermore, the widely adopted term HCCI was adopted by Thring [78], referring to a strategy in which fuel is introduced through an air path injection (API) system to ensure a uniformly mixed charge. HCCI combustion has been investigated for use with both diesel-like fuels [1] and gasoline-like fuels, including methanol [27].

Premixed charge compression ignition (PCCI) shares the core principle of HCCI by targeting fully premixed lean combustion initiated by autoignition [37]. It is often viewed as the DI counterpart of the HCCI concept [28]. To precisely control combustion timing in fully premixed modes, a refined approach is introduced involving two injection events: an early injection to create a premixed charge and a secondary injection timed to initiate combustion. Although this method retains bulk autoignition as its primary ignition source and is classified under the HCCI mode, it has been described using terms such as the Uniform Bulky Combustion System (UNIBUS) [29] and two-stage PCCI [42]. In addition, multi-pulse ultra-high-pressure injection strategies have been investigated in the context of PCCI [23, 23].

The two- or multi-stage injection approach is commonly known as Partially Premixed Combustion (PPC) [67, 101], which aims to decouple the initial fuel injection from combustion initiation [53]. Comparable techniques in diesel engines are also referred to as split-premixed compression ignition (split-PCI) [61] or partially premixed compression ignition (PPCI) [95]. To reduce ambiguity, this chapter clearly differentiates PPC from MCCI, as both terms have occasionally been used to describe similar combustion strategies—specifically, those involving a pre-TDC injection for partial premixing followed by a later injection that governs combustion phasing through diffusion-like burning [67]. In this context, PPC refers to cases where the majority of the fuel is injected well before

TDC [20], whereas MCCI involves injection much closer to TDC [25][1]. Although efforts are made here to distinguish PPC from PCCI, we acknowledge differences in terminology across the literature. Lastly, spark assisted compression ignition (SACI) is another studied approach that relies on premixed autoignition. Here, a spark plug initiates reaction kinetics locally, leading to autoignition throughout the premixed charge [65, 47].

2.2.2 Dual-fuel strategies

While the term *DF strategy* is often associated with natural gas-fuelled engines, it can also apply to other LRFs, such as alcoholic fuels [39]. The diesel–methanol blending approach is not shown in Figure 2.3, as methanol's emulsion-related limitations restrict its viability in such strategies [74], typically limiting its blend ratio up to 20%. DF engines use an HRF, such as diesel, to ignite low cetane number[2] fuels like methanol. In DF engines, the HRF injection method is generally fixed, with HP-DI being the most prevalent, while the methanol injection method varies across three typical strategies: API, low-pressure direct injection (LP-DI), and HP-DI. Among these, similarly as in mono-fuel SI engines, the API method—using either SPI or multipoint PFI—is the simplest and most widely used approach for methanol injection in DF engines.

This injection strategy has been designated as "fumigation" in the context of alcohol DF engines [11]. Alperstein et al.[7] introduced the term in 1958 to characterize diesel low pressure (LP) PFI into the intake system, primarily to address challenges related to fuel-air mixing and smoke emissions in diesel engines. Originally, fumigation referred to the delivery of liquid fuel—such as diesel—as a fine mist or "fumes" into the intake port. Over time, the definition broadened to include the introduction of alternative fuels into the intake air upstream of the manifold through a carburettor or LP injector [32, 22]. Currently, "fumigation" generally refers to methanol injection along the intake air path [15]. However, this term has become ambiguous, straying significantly from its original intent and raising uncertainty about the precise injection location and evaporation behaviour. Therefore, this chapter proposes discontinuing the use of "fumigation" and instead adopting the more precise term *air path injection (API)* to describe any form of methanol injection along the intake path.

Another LP injection approach involves directly injecting methanol into the cylinder, a method commonly used in large two-stroke marine natural gas dual-fuel engines [41, 18]. In these premixed strategies, combustion is initiated by the DI of an HRF, such as diesel. This configuration can lead to two separate combustion strategies: reactivity-controlled compression ignition (RCCI) [68] and premixed dual-fuel (PRDF). RCCI emerged as a more controllable alternative to earlier premixed autoignition approaches like HCCI and PCCI, using API of the LRF to create a homogeneous mixture. Following, early DI of the HRF is conducted to calibrate the mixture reactivity well before TDC. In contrast, PRDF retains a diesel injection timing similar to that of CDC, with a late pilot injection near TDC triggering ignition of the premixed methanol-air mixture. This PRDF mode is often

[1] PPC and RCCI typically involves fuel injection during the compression stroke at around −80° to −30° crank angles before TDC. On the other hand, MCCI typically refers to injection during the ignition, similar to diesel-style injection.

[2] The cetane number represents the autoignition tendency of a fuel.

labelled as conventional dual-fuel (CDF) [39, 59, 64]. In the context of methanol, it is typically referred to as diesel methanol dual-fuel (DMDF) [83, 17, 16] or diesel methanol compound combustion (DMCC) [93, 98, 82]. However, since these names do not clearly reflect the underlying injection or combustion processes, this chapter adopts the term methanol PRDF to better define the specific combustion strategy.

In dual-fuel strategies using HP-DI for both fuels, methanol injection timing can be varied to enable different combustion regimes [50]. This approach is currently used in large marine dual-fuel engines [41], and involves injecting both methanol and the HRF near TDC. This approach closely mimics CDC, but is applied to both fuels [21]. This setup generally follows the typical sequence of a late diesel injection close to TDC, followed by the LRF injection [3], as reported in multiple methanol studies [85, 71]. When methanol is injected before diesel [60, 94], its cooling effect extends the ignition delay, leading to a more premixed combustion behaviour, which resembles the PRDF strategy [99]. To support the experimental work and optimize this approach, several simulation studies have been conducted. For instance, Li et al. [49] explored a split injection strategy involving methanol injection both before and after diesel—referred to as methanol/diesel/methanol (M/D/M). Similarly, Yang et al. [92] studied how varying the structure of the pilot fuel injection can improve methanol combustion performance. This review chapter adopts the term methanol dual-fuel diffusion combustion (DFDC) to describe this approach, where both fuels predominantly undergo diffusion-controlled combustion.

Premixed autoignition combustion, as seen in RCCI, can also be realized through early HP-DI of both fuels during the compression stroke. This direct dual-fuel stratification (DDFS) approach blends features from both RCCI and PPC [88, 89], enabling flexible injection pulses for each fuel [48]. This flexibility offers improved control over the spatial distribution of fuel concentration and reactivity compared to conventional RCCI. Similar concepts focused on flexible stratified combustion have been referred to as intelligent charge compression ignition (ICCI) [33] and premixed micro pilot combustion (PMPC) [55]. To promote consistency in terminology, this review chapter recommends using the term DDFS to describe strategies that aim to achieve LTC through stratification provided by the DI of both fuels. To summarize the mentioned combustion strategies, Figure 2.5 displays the cylinder layout for the four main DF ignition strategies.

A notable and unique approach is the jet controlled compression ignition (JCCI) strategy [96], developed to improve combustion control in HCCI and PCCI systems. JCCI uses a small ignition chamber—similar to the pre-chamber TJI concept—mounted on the cylinder and equipped with a spark plug and an HRF injector [51]. Spark-initiated combustion from the chamber produces hot, reactive jets that are discharged through narrow orifices into the main chamber, initiating autoignition of the premixed charge. Unlike traditional TJI, which depends on flame propagation, JCCI is designed to achieve premixed autoignition, similar to HCCI, SACI, PCCI, PPC, RCCI, and DDFS. This technique has also been applied to ammonia-methanol blends, where hydrogen-fuelled jets from the pre-chamber ignite the main charge [87]. Although JCCI expands the combustion pathways for both mono- and dual-fuel CI engines [66, 87], its inclusion in Figure 2.3 would complicate the classification framework, which is intended to remain concise and accessible.

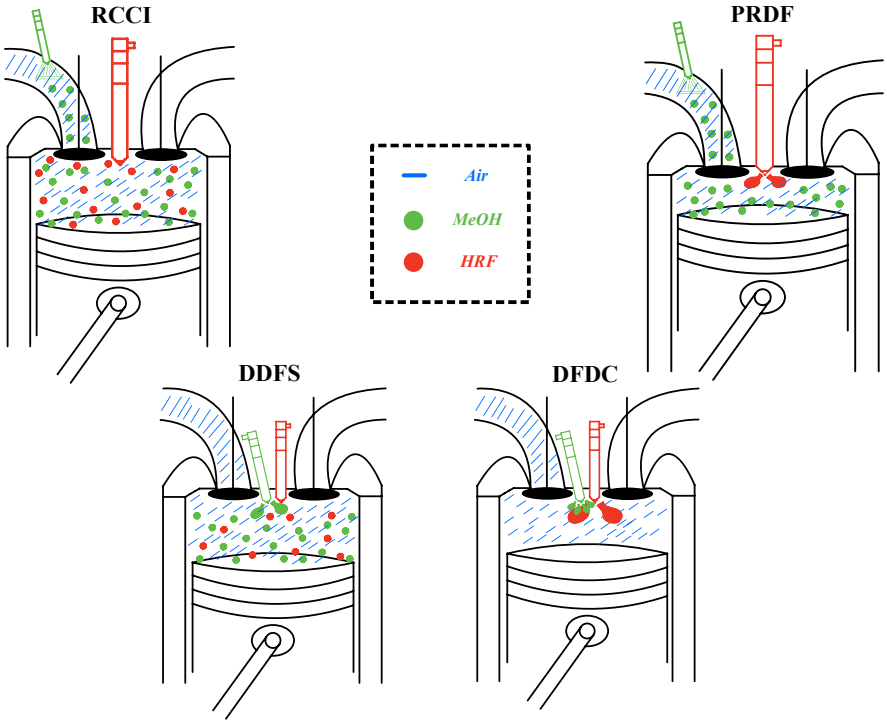

Figure 2.5: Dual-fuel main ignition combustion strategies [40]

The combustion behaviour in PRDF strategies is strongly influenced by the methanol-to-HRF ratio. In these PRDF engines, the objective is to minimize the quantity of diesel pilot required for combustion initiation [76]. However, issues such as misfiring and knocking often require lowering the methanol content to ensure safe engine operation [52]. Several studies have confirmed that methanol PRDF combustion is highly sensitive to changes in the methanol-to-HRF ratio [9, 38, 91, 4, 52]. At high methanol-to-HRF ratios, the small quantity of HRF can act as a "liquid spark," initiating combustion that resembles premixed flame propagation [9]. This forms the basis of the micro pilot dual fuel (MPDF) concept, also referred to as CDF [39]. In MPDF, the pilot fuel ignites at multiple points, creating several flame fronts that spread through the chamber and ignite the methanol-air mixture in a premixed manner [13]. Since this process depends on flame propagation similar to that in SI engines, MPDF can be classified as a deflagration-driven combustion strategy [18]. However, these systems are susceptible to knocking, a condition where pressure waves from the flame compress and autoignite the unburned mixture ahead of the flame front [63]. To counteract knock in diesel engines adapted for PRDF operation, reducing the CR is a common approach, similar to SI engine design.

At lower methanol-to-HRF ratios in a PRDF engine, the mixture ahead of the flame remains lean, while the combustion behaviour closely resembles that of CDC, as shown in Figure 2.6. As the methanol ratio increases toward levels typical of the MPDF strategy,

the combustion process becomes more intricate due to richer mixtures promoting both flame propagation and premixed autoignition. Figure 2.7 illustrates the three distinct combustion phases characteristic of the PRDF strategy, each contributing to the overall heat release rate (HRR) profile:

1. The first phase originates from the combustion of the HRF.
2. The second phase, which relies on the initial stage, is driven by the autoignition of the premixed methanol near or ahead of the flame front.
3. The third phase is governed by the HRR of the turbulent flame propagation through the remaining unburned methanol-air mixture.

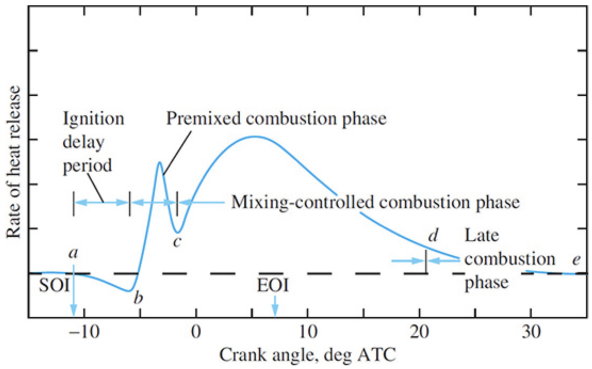

Figure 2.6: Typical combustion phases in a CDC [31]

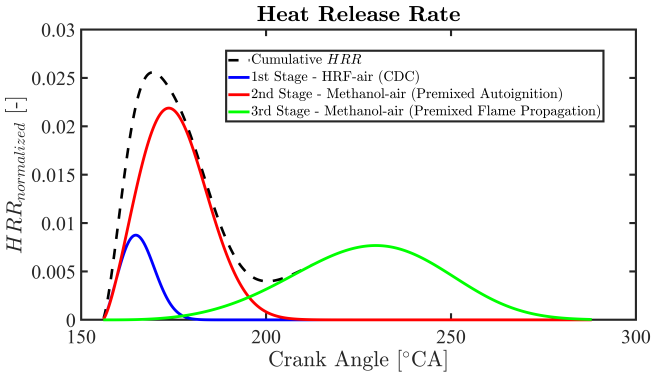

Figure 2.7: Typical combustion phases in a PRDF strategy [39]

With an increasing methanol-to-HRF ratio, the unburned mixture in front of the flame becomes richer, causing the HRF to burn predominantly in a premixed manner, which increases knocking occurrence [4]. This combustion process becomes increasingly complex, involving interactions between flame fronts initiated by the HRF and the premixed

autoignition of the methanol-air mixture near the flame front. In an attempt to emulate the SACI combustion process, Azimov et al. [8] explored a novel PRDF strategy. In their strategy, combustion was driven by the autoignition of a carefully managed premixed natural gas-air mixture, designed to prevent knocking [9]. They referred to this approach as the premixed mixture ignition in the end-gas region (PREMIER) mode, which is dominated by premixed autoignition. Although this PREMIER mode has since been further investigated for fuels such as methane [6], methane–hydrogen blends [5], and syngas [10, 80], no known studies have applied this concept specifically to methanol.

2.3 Conclusions

THIS chapter has reviewed the state-of-the-art strategies for using methanol in heavy-duty (HD) engines, covering both mono-fuel and dual-fuel combustion concepts. For mono-fuel applications, strategies such as SI, HCCI, PCCI, PPC, SACI, and MCCI have been explored to capitalize on methanol's clean-burning characteristics. While these approaches can achieve high efficiency and low emissions, they also face challenges with knocking. Dual-fuel strategies address these limitations by introducing a high-reactivity fuel (HRF), typically diesel, to initiate combustion of the low-reactivity methanol. Configurations like PRDF, RCCI, DFDC, and DDFS enable flexible ignition control; however, combustion behavior remains highly sensitive to methanol-to-HRF ratios, with increased methanol substitution amplifying the risks of knocking. Across all strategies, the methanol injection method differs between PFI and DI, with DI operating at either high or low injection pressure, depending on the injection timing.

To address inconsistencies in terminology and strategy classification across the literature—particularly in the context of dual-fuel technology—this study proposed a systematic framework for injection and ignition strategies. This includes the replacement of ambiguous terms such as "fumigation" with clearer descriptors like air path injection (API), and the introduction of classification diagrams (Figure 2.2, Figure 2.3, and Figure 2.4) to outline methanol combustion modes in HD SI and CI engines. By organizing the diverse strategies into coherent categories, the presented framework aims to guide future research toward more consistent comparisons and targeted optimization of methanol-based engine technologies. To aid engine optimization, this thesis focuses on validating CFD methanol spray models for low pressure PFI, high pressure PFI, and DI, covering the presented injection strategies found in the respective combustion modes.

Bibliography

[1] Allen W. (Bill) Gray et al. “Homogeneous Charge Compression Ignition (HCCI) of Diesel Fuel”. In: May 1997, SAE Technical Paper 971676. DOI: 10.4271/971676.

[2] Päivi T. Aakko-Saksa et al. “Renewable Methanol with Ignition Improver Additive for Diesel Engines”. In: *Energy & Fuels* 34.1 (Jan. 2020), pp. 379–388. ISSN: 0887-0624, 1520-5029. DOI: 10.1021/acs.energyfuels.9b02654.

[3] Vilmar AEsoy et al. “LNG-Fuelled Engines and Fuel Systems for Medium-Speed Engines in Maritime Applications”. In: SAE Technical Paper 2011-01-1998. Aug. 2011. DOI: 10.4271/2011-01-1998.

[4] Zeeshan Ahmad et al. “A parametric investigation of diesel/methane dual-fuel combustion progression/stages in a heavy-duty optical engine”. In: *Applied Energy* 251 (Oct. 2019), p. 113191. ISSN: 0306-2619. DOI: 10.1016/j.apenergy.2019.04.187. URL: https://linkinghub.elsevier.com/retrieve/pii/S0306261919308505 (visited on 10/19/2023).

[5] Cagdas Aksu et al. “Effect of Hydrogen Concentration on Engine Performance, Exhaust Emissions and Operation Range of PREMIER Combustion in a Dual Fuel Gas Engine Using Methane-Hydrogen Mixtures”. In: SAE Technical Paper 2011-01-19982015–01–1792. Sept. 2015. DOI: 10.4271/2015-01-1792.

[6] Cagdas Aksu et al. “Extension of PREMIER combustion operation range using split micro pilot fuel injection in a dual fuel natural gas compression ignition engine: A performance-based and visual investigation”. In: *Fuel*. SAE Technical Paper 2016-07-120 185 (Dec. 2016). ISSN: 0016-2361. DOI: 10.1016/j.fuel.2016.07.120.

[7] M. Alperstein et al. “*FUMIGATION KILLS SMOKE* - - IMPROVES DIESEL PERFORMANCE”. In: SAE Technical Paper 580058. Jan. 1958. DOI: 10.4271/580058.

[8] U Azimov et al. “Premixed mixture ignition in the end-gas region (PREMIER) combustion in a natural gas dual-fuel engine: operating range and exhaust emissions”. In: *International Journal of Engine Research* 12.5 (Oct. 2011), pp. 484–497. ISSN: 1468-0874, 2041-3149. DOI: 10.1177/1468087411409664. (Visited on 09/27/2024).

[9] Ulugbek Azimov et al. “Combustion and Exhaust Emission Characteristics of Diesel Micro-Pilot Ignited Dual-Fuel Engine”. In: *Diesel Engine - Combustion, Emissions and Condition Monitoring*. Ed. by Saiful Bari. InTech, Apr. 2013. ISBN: 978-953-51-1120-7. DOI: 10.5772/54613. (Visited on 10/18/2023).

[10] Ulugbek Azimov et al. “Effect of syngas composition on combustion and exhaust emission characteristics in a pilot-ignited dual-fuel engine operated in PREMIER combustion mode”. In: *International Journal of Hydrogen Energy* 36.18 (Sept. 2011), pp. 11985–11996. ISSN: 0360-3199. DOI: 10.1016/j.ijhydene.2011.04.192. URL: https://linkinghub.elsevier.com/retrieve/pii/S0360319911010895 (visited on 09/27/2024).

[11] Rodica A. Baranescu. “Fumigation of Alcohols in a Multicylinder Diesel Engine-Evaluation of Potential”. In: SAE Technical Paper 860308. Mar. 1986. DOI: 10.4271/860308.

[12] Zhifang Chen et al. “The impact of methanol injecting position on cylinder-to-cylinder variation in a diesel methanol dual fuel engine”. In: *Fuel* 191 (Mar. 2017), pp. 150–163. ISSN: 0016-2361. DOI: 10.1016/j.fuel.2016.11.072.

[13] Minhoo Choi et al. “Effects of methane ratio on MPDF (micro-pilot dual-fuel) combustion characteristic in a heavy-duty single cylinder engine”. In: *Scientific Reports* 11.1 (May 2021), p. 9740. ISSN: 2045-2322. DOI: 10.1038/s41598-021-89161-z. URL: https://www.nature.com/articles/s41598-021-89161-z (visited on 10/18/2023).

[14] Rasmus F. Cordtz et al. “Combustion of Methanol Blended with a Fuel Additive in a CI Engine”. In: *MTZ worldwide* 82.11 (Nov. 2021), pp. 54–59. ISSN: 2192-9114. DOI: 10.1007/s38313-021-0703-6. (Visited on 09/25/2024).

[15] Jakob Coulier et al. “Using alcohol fuels in dual fuel operation of compression ignition engines: a review”. In: *28th CIMAC World Congress on Combustion Engine*. CIMAC, 2016. ISBN: 2194-8690.

[16] Khanh Cung et al. “Engine-out Gaseous Emissions in a Diesel Engine using Methanol as a Low-carbon Fuel under Dual-fuel Operation”. In: SAE Technical Paper 2024–01–2364. Apr. 2024. DOI: 10.4271/2024-01-2364.

[17] Khanh Cung et al. “Improved combustion efficiency in methanol/renewable diesel dual fuel combustion by advanced injection timing and increased intake temperature: Single-cylinder experiment”. In: SAE Technical Paper 2023-01-1641. Oct. 2023. DOI: 10.4271/2023-01-1641.

[18] Scott Curran et al. “The future of ship engines: Renewable fuels and enabling technologies for decarbonization”. In: *International Journal of Engine Research* (Aug. 2023), p. 14680874231187954. ISSN: 1468-0874, 2041-3149. DOI: 10.1177/14680874231187954. (Visited on 09/02/2023).

[19] A Das et al. “Development of a natural gas spark ignition engine for optimum performance”. In: *Proceedings of the Institution of Mechanical Engineers, Part D: Journal of Automobile Engineering* 211.5 (May 1997), pp. 361–378. ISSN: 0954-4070, 2041-2991. DOI: 10.1243/0954407971526506. (Visited on 11/03/2023).

[20] Adam B Dempsey et al. “Comparison of low temperature combustion strategies for advanced compression ignition engines with a focus on controllability”. en. In: *Combust. Sci. Technol.* 186.2 (Feb. 2014), pp. 210–241. DOI: 10.1080/00102202.2013.858137.

[21] Yabin Dong et al. “High-pressure direct injection of methanol and pilot diesel: A non-premixed dual-fuel engine concept”. In: *Fuel* 277 (Oct. 2020), p. 117932. ISSN: 0016-2361. DOI: 10.1016/j.fuel.2020.117932.

[22] E. Eugene Ecklund et al. “State-of-the-Art Report on the Use of Alcohols in Diesel Engines”. In: SAE Technical Paper 840118. Feb. 1984. DOI: 10.4271/840118.

[23] Pop-Paul Ewphun et al. “Investigation on premixed charge compression ignition combustion control using multi pulse ultrahigh pressure injection”. In: *SAE Technical Paper Series*. 2019-01-1155. SAE International, Apr. 2019. DOI: 10.4271/2019-01-1155.

[24] Brian Gainey et al. “Mixing controlled compression ignition with methanol: An experimental study of injection and EGR strategy”. In: *Int. J. Engine Res.* 24.5 (May 2023), pp. 1961–1972. DOI: 10.1177/14680874221105161.

[25] John Gandolfo et al. “An Experimental Comparison of Methanol Combustion Strategies: Spark Ignition Versus Compression Ignition”. In: *ASME ICE Forward Conference (ICEF2024)*. San Antonio, Texas, USA, 2024.

[26] Antonio García et al. “Parametric evaluation of neat methanol combustion in a light-duty compression ignition engine”. en. In: *Fuel Process. Technol.* 249.107850 (Oct. 2023), p. 107850. DOI: 10.1016/j.fuproc.2023.107850.

[27] Ayat Gharehghani. “Load limits of an HCCI engine fueled with natural gas, ethanol, and methanol”. In: *Fuel* 239 (Mar. 2019), pp. 1001–1014. ISSN: 0016-2361. DOI: 10.1016/j.fuel.2018.11.066. URL: https://linkinghub.elsevier.com/retrieve/pii/S001623611831963X (visited on 10/03/2022).

[28] W. L. Hardy et al. “A Study of the Effects of High EGR, High Equivalence Ratio, and Mixing Time on Emissions Levels in a Heavy-Duty Diesel Engine for PCCI Combustion”. In: SAE Technical Paper 2006-01-0026. Apr. 2006. DOI: 10.4271/2006-01-0026.

[29] Ryo Hasegawa et al. “HCCI Combustion in DI Diesel Engine”. In: SAE Technical Paper 2003-01-0745. Mar. 2003. DOI: 10.4271/2003-01-0745.

[30] J. Hélie et al. “Turbulent flame propagation in partially premixed combustion”. In: *Symposium (International) on Combustion* 27.1 (Jan. 1998), pp. 891–898. ISSN: 0082-0784. DOI: 10.1016/S0082-0784(98)80486-4. URL: https://linkinghub.elsevier.com/retrieve/pii/S0082078498804864 (visited on 09/25/2024).

[31] John B. Heywood. *Internal combustion engine fundamentals*. Second edition. McGraw-Hill Education, 2018. ISBN: 978-1-260-11610-6.

[32] K. R. Houser et al. “Methanol Fumigation of a Light Duty Automotive Diesel Engine”. In: SAE Technical Paper 801379. Oct. 1980. DOI: 10.4271/801379.

[33] Guan Huang et al. “Effects of fuel injection strategies on combustion and emissions of intelligent charge compression ignition (ICCI) mode fueled with methanol and biodiesel”. In: *Fuel* 274 (Aug. 2020), p. 117851. ISSN: 0016-2361. DOI: 10.1016/j.fuel.2020.117851.

[34] T. Humerfelt et al. “Development of The Rolls-Royce C26: 33 Marine Gas Engine Series”. In: *26th CIMAC World Congress*. 2010, paper. no. 54.

[35] Y. Iwamoto et al. “Development of Gasoline Direct Injection Engine”. In: SAE Technical Paper 970541. Feb. 1997. DOI: 10.4271/970541.

[36] Gernot Kammel et al. “Simulation based predesign and experimental validation of a prechamber ignited HPDI gas combustion concept”. In: *SAE Technical Paper Series*. 2019-01-0259. 400 Commonwealth Drive, Warrendale, PA, United States: SAE International, Apr. 2019. DOI: https://doi.org/10.4271/2019-01-0259.

[37] Tomohiro Kanda et al. “PCCI Operation with Early Injection of Conventional Diesel Fuel”. In: SAE Technical Paper 2005-01-0378. Apr. 2005. DOI: 10.4271/2005-01-0378.

[38] Ghazi A. Karim. “A review of combustion processes in the dual fuel engine—The gas diesel engine”. In: *Progress in Energy and Combustion Science* 6.3 (Jan. 1980), pp. 277–285. ISSN: 0360-1285. DOI: 10.1016/0360-1285(80)90019-2. (Visited on 10/19/2023).

[39] Ghazi A. Karim. *Dual-Fuel Diesel Engines*. CRC Press, Mar. 2015. ISBN: 978-0-429-06976-5. DOI: 10.1201/b18163. (Visited on 01/04/2023).

[40] K. I. Kiouranakis et al. “Methanol for heavy-duty internal combustion engines: Review of experimental studies and combustion strategies.” In: *Renewable and Sustainable Energy Reviews* (2025).

[41] K.I. Kiouranakis et al. “Methanol as a Fuel in Shipping: Review and Outlook to ICE Research within MENENS”. In: *TRA2024*. Springer, 2024.

[42] Sanghoon Kook et al. “Combustion Control Using Two-Stage Diesel Fuel Injection in a Single-Cylinder PCCI Engine”. In: SAE Technical Paper 2004-01-0938. Mar. 2004. DOI: 10.4271/2004-01-0938.

[43] M. Krishnamoorthi et al. “A review on low temperature combustion engines: Performance, combustion and emission characteristics”. In: *Renewable and Sustainable Energy Reviews* 116 (Dec. 2019), p. 109404. ISSN: 1364-0321. DOI: 10.1016/j.rser.2019.109404. URL: https://linkinghub.elsevier.com/retrieve/pii/S1364032119306124 (visited on 09/26/2024).

[44] T. Sathish Kumar et al. “Critical review on combustion phenomena of low carbon alcohols in SI engine with its challenges and future directions”. In: *Renewable and Sustainable Energy Reviews* 152 (Dec. 2021), p. 111702. ISSN: 1364-0321. DOI: 10.1016/j.rser.2021.111702. URL: https://linkinghub.elsevier.com/retrieve/pii/S136403212100976X (visited on 10/12/2022).

[45] Xianyin Leng et al. “A preliminary numerical study on the use of methanol as a Mono-Fuel for a large bore marine engine”. In: *Fuel* 310 (Feb. 2022), p. 122309. ISSN: 0016-2361. DOI: 10.1016/j.fuel.2021.122309. URL: https://linkinghub.elsevier.com/retrieve/pii/S0016236121021839 (visited on 11/28/2023).

[46] Jun Li et al. “Effect of injection and ignition timings on performance and emissions from a spark-ignition engine fueled with methanol”. In: *Fuel* 89.12 (Dec. 2010), pp. 3919–3925. ISSN: 0016-2361. DOI: 10.1016/j.fuel.2010.06.038. URL: https://linkinghub.elsevier.com/retrieve/pii/S0016236110003200 (visited on 09/16/2022).

[47] Xiaona Li et al. “Effect of air and gas dilution on combustion and emission characteristics in alcohol-gasoline fueled SACI engine”. In: *Energy Conversion and Management* 313 (Aug. 2024), p. 118631. ISSN: 0196-8904. DOI: 10.1016/j.enconman.2024.118631. URL: https://linkinghub.elsevier.com/retrieve/pii/S0196890424005727 (visited on 09/27/2024).

[48] Yaopeng Li et al. “Multiple-objective optimization of methanol/diesel dual-fuel engine at low loads: A comparison of reactivity controlled compression ignition (RCCI) and direct dual fuel stratification (DDFS) strategies”. In: *Fuel* 262 (Feb. 2020), p. 116673. ISSN: 0016-2361. DOI: 10.1016/j.fuel.2019.116673. URL: https://linkinghub.elsevier.com/retrieve/pii/S0016236119320277 (visited on 09/30/2022).

[49] Zhiyong Li et al. “Effect of injection strategy on a diesel/methanol dual-fuel direct-injection engine”. In: *Applied Thermal Engineering* 189 (May 2021), p. 116691. ISSN: 1359-4311. DOI: 10.1016/j.applthermaleng.2021.116691. URL: https://linkinghub.elsevier.com/retrieve/pii/S1359431121001460 (visited on 09/27/2024).

[50] Zhiyong Li et al. “To achieve high methanol substitution ratio and clean combustion on a diesel/methanol dual fuel engine: A comparison of diesel methanol compound combustion (DMCC) and direct dual fuel stratification (DDFS) strategies”. In: *Fuel* 304 (Nov. 2021), p. 121466. ISSN: 0016-2361. DOI: 10.1016/j.fuel.2021.121466.

[51] Wuqiang Long et al. “Effects of dual-direct injection parameters on performance of fuel Jet Controlled Compression Ignition mode on a high-speed light duty engine”. In: *Fuel* 235 (Jan. 2019), pp. 658–669. ISSN: 0016-2361. DOI: 10.1016/j.fuel.2018.08.043. URL: https://linkinghub.elsevier.com/retrieve/pii/S0016236118314133 (visited on 09/27/2024).

[52] Baodong Ma et al. “Multiple combustion modes existing in the engine operating in diesel methanol dual fuel”. In: *Energy* 234 (Nov. 2021), p. 121285. ISSN: 0360-5442. DOI: 10.1016/j.energy.2021.121285.

[53] Vittorio Manente et al. “Effects of Ethanol and Different Type of Gasoline Fuels on Partially Premixed Combustion from Low to High Load”. In: SAE Technical Paper 2010-01-0871. Apr. 2010. DOI: 10.4271/2010-01-0871.

[54] Manuel Alejandro Echeverri Marquez et al. “A Pathway to Ultra-Lean IC Engine Combustion: The Narrow Throat Pre-chamber”. In: *Engines and Fuels for Future Transport*. Ed. by Gautam Kalghatgi et al. Springer Singapore, 2022, pp. 175–203. ISBN: 9789811687167 9789811687174. DOI: 10.1007/978-981-16-8717-4_8. (Visited on 10/23/2023).

[55] Ian May et al. “Reduction of Methane Slip Using Premixed Micro Pilot Combustion in a Heavy-Duty Natural Gas-Diesel Engine”. In: SAE Technical Paper 2015–01–1798. Sept. 2015. DOI: 10.4271/2015-01-1798.

[56] A. McIlroy et al. *Basic Research Needs for Clean and Efficient Combustion of 21st Century Transportation Fuels*. Tech. rep. 935428. Nov. 2006. DOI: 10.2172/935428.

[57] Stanley P Miller. “DDC’s Production 6V-92TA Methanol Bus Engine”. In: SAE Technical Paper 911631. SAE International, Aug. 1991. DOI: 10.4271/911631.

[58] Paul M. Najt et al. “Compression-Ignited Homogeneous Charge Combustion”. In: SAE Technical Paper 830264. Feb. 1983. DOI: 10.4271/830264.

[59] Derek E. Nieman et al. “Methods of Improving Combustion Efficiency in a High-Efficiency, Lean Burn Dual-Fuel Heavy-Duty Engine”. In: SAE Technical Paper 2019–01–0032. Jan. 2019. DOI: 10.4271/2019-01-0032.

[60] Le Ning et al. “A comparative study on the combustion and emissions of a non-road common rail diesel engine fueled with primary alcohol fuels (methanol, ethanol, and n-butanol)/diesel dual fuel”. In: *Fuel* 266 (Apr. 2020), p. 117034. ISSN: 0016-2361. DOI: 10.1016/j.fuel.2020.117034.

[61] Keiichi Okude et al. “Premixed Compression Ignition (PCI) Combustion for Simultaneous Reduction of NOx and Soot in Diesel Engine”. In: SAE Technical Paper 2004-01-1907. June 2004. DOI: 10.4271/2004-01-1907.

[62] Shigeru Onishi et al. “Active Thermo-Atmosphere Combustion (ATAC) - A New Combustion Process for Internal Combustion Engines”. In: SAE Technical Paper 790501. Feb. 1979. DOI: 10.4271/790501.

[63] J. Pan et al. “A Theoretical and Experimental Study of the Modes of End Gas Autoignition Leading to Knock in S. I. Engines”. In: SAE Technical Paper 942060. Oct. 1994. DOI: 10.4271/942060.

[64] Hyunwook Park et al. “Comparative evaluation of conventional dual fuel, early pilot, and reactivity-controlled compression ignition modes in a natural gas-diesel dual-fuel engine”. In: *Energy* 268 (Apr. 2023), p. 126769. ISSN: 0360-5442. DOI: 10.1016/j.energy.2023.126769. URL: https://linkinghub.elsevier.com/retrieve/pii/S0360544223001639 (visited on 09/27/2024).

[65] H. Persson et al. “Investigation of the Early Flame Development in Spark Assisted HCCI Combustion Using High Speed Chemiluminescence Imaging”. In: SAE Technical Paper 2007–01–0212. Apr. 2007. DOI: 10.4271/2007-01-0212.

[66] Yi-Hao Pu et al. “Renewable Methanol as a Fuel for Heavy-Duty Engines: A Review of Technologies Enabling Single-Fuel Solutions”. In: *Energies* 17.7 (Apr. 2024), p. 1719. ISSN: 1996-1073. DOI: 10.3390/en17071719. URL: https://www.mdpi.com/1996-1073/17/7/1719 (visited on 09/25/2024).

[67] Mateusz Pucilowski et al. “Effect of start of injection on the combustion characteristics in a heavy-duty DICI engine running on methanol”. In: *SAE Technical Paper Series*. 2017-01-0560. SAE International, Mar. 2017. DOI: 10.4271/2017-01-0560.

[68] Rolf D. Reitz et al. “Review of high efficiency and clean reactivity controlled compression ignition (RCCI) combustion in internal combustion engines”. In: *Progress in Energy and Combustion Science* 46 (Feb. 2015), pp. 12–71. ISSN: 0360-1285. DOI: 10.1016/j.pecs.2014.05.003. URL: https://linkinghub.elsevier.com/retrieve/pii/S0360128514000288 (visited on 01/13/2023).

[69] B.G. Richards. “Methanol-Fueled Caterpillar 3406 Engine Experience in On-Highway Trucks”. In: SAE Technical Paper 902160. Oct. 1990. DOI: 10.4271/902160.

[70] Thomas W. Ryan et al. “Combustion and Emissions Characteristics of Minimally Processed Methanol in a Diesel Engine Without Ignition Assist”. In: Mar. 1994, p. 940326. DOI: 10.4271/940326.

[71] Michael Saccullo et al. “Dual Fuel Methanol and Diesel Direct Injection HD Single Cylinder Engine Tests”. In: Apr. 2018, pp. 2018–01–0259. DOI: 10.4271/2018-01-0259. URL: https://www.sae.org/content/2018-01-0259/ (visited on 09/30/2022).

[72] Richard Samson et al. “Effects of the Combustion Enhancer Containing Alkyl Nitrate (CEN) to Methanol in a Direct-Injection Compression Ignition (DICI) Engine”. In: SAE Technical Paper 2023-01-1619. Oct. 2023. DOI: 10.4271/2023-01-1619.

[73] Harsh Sapra et al. “Hydrogen-natural gas combustion in a marine lean-burn SI engine: A comparitive analysis of Seiliger and double Wiebe function-based zero–dimensional modelling”. In: *Energy Conversion and Management* 207 (Mar. 2020), p. 112494. ISSN: 0196-8904. DOI: 10.1016/j.enconman.2020.112494.

[74] Mohit Raj Saxena et al. “Assessment of performance, combustion and emissions characteristics of methanol-diesel dual-fuel compression ignition engine: A review”. In: *Journal of Traffic and Transportation Engineering (English Edition)* 8.5 (Oct. 2021), pp. 638–680. ISSN: 2095-7564. DOI: 10.1016/j.jtte.2021.02.003. URL: https://linkinghub.elsevier.com/retrieve/pii/S2095756421000866 (visited on 12/09/2023).

[75] Sam Shamun et al. “Experimental investigation of methanol compression ignition in a high compression ratio HD engine using a Box-Behnken design”. en. In: *Fuel* 209 (Dec. 2017), pp. 624–633. DOI: 10.1016/j.fuel.2017.08.039.

[76] S Singh et al. “Effect of pilot injection timing, pilot quantity and intake charge conditions on performance and emissions for an advanced low-pilot-ignited natural gas engine”. In: *International Journal of Engine Research* 5.4 (Aug. 2004), pp. 329–348. ISSN: 1468-0874, 2041-3149. DOI: 10.1243/146808704323224231. (Visited on 09/27/2024).

[77] Magnus Svensson et al. “The development and certification of a single fuel high speed marine CI engine on methanol”. In: *30th CIMAC World Congress*. 2023.

[78] R. H. Thring. “Homogeneous-Charge Compression-Ignition (HCCI) Engines”. In: SAE Technical Paper 892068. Sept. 1989. DOI: 10.4271/892068.

[79] Shrey Trivedi et al. “Turbulence Intensity and Length Scale Effects on Premixed Turbulent Flame Propagation”. In: *Flow, Turbulence and Combustion* 109.1 (June 2022), pp. 101–123. ISSN: 1386-6184, 1573-1987. DOI: 10.1007/s10494-021-00315-5. (Visited on 10/23/2023).

[80] Alireza Valipour Berenjestanaki et al. “Performance, emissions and end-gas autoignition characteristics of PREMIER combustion in a pilot fuel-ignited dual-fuel biogas engine with various CO2 ratios”. In: *Fuel* 286 (Feb. 2021), p. 119330. ISSN: 0016-2361. DOI: 10.1016/j.fuel.2020.119330. URL: https://linkinghub.elsevier.com/retrieve/pii/S0016236120323267 (visited on 09/27/2024).

[81] J. Vancoillie et al. “The potential of methanol as a fuel for flex-fuel and dedicated spark-ignition engines”. In: *Applied Energy* 102 (Feb. 2013), pp. 140–149. ISSN: 0306-2619. DOI: 10.1016/j.apenergy.2012.05.065. URL: https://linkinghub.elsevier.com/retrieve/pii/S0306261912004692 (visited on 09/16/2022).

[82] Hui Wang et al. “Investigation to meet China II emission legislation for marine diesel engine with diesel methanol compound combustion technology”. In: *Journal of Environmental Sciences* 96 (Oct. 2020), pp. 99–108. ISSN: 1001-0742. DOI: 10.1016/j.jes.2020.04.017.

[83] Jian Wang et al. “Experimental investigation on combustion and emission characteristics of diesel methanol dual fuel (DMDF) engine at various altitudes”. In: *Energy & Environment* 35.1 (Feb. 2024), pp. 331–352. ISSN: 0958-305X, 2048-4070. DOI: 10.1177/0958305X221130140. (Visited on 09/27/2024).

[84] Peng Wang et al. “Combustion characteristics of methanol engine applying TJI-HPDI with optimized pre-chamber nozzle structure under different injection and spark strategy”. en. In: *Energy (Oxf.)* 312.133503 (Dec. 2024), p. 133503. DOI: https://doi.org/10.1016/j.energy.2024.133503.

[85] Yang Wang et al. “Study on the performance of diesel-methanol diffusion combustion with dual-direct injection system on a high-speed light-duty engine”. In: *Fuel* 317 (June 2022), p. 123414. ISSN: 0016-2361. DOI: 10.1016/j.fuel.2022.123414.

[86] Zhi Wang et al. “Knocking combustion in spark-ignition engines”. In: *Progress in Energy and Combustion Science* 61 (2017), pp. 78–112.

[87] Fuxing Wei et al. “Visualization investigation of jet ignition ammonia-methanol by an ignition chamber fueled H2”. In: *Fuel* 349 (Oct. 2023), p. 128658. ISSN: 0016-2361. DOI: 10.1016/j.fuel.2023.128658. URL: https://linkinghub.elsevier.com/retrieve/pii/S0016236123012711 (visited on 09/27/2024).

[88] Martin Wissink et al. “Direct Dual Fuel Stratification, a Path to Combine the Benefits of RCCI and PPC”. In: *SAE International Journal of Engines* 8.2 (Apr. 2015), pp. 878–889. ISSN: 1946-3944. DOI: 10.4271/2015-01-0856.

[89] Martin Wissink et al. “Exploring the Role of Reactivity Gradients in Direct Dual Fuel Stratification”. In: *SAE International Journal of Engines* 9.2 (Apr. 2016), pp. 1036–1048. ISSN: 1946-3944. DOI: 10.4271/2016-01-0774. URL: https://www.sae.org/content/2016-01-0774/ (visited on 09/27/2024).

[90] Changchun Xu et al. “Effect on the performance and emissions of methanol/diesel dual-fuel engine with different methanol injection positions”. In: *Fuel* 307 (Jan. 2022), p. 121868. ISSN: 0016-2361. DOI: 10.1016/j.fuel.2021.121868.

[91] Shuonan Xu et al. “A phenomenological combustion analysis of a dual-fuel natural-gas diesel engine”. In: *Proceedings of the Institution of Mechanical Engineers, Part D: Journal of Automobile Engineering* 231.1 (Jan. 2017), pp. 66–83. ISSN: 0954-4070, 2041-2991. DOI: 10.1177/0954407016633337. (Visited on 01/24/2023).

[92] Yong Yang et al. “Performance of large-bore methanol/diesel dual direct injection engine applying asymmetrical diesel nozzle strategies”. en. In: *Appl. Therm. Eng.* 244.122674 (May 2024), p. 122674. DOI: https://doi.org/10.1016/j.applthermaleng.2024.122674.

[93] Chunde Yao et al. “Effect of Diesel/methanol compound combustion on Diesel engine combustion and emissions”. In: *Energy Conversion and Management* 49.6 (June 2008), pp. 1696–1704. ISSN: 0196-8904. DOI: 10.1016/j.enconman.2007.11.007. URL: https://linkinghub.elsevier.com/retrieve/pii/S0196890407004104 (visited on 09/27/2024).

[94] Xiaojun Yin et al. “A comparative study on operating range and combustion characteristics of methanol/diesel dual direct injection engine with different methanol injection timings”. In: *Fuel* 334 (Feb. 2023), p. 126646. ISSN: 0016-2361. DOI: 10.1016/j.fuel.2022.126646.

[95] Fan Zhang et al. “Investigation into Light Duty Dieseline Fuelled Partially-Premixed Compression Ignition Engine”. In: *SAE International Journal of Engines* 4.1 (Apr. 2011), pp. 2124–2134. ISSN: 1946-3944. DOI: 10.4271/2011-01-1411. URL: https://www.sae.org/content/2011-01-1411/ (visited on 09/26/2024).

[96] Qiang Zhang et al. “Experimental and Numerical Study of Jet Controlled Compression Ignition on Combustion Phasing Control in Diesel Premixed Compression Ignition Systems”. In: *Energies* 7.7 (July 2014), pp. 4519–4531. ISSN: 1996-1073. DOI: 10.3390/en7074519. URL: https://www.mdpi.com/1996-1073/7/7/4519 (visited on 09/27/2024).

[97] Yu Zhang et al. “Mixing-controlled combustion of conventional and higher reactivity gasolines in a multi-cylinder heavy-duty compression ignition engine”. In: *SAE Technical Paper Series*. 2017-01-0696. SAE International, Mar. 2017. DOI: 10.4271/2017-01-0696.

[98] Z.H. Zhang et al. “Experimental investigation on regulated and unregulated emissions of a diesel/methanol compound combustion engine with and without diesel oxidation catalyst”. In: *Science of The Total Environment* 408.4 (Jan. 2010), pp. 865–872. ISSN: 0048-9697. DOI: 10.1016/j.scitotenv.2009.10.060.

[99] Yifan Zhao et al. “Combustion Mode Evaluation of a Methanol–Diesel Dual Direct Injection Engine with a Control of Injection Timing and Energy Substitution Ratio”. In: *SAE International Journal of Engines* 18.1 (Aug. 2024), pp. 03–18–01–0002. ISSN: 1946-3936, 1946-3944. DOI: 10.4271/03-18-01-0002. URL: https://www.sae.org/content/03-18-01-0002 (visited on 09/27/2024).

[100] Lijia Zhong et al. “Experimental observation of the combustion characteristics of methanol/air by turbulent jet ignition”. In: *30th CIMAC World Congress*. June 2023.

[101] Burak Zincir et al. “Investigation of Effects of Intake Temperature on Low Load Limitations of Methanol Partially Premixed Combustion”. In: *Energy & Fuels* 33.6 (June 2019), pp. 5695–5709. ISSN: 0887-0624, 1520-5029. DOI: 10.1021/acs.energyfuels.9b00660.

Chapter 3

Spray Modelling of Methanol Port Fuel Injection Systems

The maritime sector aims to achieve short and medium-term sustainability targets through the conversion of Internal Combustion Engines to methanol operation. For small to medium sized engines, Port Fuel Injection (PFI) is the most viable injection method to achieve this conversion. However, the knowledge of methanol's behaviour in combustion engines, particularly its spray characteristics under PFI conditions, is limited. To better understand liquid methanol sprays, this chapter examines the injection of methanol in marine PFI conditions using Computational Fluid Dynamics (CFD) modeling. The CFD models employ the Lagrangian-Eulerian (LE) coupling method within the Reynolds Averaged Navier Stokes (RANS) turbulence framework. Numerical results have been validated using dedicated methanol experiments from the literature for both high and low injection pressures. Subsequently, this predictive CFD framework was applied to various injection pressures and scaled injection quantities, representing marine applications. Moreover, we demonstrate that high injection pressure improves atomization and, thus, evaporation prior to wall impingement. This work significantly contributes to our understanding of marine PFI methanol engines by modelling fuel quantities relevant to ship applications. The presented approach can be implemented in full engine simulations to address evaporation challenges commonly encountered in small-bore methanol marine engines.

This chapter was reproduced from [66]:
Zoumpourlos, K., Bekdemir, C., Geertsma, R., van de Ketterij, R., & Coraddu, A. (2025). Methanol sprays in marine engines: CFD modelling of port fuel injection systems. Journal of Marine Engineering & Technology, 1–17. DOI: https://doi.org/10.1080/20464177.2025.2473184

3.1 Introduction

FOR methanol operation, installing port fuel injection (PFI) systems is the most viable conversion method for current four-stroke medium- and high-speed maritime engines [57, 13], as space and cost issues limit the adoption of direct injection (DI) systems. However, integrating methanol in marine ICEs involves a high degree of complexity. This complexity is caused by its high latent heat of evaporation, which hinders the mixture formation [57]. The spray characteristics and mixture formation process of methanol are insufficiently studied. For these reasons, evaluating the physical phenomena in PFI methanol sprays is essential.

Previous experimental research on methanol sprays has mainly focused on atmospheric ambient temperature conditions and relatively low to medium injection pressures [58, 20, 63, 64, 30, 60]. These studies reported similarities between the spray structure of methanol and conventional fuels, indicating only minor differences in the cone angle and spray penetration length. In a study by Zeng et al. [62], flash boiling methanol sprays were evaluated at 50 bar injection pressure. The authors stated that the flash boiling phenomenon could improve the start-ability of the engines under cold-start conditions due to enhanced atomization. In another study by Badawy et al. [5], lowering the ambient pressure in the flashing regime decreased the droplet sizes, thereby improving mixture formation.

More recently, several studies [35, 18, 59] have addressed DI engine conditions under high injection pressures and high ambient temperatures and pressures. In particular, Wang et al. [59] conducted experiments under compression ignition (CI) conditions and compared methanol with diesel sprays. They reported that at moderate ambient temperatures (600 K), methanol shows improved evaporation due to its lower boiling point. Generally, the reported experiments highlighted many similarities in the macroscopic spray structure between methanol and conventional fuels. However, these studies do not quantify the evaporation cooling effect of methanol and its implications for air-fuel mixture formation. Therefore, to sufficiently understand methanol sprays, predictive computational fluid dynamics (CFD) models are essential for appropriately characterizing spray structure and behaviour under engine conditions. However, the limitations of the current experimental studies make CFD model validation difficult.

To validate the CFD model, the Engine Combustion Network (ECN), an international collaboration among several institutions, was established, providing an online database of experimental data for conventional fuels [15, 33]. Although quite extensive, this database does not cover methanol sprays, particularly for PFI conditions. Very limited research has been published regarding CFD studies, as experimental data is scarce. Only one study has investigated methanol sprays numerically [37]. In that study, Moreno Cabezas et al. [37] developed a validated gasoline CFD model, which incorporated data from the ECN Spray G [17]. The validated spray model was applied to a number of methanol spray conditions representing a spark ignition (SI) DI engine. The authors reported that methanol flash-boiling conditions exhibit an increased evaporation rate, which agrees with previous experimental efforts [62, 5]. This demonstrates that CFD simulations can accurately represent the underlying spray physics during flash boiling. While the work by Moreno Cabezas et al. [37] improved our understanding of DI methanol engines, a similar

CFD approach for PFI methanol engines does not exist, indicating a gap in knowledge.

3.1.1 Aim & Novelty

This chapter aims to investigate the injection of methanol under marine PFI conditions (i.e., low ambient pressure and temperature, and low injection pressure). The novelty of the present work lies in a spray modelling approach, which is validated using experimental data for methanol at both high and low injection pressures. This approach can be implemented in the modelling of methanol engine conversion to achieve robust operation under PFI conditions. For the spray analysis, we employed CFD simulations with Lagrangian-Eulerian (LE) coupling methods to treat liquid droplets and the air-fuel gaseous mixture. To validate our models, we benchmarked two methanol injection experiments, reminiscent of PFI conditions, which comprised a relatively low ambient pressure. These included a high pressure (HP) injection experiment by Ghosh et al. [19], and a low pressure (LP) injection experiment by Liu et al. [30].

To achieve an acceptable prediction of liquid penetration, we assessed the choice of various spray parameters (i.e., rate of injection, cone angle, and turbulence model). The assessment demonstrated the influence of these parameters on spray characteristics, such as the liquid length. Moreover, we increased the injection quantity of the validated model to examine the resulting methanol spray characteristics in marine engines. This study offers insights into the impact of injection pressure on droplet breakup, evaporation, and the magnitude of droplet velocity. The results indicated that increased injection pressure significantly improves spray atomization due to enhanced air entrainment.

Coupling the presented modelling framework with 3D engine models can provide a solid modelling methodology to support methanol engine conversion. Our study addresses previously reported limitations in increasing the methanol energy fraction and mitigating combustion instability in small-bore marine and heavy-duty automotive engines by using PFI of methanol. These findings can potentially contribute to methanol implementation in the maritime sector by guiding the CFD modelling of future methanol ICEs.

3.2 Background

3.2.1 Methanol in Marine Engines

METHANOL offers desirable physical and chemical properties, which render it suitable for marine engines [11]. Depending on the engine size, methanol is injected either in the port, through a PFI system, or through a DI system in the cylinder. Based on the piston size, Curran et al. [11] classified marine engines as small-bore (up to 280 mm), medium-bore (280-500 mm), and large-bore (500-960 mm). Large-bore marine engines typically employ a DI system for methanol injection through a second injector [34] or a co-axial dual fuel injector [46]. On the other hand, small-bore marine engines, due to space and cost limitations, use a PFI system for methanol premixing and a DI system for diesel pilot ignition [12, 13, 3]. However, PFI systems are notable for their poor mixture formation because of the low injection pressure, and low ambient pressure and

temperature environment in the intake manifold [65, 67]. Therefore, retrofitting these engines poses a challenge to both engine manufacturers and ship owners, and delays the implementation of methanol in the maritime sector.

For efficient methanol conversion, CFD modelling offers insight into the mixture formation and can potentially identify the best routes to overcome the aforementioned challenges. To model PFI conditions, we distinguish three categories of CFD simulations: spray modelling, wall wetting, and flow dynamics in the intake manifold, as shown in Fig. 3.1. Spray modelling focuses on the spray formation and its spatial characteristics, such as liquid penetration length, Sauter mean diameter (SMD), cone angle, and jet velocity (Fig. 3.2). Next, wall wetting is the outcome of the spray interacting with the engine's internal parts. The impinging spray may form a liquid wall film, which hinders the mixture formation and prevents the engine from operating normally. Especially in methanol engines, due to increased latent heat of evaporation, the wall film evaporation is significantly slower than in gasoline engines. Therefore, these wall deposits have a significant impact on engine stability, causing cyclic variations and limiting the increase in methanol energy fractions in converted methanol-diesel dual-fuel engines. Finally, the liquid droplets interact with the flow field of the intake manifold. This flow field is distinctive for each engine due to its design and geometrical features, and determines the degree of mixing.

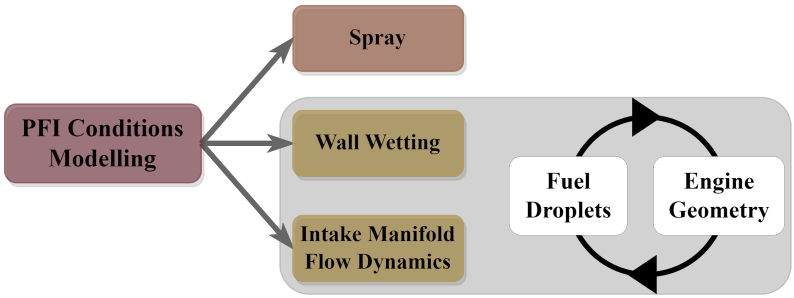

Figure 3.1: Schematic overview of modelling aspects for CFD modelling of PFI engines, demonstrating the decoupling of spray modelling, proposed in this work, from wall wetting effects and intake manifold flow dynamics, subject to future research.

In an attempt to decouple the aforementioned modelling aspects, our study focuses on the spray modelling of PFI conditions. This chapter provides a spray modelling framework that could be adapted to any specific 3D engine model (Fig. 3.2). We validated the model specifically for methanol to operate robustly in a range of injection pressures in PFI ambient conditions. Coupling the framework with wall wetting models can serve as a valuable tool for studying mixture formation and identifying the optimal retrofitting solution. CFD can provide a toolbox to study different injection pressures, injection locations, and timings a priori. Ultimately, these results reveal trends in atomization, evaporation, and jet velocity, which can provide valuable insights into the necessary development direction for methanol PFI engine technology.

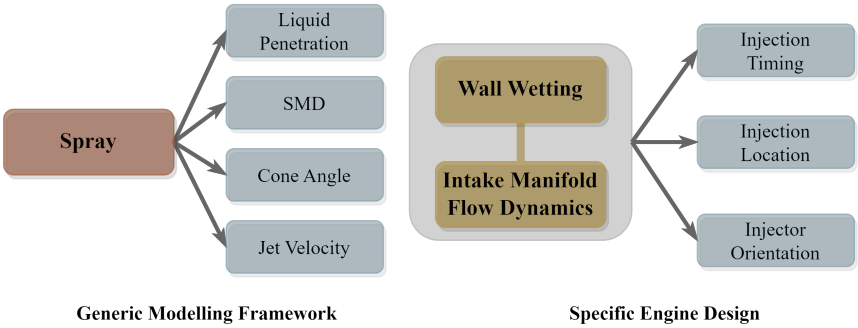

Figure 3.2: Pillars of PFI conditions modelling

3.2.2 Experimental Background

We selected two methanol spray experiments from the literature to validate our numerical models, which investigated the characteristics of methanol sprays in CVC environments. These configurations were capable of offering controlled ambient conditions while allowing optical access for spray penetration and cone angle measurements. The experiments included a low injection pressure study [30], and a high injection pressure study [19], denoted as LP case and HP case, respectively. For our study, we utilised liquid penetration data of these sprays under low-ambient temperature and low-ambient pressure conditions. These conditions match the intake manifold environment and are closely linked to the operating points of small-bore marine engines. The utilised experiments aimed to accommodate both low and high injection pressures in the engine intake manifold. The details of the experimental conditions for each case are presented in Table 3.1.

Table 3.1: Experimental Conditions

Item	LP Case Liu et al. [30]	HP Case Ghosh et al. [19]
Ambient Pressure [bar]	2	3
Injection Duration [ms]	10	2.5
Injection Pressure [bar]	6	200
Injection Quantity [mg]	4.67 (estimation)	14.23 (estimation)
Ambient Temperature [°C]	25	103
Fuel Temperature [°C]	25	90 (estimation)
Nozzle Diameter [mm]	0.15 (estimation)	0.23

In the LP case, Liu et al. [30] used backlight imaging and high-speed photography to capture the spray morphology of methanol in intake manifold conditions. The study employed a 14-hole injector and investigated the influence of ambient temperature and pressure, as well as fuel temperature, on spray penetration. The authors concluded that higher ambient and fuel temperatures induce flash boiling, which results in faster evaporation times and larger liquid penetration and cone angles.

On the other hand, in the HP case, Ghosh et al. [19] employed a Mie-scattering technique via high-speed imaging to measure liquid penetration of methanol under a range of ambient pressures ranging from 3 to 40 bar. For our study, we used the 3 bar condition to validate our results. The elevated injection pressure was achieved through a common rail DI-style injector, utilising a relatively large nozzle diameter (0.23 mm) with an L/D ratio of 4.9, which is suitable for heavy-duty applications.

Both methanol experiments used light-duty and medium-duty automotive methanol quantities, which are orders of magnitude lower than those used in marine injection. In this thesis, we employed spray models that rely on non-dimensional fluid mechanics principles (Section 3.3). When scaled up, these models can produce physically rational conclusions. This is justified by previous research on diesel sprays, which reported that automotive-engine spray models can adequately predict the liquid penetration for marine engines [27]. Therefore, the CFD models can be validated through lower quantities and then scaled up for increased maritime quantities.

3.3 Computational Methodology

IN the present chapter, we used the commercial CONVERGE v3.0 CFD software [52, 54], which contains a numerical framework for multiphase flow simulations. The framework applies the finite volume method to solve the Navier-Stokes equations, accounting for the conservation of mass, momentum, and energy [10]. The conservation of mass, momentum, and energy is formulated according to Equations 3.1, 3.2, and 3.4 respectively:

$$\frac{\partial \rho}{\partial t} + \frac{\partial (\rho u_i)}{\partial x_i} = S, \tag{3.1}$$

$$\frac{\partial (\rho u_i)}{\partial t} + \frac{\partial}{\partial x_j}[\rho u_i u_j + P\delta_{ij} - \sigma_{ij}] = S_i, \tag{3.2}$$

where σ is the viscous stress tensor:

$$\sigma_{ij} = \mu(\frac{\partial u_i}{\partial x_j} + \frac{\partial u_j}{\partial x_i}) + (\mu_v - \frac{2}{3}\mu)\frac{\partial u_k}{\partial x_k}\delta_{ij}, \tag{3.3}$$

$$\frac{\partial (\rho e_0)}{\partial t} + \frac{\partial}{\partial x_j}(\rho u_j e_0 + u_j P - K\frac{\partial T}{\partial x_j} - u_i \sigma_{ij} - \rho \sum_m D_m h_m \frac{\partial Y_m}{\partial x_j}) = S, \tag{3.4}$$

where the total specific energy is $e_0 \equiv e + \frac{u_k u_k}{2}$, ρ is the fluid density, S is the source term (accounting for evaporation and chemical reactions), u is the velocity in each axis, P is the pressure, μ is the viscosity, μ_v is the dilatational viscosity (set to zero), δ_{ij} is the Kronecker delta, T is the temperature, K is the thermal conductivity, m are the species, Y_m is the mass fraction of species, D_m is the species mass diffusion coefficient, and h_m is the species specific enthalpy. These conservation equations are applicable for the remainder of the work in the present thesis.

To model turbulence, the RANS approach was used employing the RNG and Standard $k-\varepsilon$ models [21]. These $k-\varepsilon$ models are based on the Reynolds-Averaged Navier-Stokes

(RANS) equations, which approximate the velocity field as a summation of a mean and a fluctuating velocity ($u = \bar{u} + u'$). The result of this assumption generates a turbulence-induced Reynolds-stress tensor in the Navier-Stokes equations. Resolving the stress tensor leads to modelling two additional transport equations accounting for the turbulent kinetic energy (k), and the rate of dissipation of turbulent kinetic energy (ε) [26, 45]. The 'mean' flow quantities correspond to the Reynolds ensemble average, consistent with standard statistically self-similar RANS turbulence modelling practice. The equations are solved for the mean quantities, while the fluctuating part, which generates the Reynolds stresses, is treated using the presented turbulence model. The transport equations for k and ε are as follows [10]:

$$\frac{\partial(\rho k)}{\partial t} + \frac{\partial(\rho u_i k)}{\partial x_i} = \tau_{ij}\frac{\partial u_i}{\partial x_j} + \frac{\partial}{\partial x_j}\frac{\mu + \mu_t}{Pr_k}\frac{\partial k}{\partial x_j} - \rho\varepsilon \tag{3.5}$$

and

$$\frac{\partial(\rho\varepsilon)}{\partial t} + \frac{\partial(\rho u_i \varepsilon)}{\partial x_i} = \frac{\partial}{\partial x_j}\left(\frac{\mu + \mu_t}{Pr_\varepsilon}\frac{\partial \varepsilon}{\partial x_j}\right) + C_{\varepsilon 3}\rho\varepsilon\frac{\partial u_i}{\partial x_i} + (C_{\varepsilon 1}\frac{\partial u_i}{\partial x_j}\tau_{ij} - C_{\varepsilon 2}\rho\varepsilon)\frac{\varepsilon}{k} - \rho R_\varepsilon, \tag{3.6}$$

where ρ is the fluid density, u is the velocity in each axis, τ_{ij} is the modelled Reynolds stress, μ is the viscosity, μ_t is the turbulent viscosity, Pr is the Prandtl number, $C_{\varepsilon 1}, C_{\varepsilon 2}$, and $C_{\varepsilon 3}$ are turbulence model parameters. Additionally, the k and μ_t terms are defined by the following expressions:

$$k = \frac{1}{2}\overline{u_i' u_i'}, \tag{3.7}$$

$$\mu_t = C_\mu \rho \frac{k^2}{\varepsilon} \tag{3.8}$$

and

$$R_\varepsilon = \frac{C_\mu \eta^3 (1 - \eta/\eta_0)}{1 + \beta\eta^3}\frac{\varepsilon^2}{k}, \tag{3.9}$$

where C_μ, η, η_0 and β are turbulence model parameters. For the Standard $k-\varepsilon$ model the last term $R_\varepsilon = 0$.

To solve the conservation equations, we used the density-based solver [10] along with the Pressure Implicit with Splitting of Operators (PISO) algorithm [25]. Moreover, the numerical scheme is first-order in time and second-order in space. For the determination of the time-step, we applied a control algorithm based on the Courant-Friedrichs-Lewy (CFL) criterion [10, 16, 26]. The thermodynamic properties of both air and methanol were modelled based on the Redlich-Kwong equation of state [22]. Lastly, the simulations were run in parallel on the DelftBlue supercomputer [1].

3.3.1 Computational Domain & Grid

A cylindrical geometry was adopted as the control volume for the numerical computations (Fig. 3.3), with a radius of 60 mm and a height of 180 mm. The dimensions of the geometry were chosen according to spray CFD literature [27, 32]. For the boundary conditions,

the cylinder walls were set as wall-type Neumann for both temperature and turbulent kinetic energy. For the meshing, CONVERGE generates the grid while the simulation is running through a modified cut-cell Cartesian technique [53]. The base cell size of the mesh is 4 mm with additional user-defined and automatic refinements in areas of interest. Specifically, we refined the spray cone region to better resolve the flow field and the interactions between the droplets and the ambient air (Fig. 3.3). This static mesh, however, is computationally expensive to implement in full engine simulations. An Adaptive Mesh Refinement (AMR) algorithm was employed to maintain a low cell count, based on velocity and species gradients. Near the nozzle exit, a small refinement cone was also enabled for the sufficient resolution of the flow, while AMR refined the transient tip of the spray.

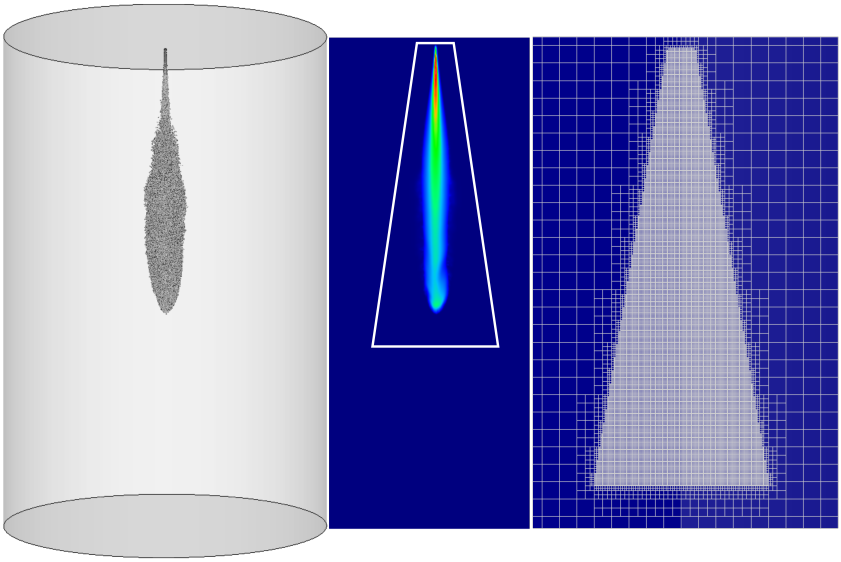

Figure 3.3: Simulation control volume: injected parcels, methanol mass fraction, and static cone mesh grid

3.3.2 Spray Model

To model the multiphase flow, we used the Lagrangian-Eulerian (LE) framework [6]. The coupling uses a Lagrangian Particle Tracking (LPT) technique, which treats the liquid droplets as Lagrangian particles [56]. The particles are tracked based on their position and motion in the computational domain. On the contrary, the gaseous phase is represented in an Eulerian way, which models the flow based on a mesh grid. In addition, a set of phenomenological spray models was used to resolve the physical phenomena that occur in the sub-grid length scales [6].

The computational parcels were injected using the Reitz et al. [49] model. The model assumes the initial discrete spherical droplets ('blobs') to be the same size as the nozzle diameter. These parcels interact with the surrounding air and break up due to instability

mechanisms. The breakup mechanism of each droplet is closely associated with the Weber (We) number, which is the ratio of the aerodynamic drag force imposed from the ambient air onto the droplet and the droplet surface tension force [39]:

$$\mathrm{We} = \frac{\rho_g u_r^2 d}{\sigma}, \tag{3.10}$$

where ρ_g is the ambient air density, u_r is the relative velocity between the droplet and the gas, d is the droplet diameter, and σ is the droplet surface tension. The droplet velocity is closely associated with the injection velocity, which is in turn closely coupled to the injection pressure. Thus, the different injection pressures used in this chapter necessitate distinct breakup models due to the altered breakup regimes. We used two separate droplet breakup models:

1. Kelvin Helmholtz - Rayleigh Taylor (KH-RT) model, suitable for HP injection conditions [7, 48].

2. Taylor Analogy Breakup (TAB) model, suitable for low We number conditions [39].

The KH-RT model is based on two separate mechanisms that occur during the primary and secondary phases of droplet breakup. Kelvin-Helmholtz hydrodynamic instabilities dominate the primary breakup phase, attributed to the unstable shear waves of the droplet-air interface [7, 49]. Likewise, the secondary breakup is caused by the aerodynamic drag force between the droplets and the air on the tip of the spray, attributed to Rayleigh-Taylor instabilities [7, 49]. In the KH model, the resulting child droplet $\mathrm{r_c}$ is proportional to the wavelength Λ_{KH} of the fastest growing unstable KH surface wave [7]:

$$\mathrm{r_c} = \mathrm{B_0}\Lambda_{\mathrm{KH}}, \tag{3.11}$$

where $\mathrm{B_0}$ is the KH model size constant. The rate of change of the parent parcel radius $\mathrm{r_p}$ is calculated with the following expression:

$$\frac{dr_p}{dt} = -\frac{(r_p - r_c)}{\tau_{KH}}, \tag{3.12}$$

where the breakup time τ_{KH} is given by:

$$\tau_{KH} = \frac{3.726 B_1 r_p}{\Lambda_{KH}\Omega_{KH}}, \tag{3.13}$$

where $\mathrm{B_1}$ is the breakup time constant, and Ω_{KH} is the growth rate of KH waves.

In the RT model, the breakup occurs due to unstable waves that are normal to the spray tip and originate from the deceleration of the droplets. Hence, the RT instabilities demonstrate growing wavelengths, which are dictated by the fastest wavelengths, similar to the KH instability [7]:

$$\Lambda_{RT} = 2\pi\sqrt{\frac{3\sigma}{\alpha(\rho_l - \rho_g)}}, \tag{3.14}$$

where α is the deceleration of the drop, and ρ_g and ρ_l are the gas and liquid densities respectively. Similar to the KH model size constant in Eq. (4.2), the RT model size constant C_{RT} dictates the wave sizes of the instability. If the length scale of the waves ($C_{RT}\Lambda_{RT}$) is larger than the parent drop diameter, breakup occurs. The growth rate of the waves (Ω_{RT}) influences the breakup time, and is defined by:

$$\Omega_{RT} = \sqrt{\frac{2}{3\sqrt{3\sigma}} \frac{[\alpha(\rho_l - \rho_g)^{\frac{3}{2}}]}{\rho_l + \rho_g}}. \tag{3.15}$$

When the RT waves have grown for a sufficient time τ_{RT}, breakup will occur accordingly:

$$\tau_{RT} = \frac{C_\tau}{\Omega_{RT}}, \tag{3.16}$$

where C_τ is the RT breakup time constant, and Ω_{RT} is the growth rate of the waves.

In the case of LP injection, we used the TAB model, which assumes that droplet distortion and breakup are proportional to a spring-mass-damper system [39]. The TAB model, however, is capable of tracking only one droplet breakup mode, for We < 12, which corresponds to the oscillation of droplets [23]. This means that TAB breakup will occur only under LP injection [67].

Marine engines require significantly larger nozzle diameters compared to automotive-style injectors to provide the demanded fuel quantities. Thus, the near-nozzle Weber number of the droplets may be high enough to create KH instabilities instead of oscillating breakup modes. The nozzle-out theoretical Bernoulli velocity (u_{th}) of the jet is defined by the following expression [42]:

$$u_{th} = \sqrt{\frac{2(P_{inj} - P_{amb}))}{\rho_f}}, \tag{3.17}$$

where P_{inj} is the injection pressure, P_{amb} is the ambient pressure, and ρ_f is the fuel density. Based on the critical Weber number (We = 12) and the nozzle-out Bernoulli velocity, the critical injection pressure P_{inj}^{cr} for a given nozzle diameter d is calculated as follows:

$$P_{inj}^{cr} = \frac{6\sigma}{d} \frac{\rho_f}{\rho_g} + P_{amb}, \tag{3.18}$$

where ρ_g is the ambient air density, and σ is the droplet surface tension. Depending on the nozzle diameter, the calculated critical injection pressure determines the most appropriate breakup model for the simulation. Hence, a lower injection pressure than the critical necessitates the use of the TAB model, whereas the KH-RT model must be used for higher injection pressures.

The spray droplets interact with each other through collisions and coalescence. The No Time Counter (NTC) algorithm [51] estimates the collisions between droplets, while the model of Post et al. [47] predicts the post-collision outcome, including bouncing, stretching, reflective separation, and coalescence. Furthermore, the droplets interact with the surrounding gas through aerodynamic drag forces and turbulent flow phenomena.

The droplet aerodynamic drag force was modelled using a dynamic drag model, where the drag coefficient changes in relation to flow conditions [29]. In the same model, the distortion of the droplet was also calculated using the TAB model calculations to secure a robust estimation of the drag coefficient.

A turbulent dispersion model was used to couple the turbulent flow of the gas with the Lagrangian parcels [38, 4]. We applied a Frossling correlation to predict evaporation phenomena, which assumes uniform temperature distribution within each droplet [10, 36]. The correlation links the Reynolds (Re) and Schmidt (Sc) numbers with the Sherwood (Sh) number of each droplet. The Sherwood number quantifies the mass transfer rate from the droplet to the ambient environment, playing a fundamental role in the evaporation process. The droplet radius rate of change is calculated as follows:

$$\frac{\mathrm{d}r_0}{\mathrm{d}t} = -\frac{\alpha_{spray}\rho_g D}{2\rho_l r_0} B_d Sh_d, \tag{3.19}$$

where r_0 is the initial drop radius, α_{spray} is a user-specified scaling mass transfer coefficient, D is the vapour mass diffusivity, ρ_g and ρ_l are the gas and liquid densities, respectively, and B_d is the fraction of vapour's mass fraction at the drop surface to the vapour mass fraction of the droplet. The vapour mass diffusivity is defined from the following expression [10]:

$$\rho_{air} D = 1.293 D_0 (\hat{T}/273)^{n_0 - 1}, \quad \hat{T} = \frac{T_{air} + 2T_d}{3}, \tag{3.20}$$

where the constants D_0 and n_0 are defined as $D_0 = 1.33e^{-05}$ and $n_0 = 1.8$ for methanol. Next, the Frossling correlation estimates the Sherwood number (Sh) as indicated by the following equation:

$$Sh_d = (2.0 + 0.6 Re_d^{\frac{1}{2}} Sc^{\frac{1}{3}}) \ln \frac{1 + B_d}{B_d}, \tag{3.21}$$

where Re_d is the droplet Reynolds number, and Sc is the Schmidt number of air. Finally, an additional boiling model was included to address the change in droplet radius under boiling regimes [10]. The rate of change of the droplet radius is calculated by the following expression:

$$\frac{\mathrm{d}r_0}{\mathrm{d}t} = \frac{k_{air}}{\rho_l c_{p,\infty} r_0} (1 + 0.23\sqrt{Re_d}) \ln \left[1 + \frac{c_{p,\infty}(T_{air} - T_d)}{h_{fg}} \right], \tag{3.22}$$

where k_{air} is the thermal conductivity of air, $c_{p,air}$ is the air specific heat capacity, h_{fg} is the enthalpy of vaporization of the droplet, and T_{air} & T_d are the temperature of air and droplet respectively. A summary of the numerical models is listed in Table 5.3, and presented visually in Figure 3.4.

Table 3.2: Numerical models

Physical Phenomena	Numerical Models
Fluid Flow	Navier Stokes, density-based solver [10]
Turbulence	RNG and Standard $k-\varepsilon$ model [21]
Droplet Injection	Blob model [49]
Liquid Breakup	KH-RT model [7] & TAB model [39]
Droplet Drag Force	Dynamic Drag Model [29]
Droplet Collision	NTC model [51]
Droplet Coalescence	Post Collision Outcome model [47]
Droplet Turbulent Dispersion	O'Rourke [38] model
Droplet Evaporation	Frossling correlation-based & boiling model [10]

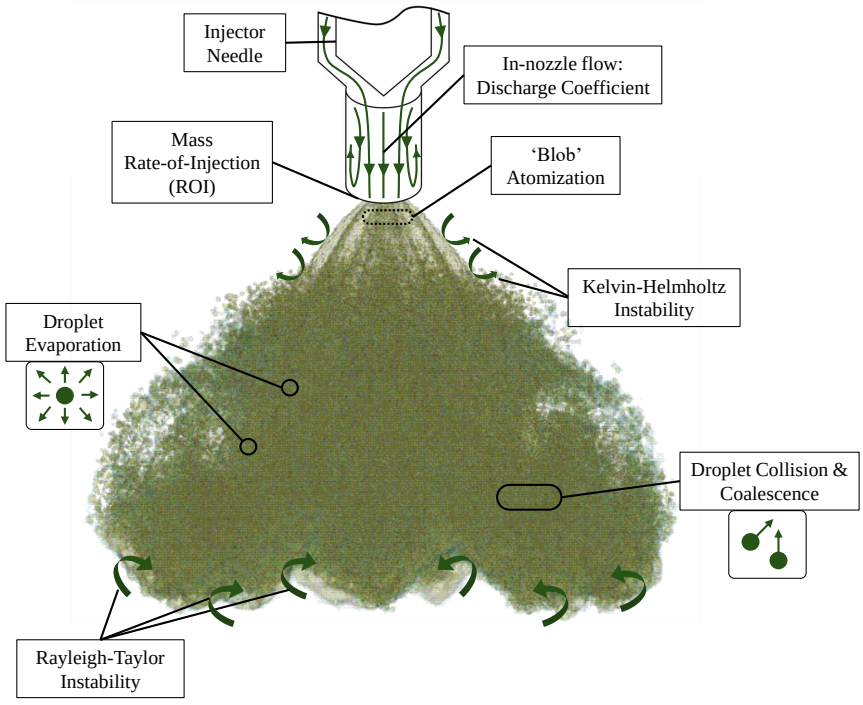

Figure 3.4: Schematic overview of the implemented spray modelling methodology.

3.3.3 Model Parameter Selection

The details of the used submodel constants are presented in Table 3.3. Apart from the constants that are associated with the nozzle characteristics, the rest have been selected based on the guidelines provided by CONVERGE [10]. The same modelling constants were used for both high and low pressure injection cases to evaluate the robustness of the modelling framework. To validate the model, we conducted a sensitivity analysis on three

modelling inputs: i) the mass rate of injection (ROI) profile, ii) the jet cone angle, and iii) the turbulence model. Specifically, the ROI profile has a significant impact on the transient response of the spray. Uncertainties in the ROI prevent CFD modelling from accurately capturing the spray development [43]. Each injector has a unique profile, which must be measured experimentally and incorporated into the CFD model [42]. Given that the ROI profile for our case study remains undetermined, we conducted a comprehensive sensitivity analysis to assess its potential impacts, as detailed in Section 5.4. Thus, we justified the selection of the most appropriate profile for PFI conditions.

On the other hand, the cone angle influences the three-dimensional spray structure and the liquid penetration. Generally, a larger cone angle leads to lower liquid penetration due to increased air entrainment [50, 14]. Detailed nozzle flow studies highlighted the importance of selecting a physically meaningful cone angle for spray simulations [50]. For both injection pressure cases, we selected the cone angle according to the experimental results. Ultimately, the turbulence model has a significant impact on the interaction between the ambient gas and the resulting spray dynamics. We compared three different turbulence model cases, using the RNG $k-\varepsilon$ model, the Standard $k-\varepsilon$ model, and the Standard $k-\varepsilon$ model with a modification. This modification included the round jet correction, where we changed the $C_{\varepsilon 1}$ constant to 1.55 [44]. This modification influences the production term of the Turbulent Kinetic Energy (TKE) dissipation rate ε, and corrects the under-prediction of liquid penetration, which was observed in diesel sprays [32].

Table 3.3: Modelling Parameters

Breakup Model	
KH Model size & breakup time constants	$B_0 = 0.61, \quad B_1 = 10$
RT Model size & breakup time constants	$C_{RT} = 0.6, \quad C_\tau = 1$
RANS Turbulence Model	
Standard $k-\varepsilon$ constants	$C_\mu = 0.09, \quad C_{\varepsilon 1} = 1.44 - 1.55, \quad C_{\varepsilon 2} = 1.92, \quad C_{\varepsilon 3} = -1.0$
RNG $k-\varepsilon$ constants	$C_\mu = 0.0845, \quad C_{\varepsilon 1} = 1.42, \quad C_{\varepsilon 2} = 1.68, \quad C_{\varepsilon 3} = -1.0$
Initial Turbulence Intensity	
Turbulent Kinetic Energy (TKE)	$k_0 = 1\,\mathrm{m}^2/\mathrm{s}^2$
TKE Dissipation Rate	$\varepsilon_0 = 100\,\mathrm{m}^2/\mathrm{s}^3$
Mass Diffusivity	
Methanol diffusivity constants	$D_0 = 1.336 \cdot 10^{-5}, \quad n_0 = 1.8$
Nozzle Characteristics	
Cone Angle	LP-case: *known variable angle (initial value:* 45°*)*, HP-case: 8°
Discharge Coefficient	$C_d = 0.79$ (both cases)

Since the injector characteristics were unknown, we calculated the nozzle discharge coefficient based on the Lichtarowicz et al. [28] correlation. The correlation estimates the discharge coefficient based on the L/D ratio of the nozzle:

$$C_d = 0.827 - 0.0085 \cdot L/D \tag{3.23}$$

For the HP injection, the ratio L/D equalled 4.9, whereas for the LP injection, it was unknown. Therefore, we kept the same value for the LP injection case. As the modelled conditions are barely evaporating and no mixing occurs, the discharge coefficient does not significantly affect the mixture formation, making our parameter choice consistent. Particularly for the LP nozzle, we assumed a single nozzle injector with the same injection characteristics (i.e., cone angle and injection duration) as in the experiment. The estimated parameters (see Table 3.1) were selected to match the experimental spray structure and liquid penetration.

In the LP case, the liquid penetration is defined as the vertical distance between the nozzle and the identified spray edge [30]. In the HP case, the authors followed the ECN guidelines by employing a Mie-scattering technique to measure liquid penetration [19]. In the numerical results, the liquid penetration was calculated by a 95 % threshold for the liquid mass fraction. Although an inherent difference exists in the definition of liquid penetration between our model and the experiments, we consider it negligible for the scope of the present study. A more strict comparison has been achieved by the ECN for gasoline sprays [17]. However, these investigations included more detailed experiments using diffused back-illumination, Mie-scattering, and PIV techniques [40, 55, 24]. Recently, the ECN has conducted dedicated methanol spray studies using an ECN spray style multi-hole injector [31], which is the subject of a subsequent chapter in this thesis. In the present chapter, we use the existing liquid penetration data dedicated to methanol PFI for our numerical investigations.

3.4 Results & Discussion

3.4.1 Simulation Plan

THE present study followed a structured simulation plan to construct a predictive framework for marine PFI sprays. The mesh size was initially analyzed by comparing a static mesh grid with an automatically refined mesh grid. After investigating the mesh influence, we performed a set of simulations to demonstrate the sensitivity of each input parameter on liquid penetration. The parameters include the mass ROI, the cone angle, and the turbulence model, as mentioned in Section 3.3.3. Consequently, we compared their influence with the experimental data and highlighted the importance of assigning realistic values in the model. Based on the outcomes of the sensitivity analysis, we selected a baseline model and scaled up the injected mass to account for marine engine operation. The marine case study examined the effect of injection pressure on breakup, evaporation, and jet velocity, as well as the impact of ambient environmental conditions on spray penetration. In Figure 3.5, we provide a visual representation of the implemented simulation plan.

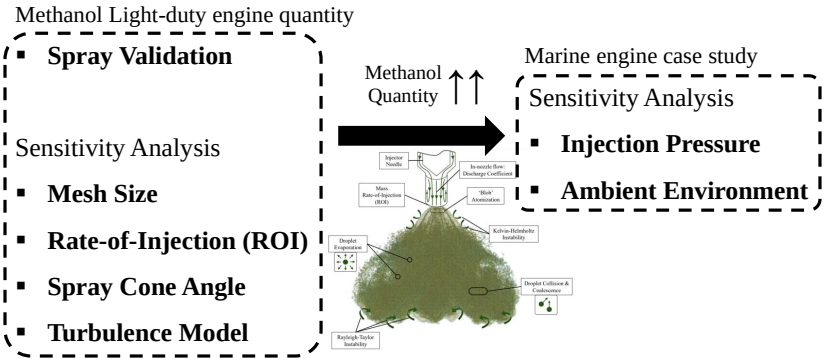

Figure 3.5: Overview of the conducted simulation cases.

3.4.2 Mesh Size Influence

For the mesh sensitivity analysis, we used four different mesh grid sizes for each injection pressure. Three cases involved a static mesh with a refinement in the cone-shaped area, as shown in Fig. 3.3, and a single AMR case with a dynamically changing grid. The refined cells were sized as 1 mm for the coarse mesh, 0.5 mm for the medium mesh, and 0.25 mm for the fine mesh cases. In the AMR case, we followed the same approach with the fine grid by using a small cone refinement close to the nozzle exit. The AMR algorithm refined the evolving spray tip with a minimum cell size of 0.25 mm. Subsequently, we compared the AMR case with the static mesh cases in terms of computational accuracy and cost. In Table 3.4, we present the mesh grid parameters, including the total cells and computational cost for each computational grid. The LP case exhibits a higher cell count because the larger cone angle of the experiment required an increased cone refinement area.

Table 3.4: Mesh grid parameters for Low Pressure (LP) and High Pressure (HP) injection

	Minimum cell size [mm]	Cell count [-]	Computational cost [core-hours]
LP coarse	1.0	0.17 M	0.15
LP medium	0.5	1 M	1.8
LP fine	0.25	7.7 M	32.9
LP AMR	0.25	0.06 M	0.19
HP coarse	1.0	0.1 M	0.13
HP medium	0.5	0.5 M	0.75
HP fine	0.25	3.4 M	9.96
HP AMR	0.25	0.5 M	1.1

In the present section, the baseline models were selected for the mesh sensitivity analysis with the parameters presented previously in Table 3.3. Moreover, we considered a top-hat ROI profile and the modified Standard $k-\varepsilon$ for both LP and HP injection cases. In Fig. 3.6, the resulting liquid penetrations are presented for both LP and HP cases. Higher injection pressure augments the penetration rate due to the increased jet velocity.

As a result, the entire spray process is faster than in the case of low injection pressure. The results demonstrated that the model predicts the liquid penetration trends satisfactorily within the experimental uncertainty limits for both injection cases.

Mesh convergence was achieved for the fine grid in both cases for a mesh size of 0.25 mm. Particularly in the LP case, a previous study using the same model employed a computationally expensive 0.125 mm grid to further demonstrate the convergence of the 0.25 mm grid [67]. The CFD model accurately captured the trends in the experimental data, providing a physical representation of the spray momentum. For both cases, the coarse grid underpredicted the liquid penetration, which aligns with trends observed in conventional fuels [54]. Interestingly, the AMR solution demonstrated similar results as the static mesh, but at significantly lower computational cost (more than 95 % cheaper simulations). This aligns with Abraham [2], who claimed that for accurate spray predictions, cell resolution must be on the order of the orifice diameter. Thus, the AMR grid was selected as the optimal grid for our numerical study, ensuring a computationally affordable and accurate solution, which can be implemented in full engine models.

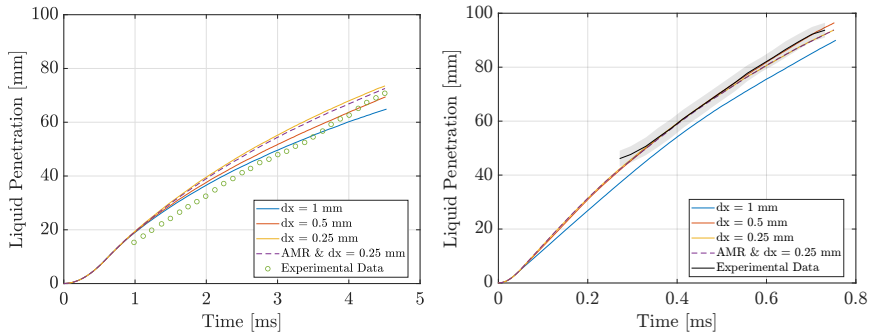

(a) Low Pressure Injection

(b) High Pressure Injection

Figure 3.6: Mesh size effect on liquid penetration

3.4.3 CFD Framework Parameter Investigation

In this section, we analyze the sensitivity of the baseline model with the AMR grid from the previous section for both LP and HP injection, examining mass ROI, cone angle, and turbulence model. The decoupled effects of each parameter are then reported and compared. In each case, we altered the parameter of interest (i.e., ROI, cone angle, and turbulence model) while using the baseline model, as reported in the mesh sensitivity study. This comparison underscores the significance of these choices in spray modelling for marine engines. Ultimately, the sensitivity analysis strives to provide a solid foundation for the proposed modelling framework.

Rate of Injection

Normally, the ROI profile for each injector is generated individually, based on mass flow rate and momentum measurements, which represent the hydraulic behaviour of the nozzle [41]. Since the ROI is unknown for the employed injectors, a modelling convention is crucial for a realistic spray outcome. This chapter aims to address this challenge by introducing an empirical ROI profile that can accurately predict the experimental liquid penetration while representing the injection conditions. The profile is based on a top-hat style profile with a modified initial transient overshoot associated with the initial needle-lift overshooting motion. This represents the overshoot observed in the Spray G profile in low ambient pressure conditions in gasoline injection [17]. This overshoot is lower in the LP case due to low ambient and injection pressure. Conversely, the overshoot is more pronounced in the HP case due to the increased initial jet momentum resulting from the high injection pressure. The normalized mass ROI profiles are presented in Fig. 3.7. Along with the proposed top-hat profiles, we compared the Spray G profile, which is closer to the HP condition, a constant mass flow profile, and a generated profile from the online "Virtual Injection Rate Generator" tool of the Clean Mobility & Thermofluids (CMT) group [9].

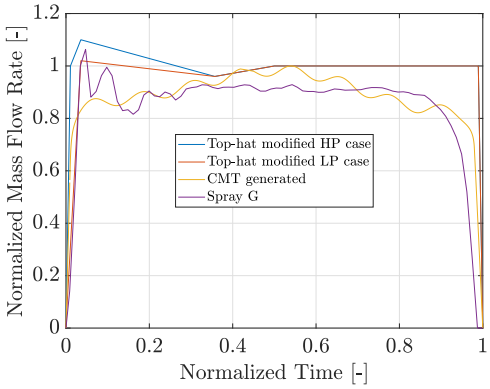

Figure 3.7: Mass ROI profiles (normalized over total injected mass)

Fig. 3.8 illustrates the liquid penetration results for the LP injection case for each ROI profile. For all simulated cases, the model overpredicted the experimental values due to the inherent uncertainty in the injector details. Thus, to mitigate this over-prediction, the model requires more accurate information on the nozzle diameter, discharge coefficient, and nozzle-hole topology. Despite this, the majority of the profiles provide reasonable predictions for the transient behaviour of the jet with less than 10 % deviation from the experimental values. This highlights that sprays in LP injection conditions are insensitive to ROI variations in the scope of PFI modelling. Hence, our model demonstrates satisfactory acceleration and initial momentum of the spray and acceptably predicts the liquid penetration.

Similar trends are also observed under HP injection in Fig. 3.9, where the liquid penetration is within the experimental uncertainty range. Despite that, the CMT tool

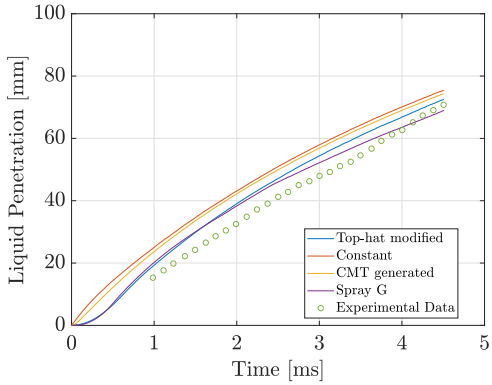

Figure 3.8: ROI profile influence on LP injection

over-predicts penetration, similar to that in diesel injection studies [43]. This is likely due to the fact that the CMT tool was developed for diesel injection in high ambient pressure environments. Under these conditions, the injector needle overshoots less due to higher resistance forces originating from the higher ambient pressure environment. These forces impede the needle motion, and, contrary to low ambient pressure injection, the injector needle displacement experiences lower overshoot.

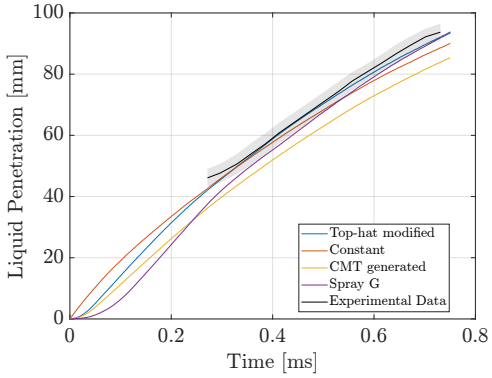

Figure 3.9: ROI profile influence on HP injection

Cone Angle

The spray cone angle influences the liquid penetration and the jet morphology [61]. By tuning it appropriately, the spray structure can be accurately captured [50]. In Fig. 3.10, the comparison of 8, 10, 12, and 16 degrees of cone angle for the HP case confirms the large influence in liquid penetration. Hence, with even 2 degrees of perturbation in cone angle input, liquid penetration results are affected significantly. Thus, high pressure injection simulations need to be assigned a realistic value for the cone angle. Small

perturbations of this parameter can lead to imprecise predictions of mixture formation due to incorrect liquid penetration. Fig. 3.11 depicts the cone angle influence for the LP

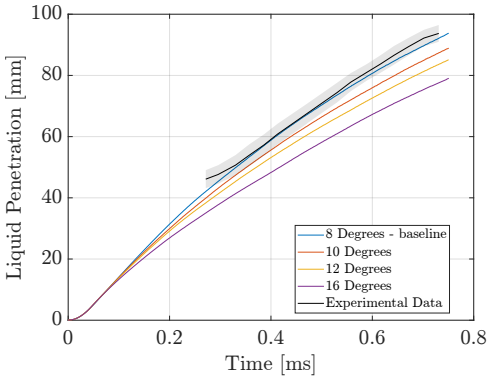

Figure 3.10: Cone angle influence on HP injection

case. Here, the different injector geometry requires larger cone angle values as input for the model. Contrary to the HP case, under low injection pressure, the cone angle slightly affects the liquid penetration, even for a wide range of jet angles (25 degrees, 35 degrees, and time-variable cone as reported by the experimental paper). This phenomenon is attributed to the low entrainment velocity experienced by the LP injection jet. Since the velocities are diminished, the jet does not entrain sufficient air into its core. Therefore, the momentum of the droplets is similar for any given jet cone angle, and the liquid penetration remains unaffected. Additional discussions on the entrainment velocity are conducted in Section 3.4.4.

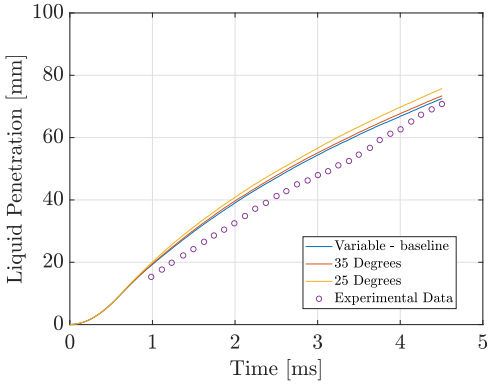

Figure 3.11: Cone angle influence on LP injection

Turbulence Model

Fig. 3.12 shows the liquid penetration results for the different turbulence model cases. As mentioned in Section 3.3.3, the turbulence model selection affects the ambient flow and spray formation. In the LP case, the effect of turbulence is negligible, indicating a low turbulent intensity. On the contrary, in the HP case, the Standard $k-\varepsilon$ model significantly under-predicts the liquid penetration, aligning with high injection pressure spray literature [32, 61, 40]. The turbulence modification is justified as the axisymmetric nature of the spray cannot use default turbulence model constants, which are typically found in boundary layer flows [44]. In addition, the RNG $k-\varepsilon$ model performs similarly to the modified Standard $k-\varepsilon$, indicating its suitability for spray and combustion simulations in ICE models.

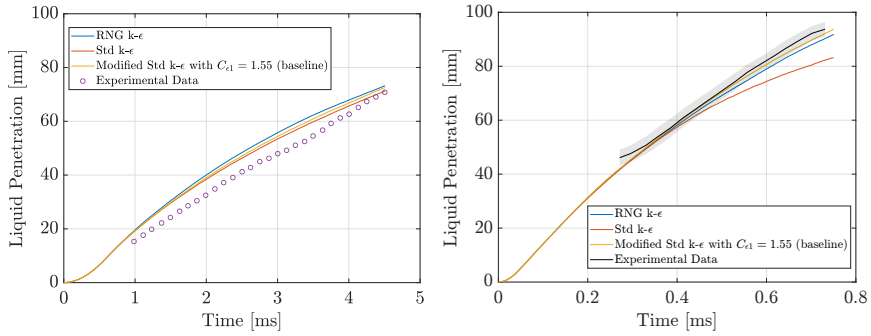

(a) Low Pressure Injection (b) High Pressure Injection

Figure 3.12: Turbulence modelling effect on liquid penetration

Sensitivity of Modelling Parameters

The sensitivity of each modelling parameter is presented in Fig. 3.13. The figure presents the relative error between the final data point of the experiments and the associated worst-case result from the CFD model. For the HP case, all of the investigated parameters exhibit a significant influence on the liquid penetration prediction. Specifically, the cone angle sensitivity is the highest among the ROI and the selection of the turbulence model. Thus, we conclude that uncertainties in cone angle and ROI during the modelling process could lead to large discrepancies in the outcome spray structure. Eliminating these uncertain parameters through experimental data or, if possible, tuning them realistically is mandatory for methanol engine simulations. On the other hand, in the LP case, the induced sensitivity is lower due to the decreased intensity of the phenomena under low injection pressures. Lower droplet velocities inevitably result in reduced droplet breakup and evaporation, and thus, the studied changes have a minor effect on the model predictions.

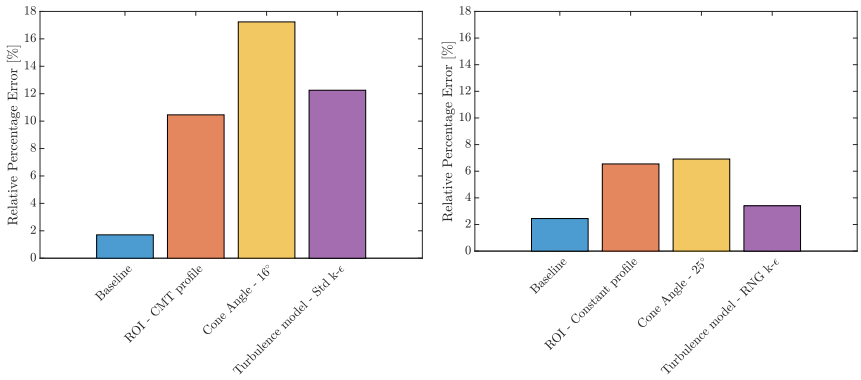

(a) HP injection sensitivity comparison (b) LP injection sensitivity comparison

Figure 3.13: Sensitivity of modelling parameters on predicted liquid penetration: comparison of ROI, cone angle, and turbulence model

Finally, to demonstrate the predictive capabilities of the present framework, Fig. 3.14 presents the liquid penetration of the HP case under varied experimental ambient pressure and temperature environments. For the increased ambient pressures, the experimental paper reported a proportional increase in ambient temperature, which promoted evaporation phenomena. As a result, the successful reproduction of the experimental results demonstrates the robustness of the present modelling framework.

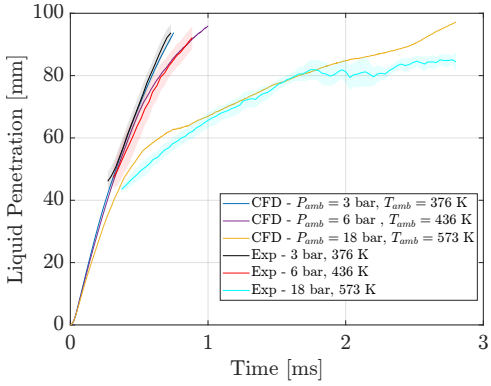

Figure 3.14: Validated HP model predictions at varying ambient pressures

3.4.4 Marine Engine Case Study

To account for marine engine fuel quantities, we increased the injected mass and conducted a case study on the effect of injection pressure on methanol sprays. Consequently, we compared the spray characteristics of the outcome for each injection pressure. The evaluation included the liquid penetration results, the occurrence of breakup (in terms

of spray SMD), and the entrainment velocity field. A larger nozzle diameter was used to replicate the conditions of small-bore marine engines, thereby facilitating the increased quantity of methanol. In Table 3.5, the ambient conditions are reported along with the details of injection quantity and nozzle diameter. The chosen conditions represent a small-bore marine engine, which was retrofitted for methanol PFI in previous research by our group [8]. In addition, Table 3.6 shows each case's injection pressure and associated injection duration. For each injection pressure, the injection duration was calculated to facilitate the predefined 400 mg of methanol. For the analysis, we used the validated modelling framework with the baseline parameters from the previous section (Section 3.4.3). The meshing strategy was the same as previously, but with a minimum cell size of 0.5 mm due to the larger nozzle diameter. Similarly as in Section 3.4.2, we achieved mesh convergence for the 0.5 mm AMR grid through testing three different cell sizes ranging from 2 mm to 0.5 mm.

Table 3.5: Marine Case Study Conditions

Item	Value
Ambient Pressure [bar]	2
Ambient Temperature [°C]	100
Fuel Temperature [°C]	90
Injection Quantity [mg]	400
Nozzle Diameter [mm]	1.0

Table 3.6: Marine Case Study: Injection Pressure & Duration

Injection Pressure [bar]	Injection Duration [ms]
6	22.5
8	19.5
10	17.5
15	14.3
20	12.4
30	10.1
40	8.7
50	7.8
100	5.5
200	3.9

To prevent fuel impingement on the computational domain walls, the simulations were run until 25 % of the total fuel quantity had been injected. While less fuel was injected during the simulation duration, we maintained a mass flow rate corresponding to 400 mg of methanol. Fig. 3.15 demonstrates the resulting liquid penetration for the range of injection pressures. For high injection pressures, the spray penetrates more quickly, thereby determining the conditions prior to wall impact. Nevertheless, similar liquid penetration is observed for the same injected quantity. Fig. 3.16 depicts the advantage of higher injection pressures in terms of droplet breakup. Moreover, the spray SMD results

demonstrate that significant improvements in droplet atomization are realized by using high injection pressures.

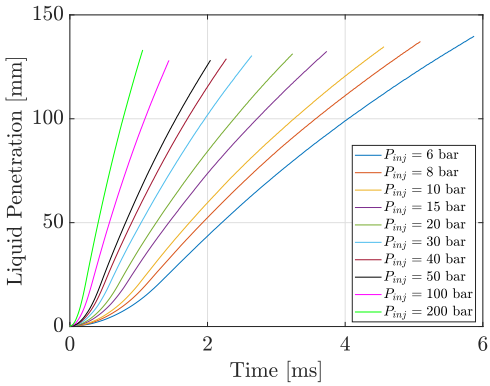

Figure 3.15: Effect of injection pressure on liquid penetration in marine PFI conditions

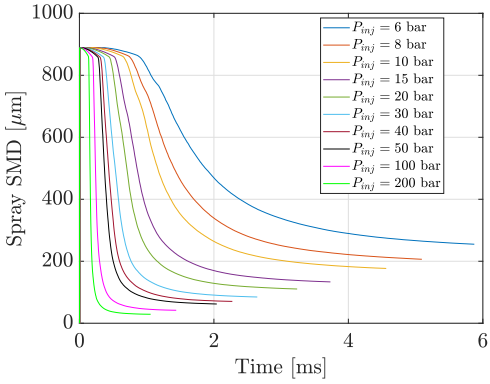

Figure 3.16: Spray SMD under different injection pressures

With improved atomization, the droplets have an increased effective area, which interacts with the surrounding gaseous medium and, thus, experiences faster evaporation. In Fig. 3.17, we illustrate a spatial comparison of the droplet diameter for each injection pressure at the moment that 25 % of the fuel quantity was injected. The spatial comparison shows that low injection pressures (< 20 bar) have a higher concentration of droplets sized between 104 μm and 216 μm. On the other hand, for injection pressures higher than 50 bar, atomization is enhanced with smaller droplets even in the vicinity of the spray.

The resulting evaporated methanol is presented in Fig. 3.18. The 200 bar case exhibits the highest evaporated quantity, confirming improved atomization with increased injection pressure. The evaporation rate is also substantially increased, whereas for the low injection pressures evaporation is minimal. Nonetheless, when compared with the total injected mass, the total evaporated quantities are up to 1 % (Fig. 3.19). Hence, evaporation will be minimal at intake port conditions, as most of the fuel will impact the walls or

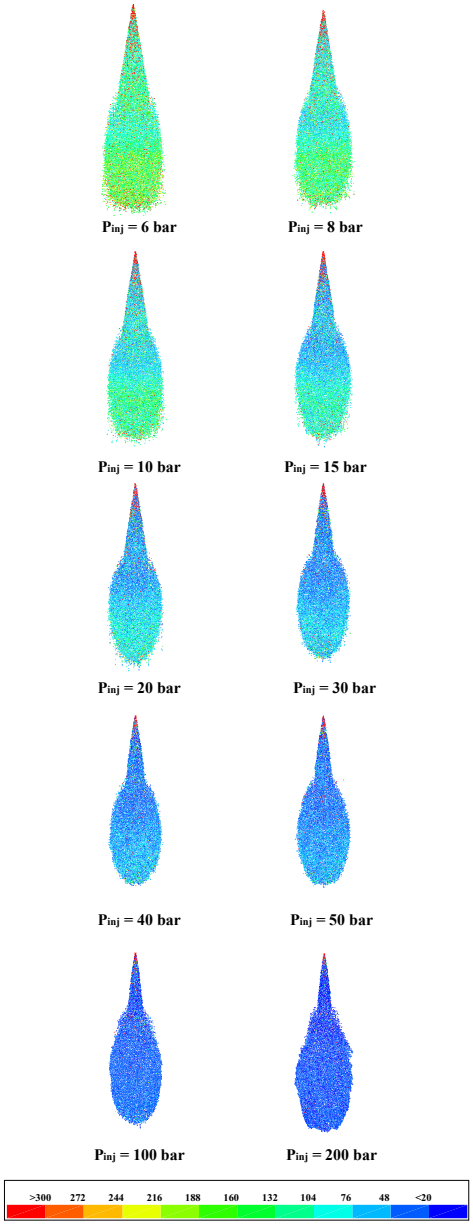

Figure 3.17: Droplet diameter (in μm) for each injection pressure

the intake valve geometry. These findings indicate that the mixture formation may be dominated by wall film and in-cylinder evaporation phenomena.

The velocity vectors for each injection pressure are shown in Fig. 3.20 for the moment

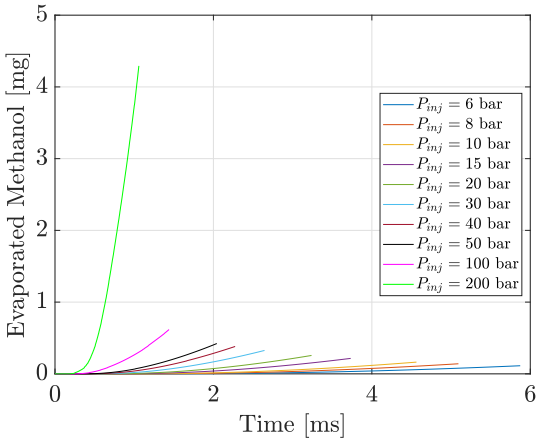

Figure 3.18: Evaporated methanol for each injection pressure

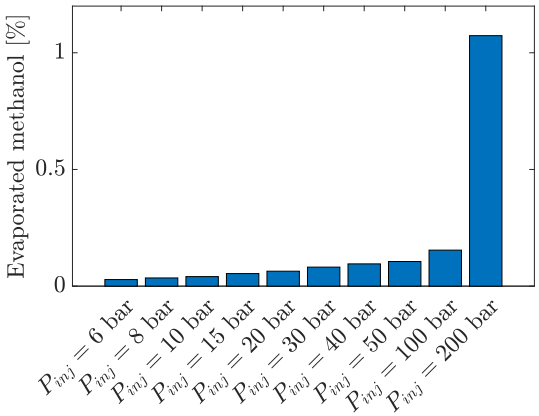

Figure 3.19: Percentage of evaporated methanol with respect to total injection quantity

when 25 % of the fuel quantity was injected. Low injection pressures result in very low air entrainment, while the core maintains high momentum due to increased spray density. On the contrary, under high injection pressure, the spray velocity and air entrainment effects are an order of magnitude higher than in lower injection pressures. This results in a more diluted spray core with less momentum and higher droplet breakup. Additionally, under high injection pressure, the wing tip vortex is located closer to the tip of the spray. Fig. 3.21 displays the velocities in the vicinity of the spray and close to the nozzle exit (air entrainment point). Under low injection pressures (< 30 bar), the air is entrained with less than 5 m/s, which is insufficient for the primary breakup of the jet. Similarly, the low injection pressures demonstrate low momentum indicating the decreased penetration rate shown in Fig. 3.15.

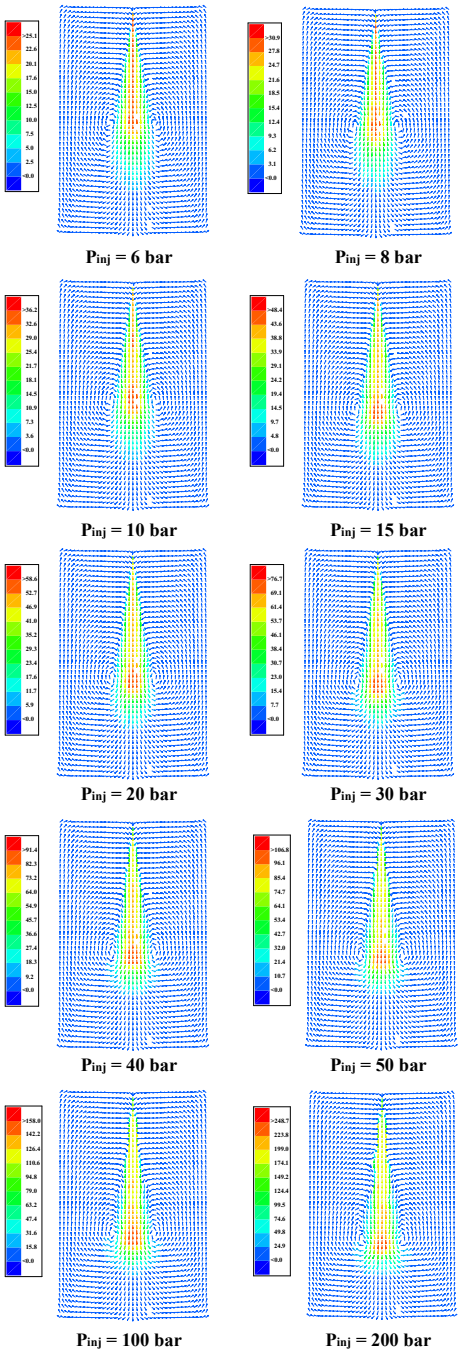

Figure 3.20: Entrainment velocity vectors for each injection pressure

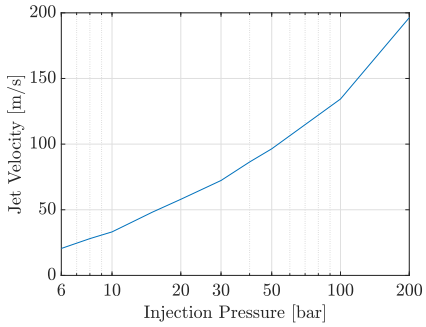

(a) Jet velocity for each injection pressure at $z = 100\,\text{mm}$ point

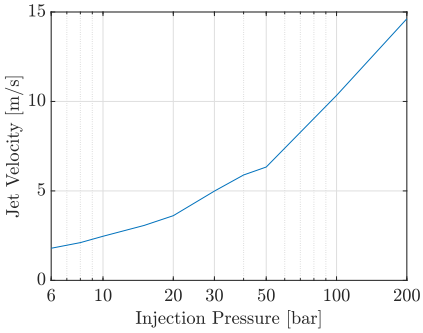

(b) Entrainment velocities for each injection pressure at $z = 14.5\,\text{mm}$ and $y = \pm 3.5\,\text{mm}$ (average of $y = \pm 3.5\,\text{mm}$ points)

Figure 3.21: Injection pressure effect on jet velocity

Finally, Table 3.7 presents the nozzle tip We number for each injection pressure. For all the injection pressures, the droplets remain in the multimode and shear breakup regime [23]. Even with low injection pressures, primary breakup is predicted correctly using the KH model, because marine nozzle dimensions produce sufficiently large droplets. These large droplets exhibit increased We numbers with higher injection pressures than the critical value, remaining outside the oscillation and deformation breakup regimes. However, automotive-style nozzles in PFI conditions may require the TAB model to predict breakup as the droplets lie within the oscillation breakup regime [67].

Table 3.7: Nozzle Exit Weber Number

Injection Pressure [bar]	We number [-]
6	50
8	68
10	85
15	123
20	170
30	260
40	350
50	430
100	850
200	1650

Influence of Ambient Environment on Marine PFI Sprays

In this section, we conduct a sensitivity analysis on the ambient pressure and temperature, and report their effect on spray formation. For the present investigation, we used the previous marine injection conditions reported in Table 3.5 along with a fixed injection

pressure of 10 bar. Figure 3.22 depicts the influence of ambient pressure on liquid penetration and SMD. For the low ambient pressure cases, the spray exhibited increased penetration and SMD due to the lower drag forces imposed on the droplet's surface. In the case of high ambient pressure, higher drag forces augmented the droplet breakup occurrence, leading to decreased penetration and SMD. Furthermore, Figure 3.23 illustrates the ambient temperature sensitivity analysis. Higher ambient temperatures lower the ambient density, and as a result, both liquid penetration and SMD are slightly increased in proportion. This is valid as long as the spray is outside the flashing regime, which is true in the presented cases. Thus, with modifications to the ambient conditions, the CFD model can provide physically accurate predictions.

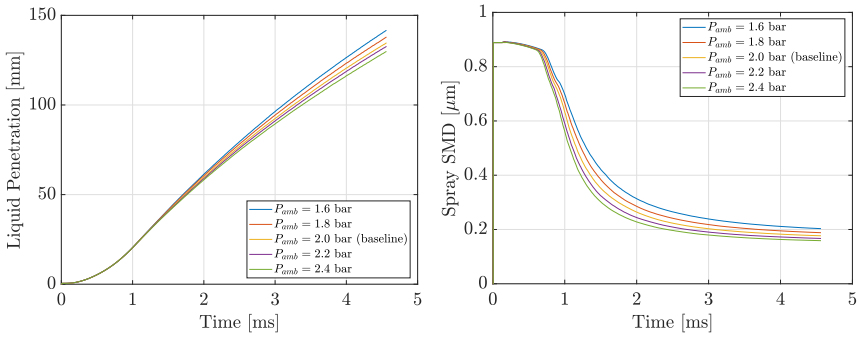

Figure 3.22: Influence of ambient pressure on liquid penetration (left) and SMD (right) for 10 bar injection pressure

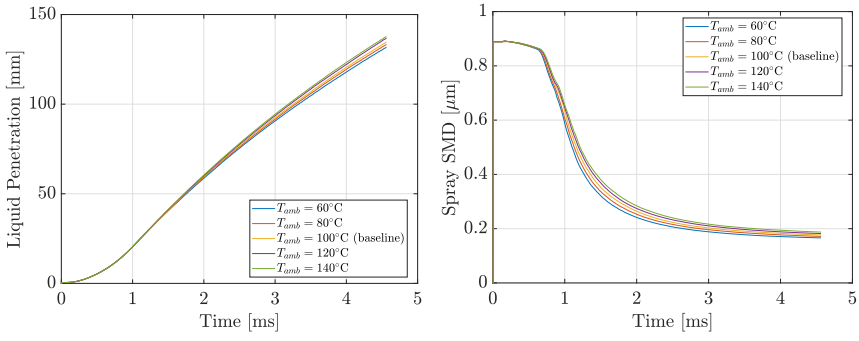

Figure 3.23: Influence of ambient temperature on liquid penetration (left) and SMD (right) for 10 bar injection pressure

3.5 Conclusions

IN this chapter, we presented a CFD framework, which uses state-of-the-art spray modelling to reproduce methanol sprays under PFI conditions with a well-established approach for diesel and gasoline. These conditions are characterized by low ambient pressure and temperature, as well as low injection pressures (ranging from 6 to 10 bar), often found in four-stroke medium- and high-speed marine engines operating with premixed methanol combustion. To overcome the challenges of poor atomization, our framework was extended to higher injection pressures up to 200 bar. The presented work is the first to use methanol experimental data for both high and low injection pressures to validate and tune the models for robust operation in PFI conditions. We investigated the sensitivity of the uncertain parameters resulting from unknown injector specifications on liquid penetration. The validated model was then applied in a marine engine case study, using increased methanol quantities, and demonstrated the evaporation and atomization challenges in PFI conditions.

Based on the model results, we found several key insights. The sensitivities of mesh, ROI, cone angle, and turbulence model have been thoroughly investigated and reported. Resolving the flow with AMR is the most efficient way to simulate engines in CFD environments. We demonstrated that with an unknown ROI, a modified top-hat profile with an initial transient response yields satisfactory results for both high and low injection pressures. Accurate spray predictions necessitate a precise definition of the cone angle, as it significantly influences the spray structure. Under low injection pressure conditions, the effects of cone angle and turbulence are negligible, whereas under high injection pressure, the modified Standard and RNG $k-\varepsilon$ models perform as expected. This is due to increased droplet velocities, making HP injection highly sensitive to ROI and cone angle inputs.

In contrast, for low-pressure (LP) injection, the jet velocity is significantly lower than in high-pressure (HP) scenarios, resulting in the spray structure and the adjacent flow phenomena having a lesser impact on the in-cylinder mixture formation. Consequently, evaporation and mixing may be more influenced by wall wetting phenomena. This suggests a potential area for further research, which could involve exploring the coupling of the current framework with wall wetting models to investigate mixture formation in intake port manifold environments. Additionally, there should be a focus on studying wall wetting evaporation parameters, like film thickness and size, in associated marine engines. For small injection quantities typical of automotive style, the low jet velocity also influences the applicability of the droplet breakup model. Thus, for an injection pressure lower than a critical value (determined by Eq. (3.18)), the TAB model should be implemented for accurate predictions of liquid penetration.

Following the spray model validation, we scaled up the injected methanol quantity to 400 mg using a larger single-hole nozzle. The simulated conditions aimed to account for a marine engine operating with methanol premixing at the intake manifold. Using the scaled up marine engine injection model, we performed a case study encompassing a set of different injection pressures ranging from 6 bar to 200 bar. Subsequently, using the 10 bar injection pressure case, we conducted a sensitivity analysis on the ambient conditions, revealing the isolated effects of ambient pressure and temperature on spray

penetration. Using higher injection pressures results in the spray jet breaking up more quickly, which promotes evaporation and enhances mixture formation. However, evaporation occurring at the initial stage of injection, before impact with the wall, is minimal. Therefore, higher jet velocities will evidently affect wall wetting in conjunction with the cross-flow of the inlet manifold. This pattern is similar to what is observed in LP injection, suggesting that wall wetting effects may still be dominant. Studies of conventional fuels have not produced consistent results about the influence of injection pressure on wall wetting [14]. This suggests a need for additional experimental and simulation work in this area, which will reveal the interaction between spray and intake air cross-flow in the intake manifold.

In summary, injection pressure dictates atomization and pre-wall impact conditions, as ambient temperature in the PFI environment is load dependent. Higher injection pressures can potentially overcome methanol evaporation challenges, as could alternative injection hardware. This chapter provided a best practice for the CFD analysis of injection timing and location for real engine geometries under a wide range of injection pressures. When combined with wall-wetting models, our approach can identify the challenges associated with converting methanol marine engines. CFD simulations can be a crucial step towards robust methanol operation and, ultimately, contribute to achieving sustainability targets.

Bibliography

[1] Delft High Performance Computing Centre (DHPC). *DelftBlue Supercomputer (Phase 1)*. 2022. URL: https://www.tudelft.nl/dhpc/ark/delftbluephase1.

[2] John Abraham. "What is adequate resolution in the numerical computations of transient jets?" In: *SAE transactions* (1997), pp. 141–155.

[3] Avinash Kumar Agarwal et al. "Fuel injection strategy optimisation and experimental performance and emissions evaluation of diesel displacement by port fuel injected methanol in a retrofitted mid-size genset engine prototype". In: *Energy* 248 (June 2022), p. 123593. ISSN: 0360-5442. DOI: 10.1016/j.energy.2022.123593.

[4] Anthony A Amsden et al. *KIVA-II: A computer program for chemically reactive flows with sprays*. Tech. rep. Los Alamos National Lab.(LANL), Los Alamos, NM (United States), 1989.

[5] Tawfik Badawy et al. "Macroscopic spray characteristics of iso-octane, ethanol, gasoline and methanol from a multi-hole injector under flash boiling conditions". en. In: *Fuel* 307 (Jan. 2022), p. 121820. DOI: 10.1016/j.fuel.2021.121820. (Visited on 11/02/2022).

[6] Carsten Baumgarten. *Mixture formation in internal combustion engines*. Springer Science & Business Media, 2006.

[7] Jennifer C Beale et al. "Modeling spray atomization with the Kelvin-Helmholtz/Rayleigh-Taylor hybrid model". In: *Atomization and sprays* 9.6 (1999).

[8] J. Bosklopper et al. "Experimental study on a retrofitted marine size spark-ignition engine running on portinjected 100% methanol". In: *INEC 2020, Delft* (2020). URL: https://repository.tno.nl/islandora/object/uuid%3A3b9a2d8e-34ab-49a9-a07f-3db8bb20be1a.

[9] CMT - Clean Mobility & Thermofluids website. *"Virtual Injection Rate Generator"*. Accessed: 2023-09-05. URL: https://www.cmt.upv.es/#/ecn/download/InjectionRateGenerator/InjectionRateGenerator/.

[10] Convergent Science Inc. *CONVERGE MANUAL v3.0*. 2022.

[11] Scott Curran et al. "The future of ship engines: Renewable fuels and enabling technologies for decarbonization". In: *International Journal of Engine Research* (2023).

[12] Jeroen Dierickx et al. “Efficiency and Emissions of a High- Speed Marine Diesel Engine Converted to Dual-Fuel Operation with Methanol.pdf”. In: 2019. DOI: oai:archive.ugent.be:8627787.

[13] Jeroen Dierickx et al. “Retrofitting a high-speed marine engine to dual-fuel methanol-diesel operation: A comparison of multiple and single point methanol port injection”. In: *Fuel Communications* 7 (June 2021), p. 100010. ISSN: 2666-0520. DOI: 10.1016/j.jfueco.2021.100010. URL: https://linkinghub.elsevier.com/retrieve/pii/S2666052021000030 (visited on 11/03/2023).

[14] Francesco Duronio et al. “Gasoline direct injection engines–A review of latest technologies and trends. Part 1: Spray breakup process”. In: *Fuel* 265 (2020), p. 116948.

[15] ECN. *Engine Combustion Network*. Accessed: 2023-09-01. URL: https://ecn.sandia.gov/.

[16] Joel H Ferziger et al. *Computational methods for fluid dynamics*. Vol. 3. Springer, 2002.

[17] ECN Spray G. *Engine Combustion Network Spray-G Conditions*. Accessed: 2023-10-07. URL: https://ecn.sandia.gov/gasoline-spray-combustion/target-condition/spray-g-operating-condition/.

[18] Anupam Ghosh et al. “Evaporating spray characteristics of methanol-in-diesel emulsions”. In: *Fuel* 290 (Apr. 2021). DOI: 10.1016/j.fuel.2020.119730.

[19] Anupam Ghosh et al. “MEASUREMENT OF LIQUID AND VAPOR PENETRATION OF EVAPORATING METHANOL SPRAYS”. In: *Atomization and Sprays* 30.10 (2020), pp. 741–757.

[20] Yanfeng Gong et al. “Investigation on methanol spray characteristics”. In: *Energy and Fuels* 21.5 (Sept. 2007), pp. 2991–2997. DOI: 10.1021/ef0605089.

[21] Zhiyu Han et al. “Turbulence modeling of internal combustion engines using RNG κ-ε models”. In: *Combustion science and technology* 106.4-6 (1995), pp. 267–295.

[22] AL Horvath. “Redlich-Kwong equation of state: review for chemical engineering calculations”. In: *Chemical Engineering Science* 29.5 (1974), pp. 1334–1340.

[23] L-P Hsiang et al. “Drop deformation and breakup due to shock wave and steady disturbances”. In: *International Journal of Multiphase Flow* 21.4 (1995), pp. 545–560.

[24] Joonsik Hwang et al. “Spatio-temporal identification of plume dynamics by 3D computed tomography using engine combustion network spray G injector and various fuels”. In: *Fuel* 280 (2020), p. 118359.

[25] Raad I Issa. “Solution of the implicitly discretised fluid flow equations by operator-splitting”. In: *Journal of computational physics* 62.1 (1986), pp. 40–65.

[26] Pijush K Kundu et al. *Fluid mechanics*. Academic press, 2015.

[27] Haohan Li et al. “Improving the calculation of evaporating sprays for medium-speed marine-engine-like conditions”. In: *Atomization and Sprays* 31.8 (2021).

[28] Andrzej Lichtarowicz et al. “Discharge coefficients for incompressible non-cavitating flow through long orifices”. In: *Journal of mechanical engineering science* 7.2 (1965), pp. 210–219.

[29] Alex B Liu et al. “Modeling the effects of drop drag and breakup on fuel sprays”. In: *SAE Transactions* (1993), pp. 83–95.

[30] Kai Liu et al. “Experimental study of the macroscopic characteristics of methanol low-pressure injection spray”. en. In: *International Journal of Energy Research* (Aug. 2022), er.8625. DOI: 10.1002/er.8625. (Visited on 11/01/2022).

[31] ECN Spray M. *Engine Combustion Network Spray-M Data*. Accessed: 2023-10-07. URL: https://ecn.sandia.gov/data/sandia-spray-m-data/.

[32] Noud Maes et al. “Experimental and numerical analyses of liquid and spray penetration under heavy-duty diesel engine conditions”. In: *SAE International Journal of Fuels and Lubricants* 9.1 (2016), pp. 108–124.

[33] Noud Maes et al. “Spray penetration, combustion, and soot formation characteristics of the ECN Spray C and Spray D injectors in multiple combustion facilities”. In: *Applied Thermal Engineering* 172 (2020), p. 115136.

[34] MAN Energy Solutions. *MAN B&W ME-LGIM two-stroke dual-fuel engine*. Accessed: 2023-10-18. URL: https://www.man-es.com/marine/products/two-stroke-engines/man-b-w-me-lgim.

[35] Alexios Matamis et al. “Optical Characterization of Methanol Sprays and Mixture Formation in a Compression-Ignition Heavy-Duty Engine”. en. In: Sept. 2020, pp. 2020–01–2109. DOI: 10.4271/2020-01-2109. (Visited on 09/01/2022).

[36] RS Miller et al. “Evaluation of equilibrium and non-equilibrium evaporation models for many-droplet gas-liquid flow simulations”. In: *International journal of multiphase flow* 24.6 (1998), pp. 1025–1055.

[37] K. Moreno Cabezas et al. “Characteristics of Methanol and Iso-Octane under Flashing and Non-Flashing Conditions in ECN-G Spray”. English. In: 2022. DOI: 10.4271/2022-01-0496.

[38] Peter J O’Rourke. “Statistical properties and numerical implementation of a model for droplet dispersion in a turbulent gas”. In: *Journal of Computational Physics* 83.2 (1989), pp. 345–360.

[39] Peter J O’Rourke et al. *The TAB method for numerical calculation of spray droplet breakup*. Tech. rep. SAE Technical Paper, 1987.

[40] Davide Paredi et al. “Validation of a comprehensive computational fluid dynamics methodology to predict the direct injection process of gasoline sprays using Spray G experimental data”. In: *International Journal of Engine Research* 21.1 (2020), pp. 199–216.

[41] R Payri et al. “Hydraulic characterization of diesel engine single-hole injectors”. In: *Fuel* 180 (2016), pp. 357–366.

[42] R Payri et al. “Using spray momentum flux measurements to understand the influence of diesel nozzle geometry on spray characteristics”. In: *Fuel* 84.5 (2005), pp. 551–561.

[43] Lyle M Pickett et al. *Transient rate of injection effects on spray development*. Tech. rep. SAE Technical Paper, 2013.

[44] SB Pope. "An explanation of the turbulent round-jet/plane-jet anomaly". In: *AIAA journal* 16.3 (1978), pp. 279–281.

[45] Stephen B Pope et al. *Turbulent flows*. Cambridge university press, 2000.

[46] Portin K. *Wärtsilä gas engine development and methanol adaptation: Classnk seminar*. Tech. rep. Accessed: 2023-10-18. 2015. URL: https://www.classnk.or.jp/classnk-rd/assets/pdf/V_Wartsila_Gas_Engine_Development_Methanol_Adaptation.pdf.

[47] Scott L Post et al. "Modeling the outcome of drop–drop collisions in Diesel sprays". In: *International Journal of Multiphase Flow* 28.6 (2002), pp. 997–1019.

[48] Rolf D Reitz. "Mechanism of breakup of round liquid jets". In: *Encyclopedia of fluid mechanics* 10 (1986).

[49] Rolf D Reitz et al. "Structure of high-pressure fuel sprays". In: *SAE transactions* (1987), pp. 492–509.

[50] Kaushik Saha et al. *Coupled Eulerian internal nozzle flow and Lagrangian spray simulations for GDI systems*. Tech. rep. SAE Technical Paper, 2017.

[51] David P Schmidt et al. "A new droplet collision algorithm". In: *Journal of Computational Physics* 164.1 (2000), pp. 62–80.

[52] Convergent Science. *CONVERGE CFD Software Website*. Accessed: 2023-11-13. URL: https://convergecfd.com/.

[53] PK Senecal et al. *A new parallel cut-cell Cartesian CFD code for rapid grid generation applied to in-cylinder diesel engine simulations*. Tech. rep. SAE Technical Paper, 2007.

[54] PK Senecal et al. "Grid-convergent spray models for internal combustion engine CFD simulations". In: *Internal Combustion Engine Division Fall Technical Conference*. Vol. 55096. American Society of Mechanical Engineers. 2012, pp. 697–710.

[55] Panos Sphicas et al. "A comparison of experimental and modeled velocity in gasoline direct-injection sprays with plume interaction and collapse". In: *SAE International Journal of Fuels and Lubricants* 10.1 (2017), pp. 184–201.

[56] Shankar Subramaniam. "Lagrangian–Eulerian methods for multiphase flows". In: *Progress in Energy and Combustion Science* 39.2-3 (2013), pp. 215–245.

[57] Sebastian Verhelst et al. "Methanol as a fuel for internal combustion engines". In: *Progress in Energy and Combustion Science* 70 (Jan. 2019), pp. 43–88. ISSN: 0360-1285. DOI: 10.1016/j.pecs.2018.10.001. URL: https://linkinghub.elsevier.com/retrieve/pii/S036012851830042X (visited on 09/16/2022).

[58] Xibin Wang et al. "Spray Characteristics of High-Pressure Swirl Injector Fueled with Methanol and Ethanol". In: *Energy & Fuels* 19.6 (Nov. 2005), pp. 2394–2401. DOI: 10.1021/ef050135w. (Visited on 06/17/2022).

[59] Yang Wang et al. “Characteristics of Evaporating Spray for Direct Injection Methanol Engine: Comparison between Methanol and Diesel Spray”. In: *Processes* 10.6 (June 2022), p. 1132. DOI: 10.3390/pr10061132. (Visited on 07/13/2022).

[60] Christian Wouters et al. “Comprehensive assessment of methanol as an alternative fuel for spark-ignition engines”. In: *Fuel* 340 (2023), p. 127627.

[61] Jacopo Zembi et al. “Numerical Study of Ammonia Spray with a GDI Engine Injector”. In: *Journal of Ammonia Energy* 1.1 (2023).

[62] Wei Zeng et al. “Atomization and vaporization for flash-boiling multi-hole sprays with alcohol fuels”. In: *Fuel* 95 (May 2012), pp. 287–297. DOI: 10.1016/j.fuel.2011.08.048. (Visited on 06/17/2022).

[63] Wei Zeng et al. “Characterization of Methanol and Ethanol Sprays from Different DI Injectors by Using Mie-scattering and Laser Induced Fluorescence at Potential Engine Cold-start Conditions”. In: *SAE Technical Papers* (2010).

[64] Wei Zeng et al. “Macroscopic characteristics for direct-injection multi-hole sprays using dimensionless analysis”. In: *Experimental Thermal and Fluid Science* 40 (July 2012), pp. 81–92. DOI: 10.1016/j.expthermflusci.2012.02.003. (Visited on 06/17/2022).

[65] Zengqiang Zhu et al. “Investigation on mixture formation and combustion characteristics of a heavy-duty SI methanol engine”. en. In: *Applied Thermal Engineering* 196 (Sept. 2021), p. 117258. DOI: 10.1016/j.applthermaleng.2021.117258. (Visited on 09/20/2022).

[66] K. Zoumpourlos et al. “Methanol sprays in marine engines: CFD modelling of port fuel injection systems.” In: *Journal of Marine Engineering Technology* (2025).

[67] Konstantinos Zoumpourlos et al. “Evaluation of Methanol Sprays in Marine Internal Combustion Engines: a Case Study for Port Fuel Injection Systems”. In: *Modelling and Optimisation of Ship Energy Systems 2023* (Dec. 2023). DOI: 10.59490/moses.2023.655. URL: https://proceedings.open.tudelft.nl/moses2023/article/view/655.

Chapter 4

CFD Modelling Approach for Late-Injection Methanol Sprays Validated with ECN Spray M

To reduce emissions, methanol is a favourable carbon-neutral, producible alternative fuel, which can substitute gasoline in direct-injection spark-ignition (DISI) engines. Robust DISI engine operation relies on a consistent air-fuel mixture. To understand the physical processes that characterize the mixture formation, predictive computational fluid dynamics (CFD) simulations are used to improve the understanding, operation, and emissions of these engines. However, using an alternative fuel, such as methanol, often poses challenges to the validity of CFD simulations due to alterations in fuel properties. This chapter presents the validation of a CFD modelling approach that can be applied to the predictive modelling of DISI methanol engines. Our methodology uses Lagrangian-Eulerian methods to model the methanol eight-hole counter-bore style Spray M injector from the Engine Combustion Network (ECN). We used the Spray M1 condition, which represents a late-injection spray in a high-ambient-pressure and temperature environment. In the present chapter, we employed both a Reynolds Averaged Navier Stokes (RANS) and a Large Eddy Simulation (LES) turbulence approach in CONVERGE-CFD. To validate our models, we used the projected liquid volume (PLV) maps generated by the tomographic liquid volume fraction (LVF) based on methanol. Subsequently, we tuned our models based on the corresponding numerical predictions of the liquid penetration and LVF distributions. The results demonstrated that both the RANS and LES models could replicate the spray morphology and liquid length. While the RANS model was unable to fully capture the complex phenomena of spray collapse and sweeping in the methanol multi-hole spray, the LES model effectively reproduced these behaviours without excessive tuning effort.

This chapter was reproduced from [59]:
Zoumpourlos, K., Bekdemir, C., Geertsma, R., van de Ketterij, R., Coraddu, A. CFD modeling approach for late-injection methanol sprays validated with ECN spray M. International Journal of Engine Research. 2025. DOI:10.1177/14680874251323931

4.1 Introduction

IN the transportation sector, spark ignition (SI) internal combustion engines (ICEs) are mainly used in light and medium-duty vehicles inducing CO_2, and other harmful emissions such as NO_x, unburned hydrocarbons (UHC), CO, and soot [24, 49, 15]. Despite the recent progress of electrified vehicles, ICEs persist as the main powering solution due to their high energy density, range, and reduced cost [41, 23]. Moreover, the increased deployment of direct-injection spark-ignition (DISI) engines over the outdated port fuel injection (PFI) technology improved the efficiency and emissions of SI engines [2, 14]. To further reduce exhaust emissions and achieve the desired climate targets, alternative fuels produced from carbon-neutral sources can decarbonize ICEs [8, 60]. Methanol is regarded as a promising alternative fuel, capable of substituting gasoline in DISI engines [1], or used as a premixed fuel in dual-fuel compression ignition engines in the marine sector [8]. In particular, methanol possesses favourable combustion properties, such as high burning velocity, low combustion temperature and high octane number, resulting in reduced NO_x and soot emissions compared to gasoline [50, 49, 45]. Methanol remains in liquid form under atmospheric conditions, making storage and handling similar to those of conventional fuels [50]. Its production can be scaled up, and it effectively offers a higher energy density than other alternative fuels such as ammonia and hydrogen [48, 61]. Given these considerations, methanol is considered a viable option for direct injection (DI) engines.

With respect to both efficient combustion and low emissions, the performance of DI engines depends on the formation of a homogeneous mixture through the spray and evaporation phenomena [14]. Therefore, studying spray formation is fundamental for controlling, improving the performance, and reducing emissions of DI engines. Computational fluid dynamics (CFD) can be employed to analyze and predict in-cylinder engine phenomena, such as spray development, mixture formation, and combustion [53].

As mentioned previously in Chapter 3, using CFD to investigate methanol spray and combustion can be challenging due to the lack of dedicated experimental data for methanol. Existing CFD modelling practices have only been verified using conventional fuels, which are calibrated based on their physical properties. In contrast, the physical properties of methanol differ significantly from those of gasoline. Methanol's latent heat of vaporization is approximately four times higher than gasoline's, which enhances the evaporation cooling effect observed in DI engines [50]. Furthermore, at elevated injection temperatures, methanol has an augmented vapor pressure and a lower boiling point. This makes it more volatile than gasoline and increases in-nozzle cavitation phenomena. This inherent disparity between the properties of methanol and gasoline affects the spray structure and evaporation phenomena; thus, the lack of methanol experimental data renders the validity of CFD simulations questionable.

Previous experimental research revealed that under low ambient temperatures, methanol displays a different spray structure compared to gasoline [51, 56, 55, 57]. These conditions comprised of low to medium injection pressures (50 to 150 bar), and variable ambient environments ranging from atmospheric to sub-atmospheric conditions linked to cold-start operation [56, 55]. While methanol demonstrated a similar spray structure with gasoline under barely evaporating conditions [51], its higher volatility increased the evaporation

rate and spray cone angle [55]. In another study by Zeng et al. [56] in a sub-atmospheric pressure environment, increasing the methanol temperature caused a faster transition to flash-boiling spray which can potentially enhance the cold-start performance.

Recent experimental studies have employed more engine-relevant multi-hole counter-bore gasoline injectors, using methanol and iso-octane, in environments with increased ambient temperatures. Particularly, the study of Badawy et al. [3] revealed a more pronounced difference in the methanol spray structure under realistic DISI conditions. In the same study, even at atmospheric pressure and 80 °C fuel temperature, the methanol spray plumes displayed evident spray collapse, highlighting a significantly different structure than that of iso-octane. Furthermore, the engine combustion network (ECN) [16] has conducted methanol spray experiments using an eight-hole counter-bore injector under the same conditions as Spray G [18]. These new Spray M experiments [32] consist of a late-injection, stratified DISI operation dataset, and an early-injection flash-boiling condition dataset. Similarly, the findings of Badawy et al. [3] are consistent with the ECN results, which showed strong spray collapsing phenomena for both tested conditions, confirming the influence of methanol's volatility. In addition, using a set of ECN Spray G conditions, Hwang et al. [21] compared iso-octane with di-isobutylene surrogate, olefinic, and the 30% ethanol blend (E30) sprays. Under the tested conditions, the non-isooctane fuels demonstrated plume collapsing due to higher volatility. These findings strongly indicate that the vapour pressure influences the spray structure under DISI engine operation.

Concerning methanol engine studies, the focus was mainly on investigating combustion performance and emissions [47, 58, 11, 33]. Due to methanol's high latent heat of vaporization, a strong cooling effect is introduced during the mixture formation, which lowers the in-cylinder temperature, and may cause cyclic variability and wall impingement [61]. Wouters et al. [54] demonstrated that methanol wall film formation is three times stronger than in gasoline operation, due to the slower evaporation rate. Matamis et al. [33] conducted experiments in an optically accessible heavy-duty methanol engine and showed increased ignition delay. This cooling-effect-induced ignition delay impeded the flame propagation, demonstrating the effect of methanol sprays during engine operation. Furthermore, Dierickx et al. [10] observed that the intensified cooling effect resulted in methanol condensation within the intake manifold. As a result of the reported lower in-cylinder and intake air temperatures, NO_x emissions and heat losses decreased compared to diesel [10, 11, 47, 58] and gasoline operation [54]. Thus, methanol operation diminishes the trade-off between thermal efficiency and emissions while improving the carbon footprint [25].

With respect to CFD modelling studies, very limited research has been conducted on methanol sprays in DI conditions due to the scarcity of experimental data. The recent Spray M experiment is the first publicly available dataset, which provides a validation basis for future methanol-dedicated spray modelling approaches [32]. Furthermore, Duronio et al. [12] applied a novel unified droplet breakup modelling approach to simulate the Spray G and M conditions. To eliminate the tuning effort required for state-of-the-art breakup models, their approach combined a flash-boiling effervescent model with a dynamic aerodynamic breakup model, successfully recreating the methanol and E00 experiments in both late and early-injection conditions. Before the recent methanol ECN datasets, previous computational efforts mainly used the established Spray G [18]

datasets to tune and validate Lagrangian spray models employing iso-octane [37, 27, 26, 29] and E30 [5]. Using a similar approach, Moreno Cabezas et al. [35] validated their volume-of-fluid (VoF) and Lagrangian modelling framework based on the iso-octane ECN Spray G. Following this, they converted the model for methanol injection using the same injection and ambient conditions. Their results illustrated increased spray plume angles for the methanol injection, confirming past experimental observations [55]. However, with the recent understanding from Spray M, the CFD model was expected to predict plume collapsing due to the volatility of methanol.

This suggests that the conventional state-of-the-art modelling approaches are not sufficient for predicting the methanol vapor pressure and latent heat effects on spray formation. While the use of iso-octane datasets and modelling frameworks offers a solid foundation for understanding DISI sprays, it is imperative to transfer this knowledge to alternative fuels, such as methanol. Thus, to ensure robust tuning and calibration of CFD models, experimental data dedicated to methanol should be employed.

4.1.1 Aim & Novelty

This chapter aims to model the ECN methanol Spray M experiment using the Lagrangian-Eulerian framework. The novelty of the present study comprises the presented modelling framework, which is able to capture the complex multiphase flow phenomena of methanol injection. While previous studies have demonstrated that CFD modelling can accurately replicate the ECN spray G data using iso-octane, a similar CFD study using the recent methanol Spray M data for tuning the conventional wave breakup model is lacking. Therefore, to accurately model sprays and understand the impact of methanol in the mixture formation, CFD model calibration should be conducted using proper methanol experiments.

For our analysis, we employed a spray model using CONVERGE-CFD [6], which incorporates both Reynolds Averaged Navier-Stokes (RANS) and Large Eddy Simulation (LES) turbulence models. Using both turbulence approaches, we tested the ability of each model to capture the plume-collapsing behaviour of methanol under the designated DISI conditions. Our aim was to accurately predict the experimental trends using computationally inexpensive RANS models, which can be employed for full engine CFD simulations at a later stage. Accordingly, the RANS models were compared with the more computationally intensive and high-fidelity LES approach.

For model validation, we used the spray M1 experimental condition, which corresponds to late-injection stratified DISI conditions. These conditions are characterized by an increased ambient pressure and temperature. To compare our numerical results with the experiments, we used the projected liquid volume (PLV) maps for liquid penetration characterization [30]. Furthermore, using the RANS approach, we conducted a sensitivity analysis over a range of modelling parameters. We tuned the cone angle (CA), plume direction (PD), and breakup model constants of the framework to capture the spray momentum and morphology. The analysis demonstrated an increased sensitivity of the Rayleigh-Taylor size and time constants on liquid penetration and spray collapsing behaviour. Despite the systematic calibration effort, the RANS model showed weaker spray collapsing compared to the experiment. Subsequently, the calibrated model

parameters were used in a matching LES model, which more accurately captured the plume collapsing phenomenon. Our findings suggest that methanol injection can be sufficiently predicted under late-injection stratified DISI conditions, using state-of-the-art high-fidelity LES modelling along with a RANS-driven calibration.

4.2 Experimental Background: ECN Spray M1 Methanol

THE present study uses the publicly available data from ECN Spray M1 methanol, which resembles stratified late-injection conditions in conventional Gasoline Direct Injection (GDI) engines [32]. The experiments deployed a new GDI-style injector consisting of an eight-hole counter-bore configuration [28] operating at an injection pressure of up to 200 bar. Figure 4.1 illustrates the configuration of the eight-hole injector along with the detailed nozzle topology. The geometrical features of the nozzle, such as the plume direction (PD), serve as input to our simulations and provide a basis for tuning the presented modelling approach. The experiments covered a range of ambient conditions, from early-injection flash boiling at low ambient pressure to late-injection at high ambient pressure and temperature. The details of the replicated ECN experiment are presented in Table 4.1.

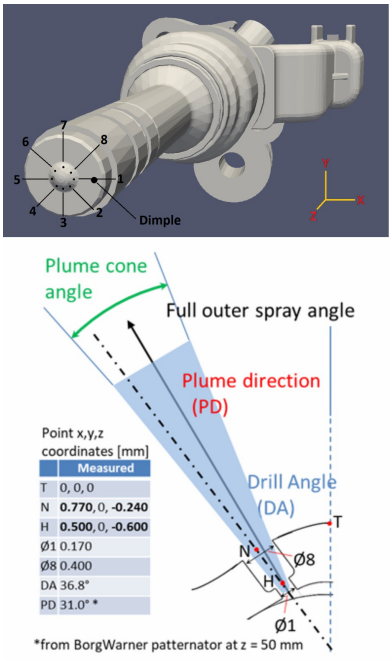

Figure 4.1: ECN Spray M nozzle geometry [32]

Table 4.1: Experimental conditions & injector details for late-injection Methanol Spray M1

Ambient Pressure	6 bar
Ambient Temperature	573 K (300 °C)
Ambient Gas	N_2
Fuel Temperature	363 K (90 °C)
Injection Pressure	200 bar
Injection Quantity	9.75 mg
Injection Duration	0.74 ms
Nozzle Diameter	0.170 mm
Counter-bore Diameter	0.400 mm
Number of Holes	8

4.2.1 Experimental Method

The Spray M experimental campaign was performed by Sandia National Laboratories in their optically accessible constant-flow spray vessel (SV). A detailed explanation of the employed imaging technique and experimental apparatus can be found in a corresponding study by Hwang et al. [21]. In particular, the characterization of the spray's liquid phase was conducted by means of projected liquid volume (PLV) using diffused back illumination (DBI) extinction imaging [52]. Using the DBI method, the liquid volume fraction (LVF) can be reconstructed in the three-dimensional space using computer tomography (CT). By measuring the emitted light intensity, the optical thickness of the spray (τ) was calculated, while the resulting PLV can be computed by the following expression:

$$PLV = \tau \frac{\pi d^3/6}{C_{ext}} = \int_{-y_\infty}^{y_\infty} (LVF)\, dy, \tag{4.1}$$

where d is the expected droplet diameter, and C_{ext} is the extinction coefficient. For the expected droplet diameter, we assumed a Sauter mean diameter (SMD) of 10 μm, while we used a C_{ext} of $79.54 \cdot 10^{-6}$mm^2 to estimate the experimental PLV maps. These values were selected according to the ECN guidelines in conjunction with the reported sensitivity analyses from similar condition gasoline and E30 studies [5, 18, 32, 21]. By setting a threshold for the PLV maps, the experimental results can be directly compared with the CFD results, as shown in the following section.

4.2.2 Collapsing Behavior of Methanol Spray & Comparison with Iso-octane

For the Spray G experiments, the ECN used iso-octane as a surrogate for gasoline fuel [18]. Compared to iso-octane, methanol exhibits vastly different physical properties, as shown in Table 5.1. Mainly, methanol's high latent heat of vaporization, which is four times higher compared to iso-octane, creates an intensive evaporation cooling effect [50]. Considering also the decreased lower heating value, methanol requires up to eight times more thermal energy to form a combustible mixture with similar energy density compared to conventional fuels [61]. Additionally, methanol is more volatile than iso-octane, due to its

higher vapor pressure. Thus, methanol evaporates faster than iso-octane while drawing more energy from the surrounding air, due to its latent heat.

Table 4.2: Fuel Properties [50, 21, 3]

Property	Iso-octane	Methanol
Lower Heating Value (LHV) [MJ/kg]	44.3	20.1
Density (at STP) [kg/m^3]	692	790
Heat of Vaporization (at 1 bar) [kJ/kg]	270	1089
Boiling Point (at 1 bar) [°C]	99	65
Vapor Pressure (at 90 °C) [kPa]	70.9	256
Surface Tension (at 20 °C) [mN/m]	18.6	23
Dynamic Viscosity (at 20 °C) [mPa·s]	0.5	0.57

These reasons render the fluid mechanics and heat transfer phenomena of methanol sprays significantly different from those of iso-octane spray cases. Different results were observed experimentally in the same GDI conditions using iso-octane [18] and methanol [32]. In both experimental cases, the iso-octane and methanol injections maintained identical injection durations, injected masses, and ambient conditions. Although the two experimental campaigns employed slightly altered injectors, the difference in the results is attributed to the inherent variation of the fuel properties. Specifically, for the same late-injection condition (573 K ambient temperature and 6 bar ambient pressure), while the liquid penetration until the end of injection (EOI) is identical (until 1.3 ms aSOI in Figure 4.2), methanol evaporation duration is prolonged increasing the liquid residence time in the SV. Although methanol is more volatile due to its high vapour pressure, its high latent heat of vaporisation slows the overall evaporation process, as more energy is absorbed from the ambient gas. These two physical properties strongly affect the methanol spray morphology, as illustrated in Figure 4.3. In the methanol case, a strong spray-collapse and sweeping behaviour are observed, which merges the spray plumes into a single centre-line plume. This phenomenon further increases the evaporation duration due to the smaller effective area for heat transfer between the liquid and the ambient gas. In the corresponding iso-octane experiment, the spray plumes remain intact, while evaporation occurs on faster time-scales without interactions between individual plumes. Eventually, the physical properties of methanol, especially its vapour pressure and latent heat, challenge the spray modelling of multi-hole counter-bore injectors.

4.3 Methodology

THIS section introduces the proposed CFD modelling approach, which was developed using the CONVERGE v3.1 CFD software [6]. Our methodology is based on the Lagrangian-Eulerian framework [46]. To model turbulence, we employed both a RANS approach, utilizing the RNG $k-\varepsilon$ model [19], and a LES approach, using the dynamic structure model [39]. To solve the conservation equations, the density-based solver [7] was used in conjunction with the Pressure Implicit with Splitting of Operators (PISO) algorithm [22]. The accuracy of the numerical scheme is first order with respect to

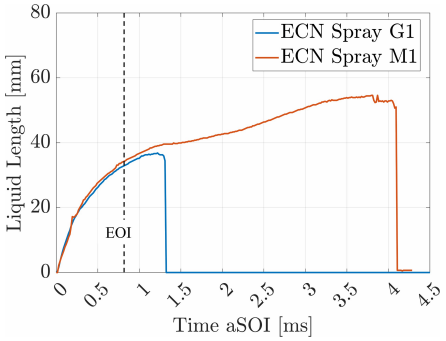

Figure 4.2: Liquid Penetration of Spray G1 & Spray M1 [18, 32]

time and second order in space. In addition, to calculate the simulation time-step, the Courant-Friedrichs-Lewy (CFL) criterion was used to ensure numerical stability [6, 17]. Finally, the thermodynamic properties of methanol and nitrogen were estimated by the Redlich-Kwong equation of state [20].

4.3.1 Lagrangian Spray Model

The multiphase modelling approach uses the Lagrangian Particle Tracking (LPT) method to simulate the liquid phase as a set of liquid parcels. For the gaseous phase, comprising the ambient medium and evaporated methanol, the Eulerian method is employed. The coupling between the liquid and gaseous phase is secured through the exchange of mass, momentum, and energy with respective source terms in the transport equations [46]. In the LPT technique, parcels require an additional set of phenomenological models that describe sub-grid fluid phenomena, such as breakup, collisions, evaporation, and turbulence effects. It should be noted that the presented Lagrangian-Eulerian framework is specifically applicable to liquid fuels injected under conditions outside the flash-boiling regime.

The computational parcels are initially injected using the Reitz and Diwakar model [42]. The injection model treats the droplets as 'blobs' with an initial diameter equal to the effective nozzle diameter. Subsequently, the parcels experience breakup due to flow instabilities originating from their interaction with the ambient gas. We used the combined wave model [4], which employs Kelvin-Helmholtz (KH) and Rayleigh-Taylor (RT) hydrodynamic instabilities to calculate the timescales and length scales for the resulting droplets (more information is provided in the following section). Moreover, the No Time Counter (NTC) algorithm [43] was used to predict the parcel collisions. We also used the model of Post and Abraham [40] to calculate the post-collision outcomes, which encompass bouncing, stretching, reflective separation, and coalescence.

To ensure the interaction of the parcels with the ambient gas, we used additional models for the aerodynamic drag forces and the turbulent phenomena. The aerodynamic drag force was calculated using the dynamic drag model, which considers the droplet distortion for calculating the drag coefficient [31]. Specifically, to consistently calculate the drag coefficient, the dynamic drag model uses the Taylor Analogy Breakup (TAB)

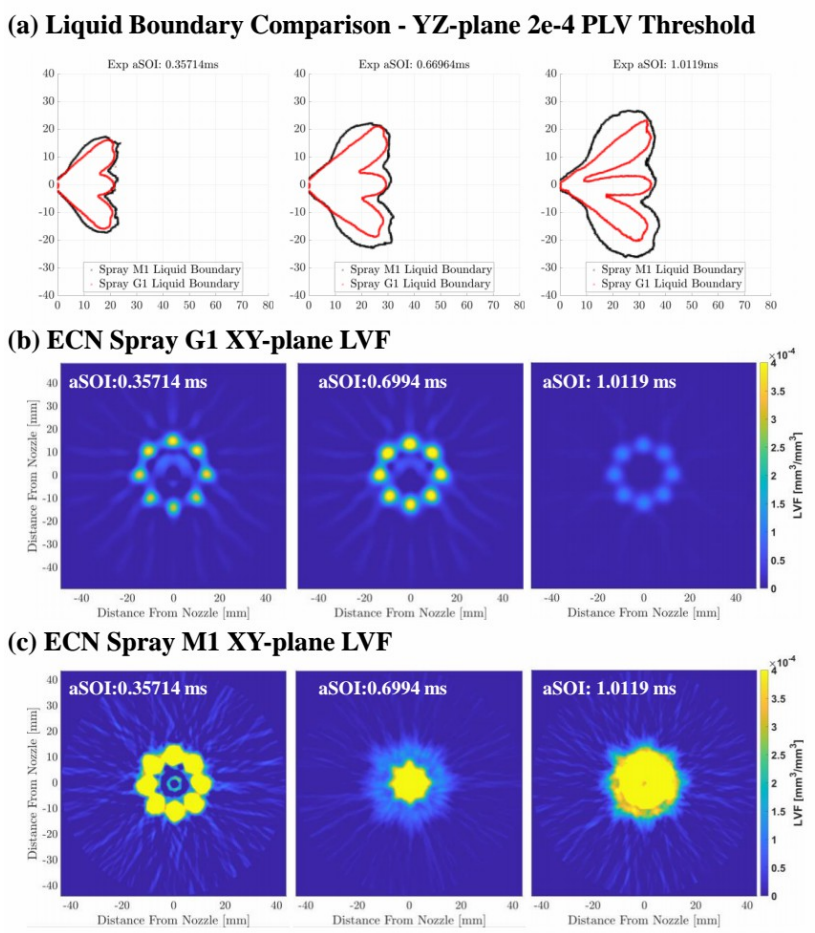

Figure 4.3: Spray G1 & Spray M1: (a) Experimental comparison of projected Liquid boundary measured by DBI extinction imaging with extinction threshold set as $0.2 \cdot 10^{-3} mm^3$(liquid)$/mm^2$. (b) & (c) LVF at perpendicular XY-plane of the injection direction - z = 15 mm distance from nozzle exit [18, 32]

model to estimate the droplet distortion. The effects of turbulence were regarded using the turbulent dispersion model of O'Rourke [36]. Lastly, the Frossling-correlation-based evaporation model was used to calculate the droplet evaporation, which assumes a uniform temperature profile within each parcel [7]. The summary of the adopted spray models is presented in Table 5.3.

Droplet Breakup Model

As mentioned in the previous section, the KH-RT model is adopted for the droplet breakup of the injected methanol [4]. For better agreement with the experiment, the breakup length of the model was set to zero, enabling immediate competition between the KH

Table 4.3: Numerical models

Physical Phenomena	Numerical Models
Fluid Flow	Navier Stokes, density-based solver [7]
Turbulence	RNG $k-\varepsilon$ model [19] & LES Dynamic Structure model [39]
Droplet Injection	Blob model [42]
Droplet Breakup	KH-RT model [4]
Droplet Drag Force	Dynamic Drag Model [31]
Droplet Collision	NTC model [43]
Droplet Coalescence	Post Collision Outcome model [40]
Droplet Turbulent Dispersion	O'Rourke [36] model
Droplet Evaporation	Frossling correlation-based & boiling model [7]

and RT breakup as each parcel exits the counter-bore region [5]. Additionally, we also tested the modified KH-RT model by Patterson and Reitz [38], which does not require a breakup length to activate the RT model. Similarly, as in a previous ECN Spray G study [27], this modified model under-predicted liquid penetration; therefore, the Beale and Reitz model [4] was selected as the most appropriate for our study. The inherent distinction between these two models lies in the need to input a predefined breakup length. The Beale and Reitz model [4] requires a predefined breakup length to establish the onset of competition between KH and RT mechanisms. In contrast, the Patterson and Reitz model [38] calculates the breakup process directly without relying on a predefined length. This approach proves inaccurate for our case, as the Patterson and Reitz model first determines the occurrence of RT instability before testing whether the KH instability criterion is met. Thus, the potential fulfilment of RT breakup omits the KH breakup criterion while favouring the RT breakup. On the contrary, the Beale and Reitz model simulates a concurrent competition between the two mechanisms.

The Kelvin-Helmholtz hydrodynamic instabilities result from unstable shear waves growing between the high velocity liquid spray surface and the ambient gas. If these surface waves grow for a sufficient time, they cause liquid detachment from the parcels and, eventually, form smaller new parcels. The newly formed child parcels have a radius r_c, which is proportional to the wavelength of the instability, and is calculated by the following expression [4]:

$$r_c = B_0 \Lambda_{KH}, \tag{4.2}$$

where Λ_{KH} is the wavelength of the fastest growing wave, and B_0 is the KH model size constant. The decreasing parent parcel radius r_p can be estimated as follows:

$$\frac{dr_p}{dt} = -\frac{(r_p - r_c)}{\tau_{KH}}, \tag{4.3}$$

where the breakup time τ_{KH} is established as:

$$\tau_{KH} = \frac{3.726 B_1 r_p}{\Lambda_{KH} \Omega_{KH}}, \tag{4.4}$$

where B_1 is the breakup time constant, and Ω_{KH} is the growth rate of the Λ_{KH} wavelength. Moreover, after droplet breakup, the child parcels accumulate liquid mass from the parent parcel. To estimate the accumulated mass, a shed factor s is used, which determines the fraction of the mass of the parent parcel that is transferred to child parcels.

Furthermore, the RT model is based on Rayleigh-Taylor hydrodynamic instabilities, which occur due to deceleration of the high-speed liquid jet exiting the nozzle. This deceleration also causes unstable waves, which are perpendicular to the spray tip and cause droplet breakup [4]. Breakup occurs once the wavelength scale ($C_{RT}\Lambda_{RT}$) becomes smaller than the diameter of the parent droplet, and given that the RT waves have grown on the droplet surface for a period longer than the breakup time. Similarly with the KH model, the RT breakup time τ_{RT} is calculated by the following equation:

$$\tau_{RT} = \frac{C_\tau}{\Omega_{RT}}, \tag{4.5}$$

where C_τ is the RT breakup time constant, and Ω_{RT} is the fastest wave growth rate. The resulting child droplet radius r_c is given by the following expression:

$$r_c = \frac{C_{RT}\Lambda_{RT}}{2} \tag{4.6}$$

4.3.2 Computational Domain & Mesh

To accommodate the numerical calculations, we generated a cylindrical geometry to replicate the SV conditions of the ECN Spray M experiment (Figure 5.2). For the cylinder dimensions, we used a radius of 54 mm and height of 83 mm, which were defined according to previous modelling practices of ECN sprays [5, 9, 61, 29]. The cylinder boundary conditions were assigned as wall-type Dirichlet for the temperature and Neumann for the turbulent kinetic energy. The wall temperature was set as 573 K, similar to the ambient temperature of the constant-flow SV. For the grid generation, we employed the CONVERGE cut-cell Cartesian method [7, 44] using a base cell size of 2 mm for the RANS simulations, and 1.3 mm for the LES cases.

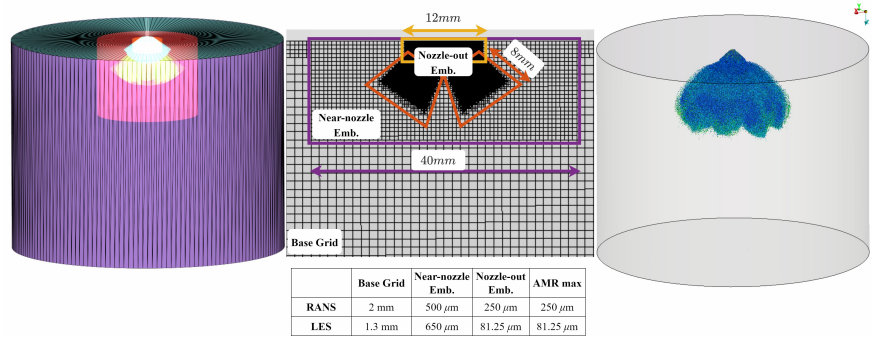

	Base Grid	Near-nozzle Emb.	Nozzle-out Emb.	AMR max
RANS	2 mm	500 μm	250 μm	250 μm
LES	1.3 mm	650 μm	81.25 μm	81.25 μm

Figure 4.4: Computational domain for the constant-flow spray vessel, the employed mesh grid strategy, and the Lagrangian parcels

To obtain a higher fidelity mesh, we applied fixed embedding in areas of interest, while the adaptive mesh refinement (AMR) algorithm was used for automatic refinements on the basis of velocity and methanol species gradients. Three different types of fixed embedding were used, two in the nozzle-out region and one in the outer near-nozzle area. To resolve the nozzle-out flow, a spray-cone and a cylindrical-style refinement were utilised, accomplishing a grid size of 250 μm for the RANS, and 81.25 μm for the LES simulations. On the other hand, the near-nozzle region was refined in a cylindrical style using a grid size of 500 μm for the RANS, and 650 μm for the LES simulations to avoid excessive computational costs. The details of the meshing strategy are presented thoroughly in Figure 5.2. Regarding the AMR strategy, in the RANS cases, the maximum embedding level was set as 3 leading to a minimum cell size of 250 μm. The adopted meshing strategy aligns with similar iso-octane and E30 study using multi-hole counterbore injectors [5]. For the LES simulations, we set a maximum embedding level of 4, obtaining a minimum cell size of 81.25 μm. Finally, the sub-grid embedding criterion for the AMR was set as 0.1 m/s for velocity refinement and 0.001 methanol mass fraction for species refinement. Based on the numerical predictions, the adopted meshing strategy was deemed trustworthy and robust in terms of numerical accuracy and computational cost [44].

4

4.3.3 Numerical Model Settings

The complete settings of the presented numerical framework are depicted in Table 5.4. To obtain a realistic value for the turbulence conditions prior to injection, we used the available ECN spray G particle-image-velocimetry (PIV) measurements to estimate the initial turbulent intensity inside the constant-flow SV [18]. As a result, more realistic predictions were achieved as the methanol experimental campaign used the same conditions as the Spray G experiments. A sensitivity analysis on the initial turbulence intensity can be found in the study by Bestel et al. [5].

Table 4.4: Model Settings

Breakup Model	
KH Model size & breakup time constants	$B_0 = 0.6, \quad B_1 = 50$
KH Shed factor	$s = 0.5$
RT Model size & breakup time constants	$C_{RT} = 0.6, \quad C_\tau = 0.5$
RANS Turbulence Model	
RNG $k-\varepsilon$ constants	$C_\mu = 0.0845, \quad C_{\varepsilon 1} = 1.42, \quad C_{\varepsilon 2} = 1.68,$ $C_{\varepsilon 3} = -1.0$
Initial Turbulence Intensity	
Turbulent Kinetic Energy (TKE)	$k_0 = 6.4 \cdot 10^{-3} m^2/s^2$
TKE Dissipation Rate	$\varepsilon_0 = 5.08 \cdot 10^{-1} m^2/s^3$ (for the RANS model only)
Mass Diffusivity	
Methanol diffusivity constants	$D_0 = 1.336 \cdot 10^{-5}, \quad n_0 = 1.8$

For the calculation of liquid penetration, we used the new ECN liquid penetration length definition [30]. The computational results were post-processed using a set of

ECN-provided Python scripts [16], which calculate the PLV maps by projecting the liquid volume fraction (LVF) across the y-direction. Using the PLV maps, the ECN recommends using a 'low' and a 'high' threshold for the comparison with the experimental data. These thresholds are calculated as follows:

$$PLV = \int_{-y_\infty}^{y_\infty} (LVF)\,dy = 0.2 \cdot 10^{-3} \frac{\text{mm}^3(\text{liquid})}{\text{mm}^2} \quad 2.0 \cdot 10^{-3} \frac{\text{mm}^3(\text{liquid})}{\text{mm}^2} \tag{4.7}$$

In our study, we used the 'low' threshold $0.2 \cdot 10^{-3}$ to plot the liquid boundary and, subsequently, compare it with the corresponding computer tomography LVF results. A visual representation of the CFD post-processing procedure and comparison with the experiments is illustrated in Figure 4.5.

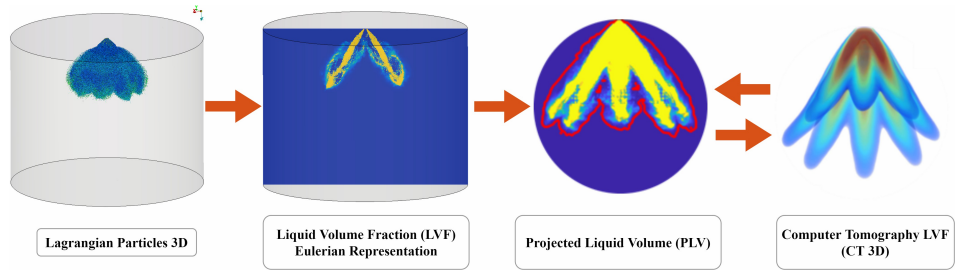

Figure 4.5: Calculation of liquid penetration and comparison with experimental DBI data [21, 29]

Injector Nozzle Parameters

Table 4.5 depicts the nozzle parameters which were used for the present study. Compared to iso-octane, methanol exhibits a higher vapour pressure and lower boiling point (Table 5.1), which increases the probability of methanol vapour in the nozzles. As a result, under similar conditions, cavitation phenomena might be increased during methanol injection, leading to a smaller effective nozzle area and higher initial jet momentum. Previous in-nozzle flow [34] and LPT [27, 26] simulations using the spray G nozzle used a discharge coefficient value of 0.4815 and 0.5, respectively. In our study, to account for this augmented methanol in-nozzle cavitation, we set the discharge coefficient C_d as 0.47 to match the initial momentum of the liquid jet based on a sensitivity study.

Due to the absence of the nozzle geometry file, the injected parcels were initialised at the counter-bore exit (N in Figure 4.1) rather than the nozzle-exit location (H in Figure 4.1). This technique was proven valid by Kumar et al. [27], who compared different injection locations for the spray G nozzle. They stated that adequate predictions can be obtained by using the counter-bore exit injection location along with the experimentally measured mass flow rate of injection (ROI) profile. Moreover, we used the Spray M1 ROI profile (Figure 4.6), which is provided by ECN [32]. Lastly, similarly to the iso-octane study of

Table 4.5: Used Nozzle Parameters for ECN Spray M1 numerical framework

Discharge Coefficient	$C_d = 0.47$
Velocity Coefficient	$C_v = 0.80$
Cone Angle	33°
Plume Direction	34°
Number of Parcels per Nozzle	RANS: 70000, LES: 150000

Bestel et al. [5], the parcels were injected using a uniform distribution, which equally allocates the parcels across the spray plumes.

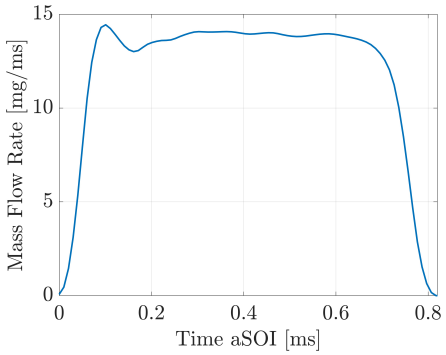

Figure 4.6: Injection Rate Profile for ECN Spray M Injector using methanol [32]

4.4 Results

OUR study adopted a structured simulation plan to investigate the predictive capabilities of the presented framework. Initially, using the RANS turbulence approach, we performed a set of simulations altering the KH-RT breakup constants. By assessing the impact of each breakup constant individually, we selected the best-performing constants and calibrated our model for methanol injection. Consequently, the calibrated model was compared with a corresponding LES model using the same breakup constants. Lastly, in the appendix, an evaluation of the plume cone angle sensitivity is presented for both the calibrated RANS and LES models.

4.4.1 Assessment of KH-RT Breakup Model Constants

Influence of KH Time Constant & Shed Factor

This section covers the parametric investigation for the KH model time constant B_1 and the shed factor. These values were altered independently each time to evaluate their individual impact on the methanol spray. The parametric sweep was systematically performed to ensure physically accurate values that adhered to mass and momentum

conservation. Thus, the KH model time constant B_1 ranged from 10 to 50, inducing fast to slow KH breakup occurrence. The shed factor ranged from 0.1 to 1.0 representing 10 % to 100 % of the parent parcel mass transferred to child parcels. The RT model parameters were kept constant according to the baseline modelling framework that was presented in Table 5.4. For all of the presented liquid plots, the 'low' threshold $0.2 \cdot 10^{-3}$ was imposed on the generated PLV maps according to ECN guidelines.

Based on the KH model formulation presented in the previous section, increasing the B_1 constant amplifies the KH breakup time τ_{KH}, which in turn decreases the breakup rate and the KH breakup occurrence. Figure 4.7 presents the spray liquid penetration and liquid width for a range of KH time constants. The spray liquid width is plotted for two axial cross-sections at 15 mm and 25 mm downstream distance from the nozzle tip. Moreover, increasing the B_1 constant does not significantly affect the liquid penetration. Contrary to that, we observe a minor increase in the 15 mm cross-section liquid width, which aligns better with the experimental liquid width. The spray morphology was also similar for all tested parameters, indicating a minor impact from the time constant calibration.

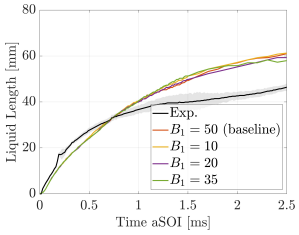

(a) KH Time Constant Sensitivity on Liquid Penetration Length

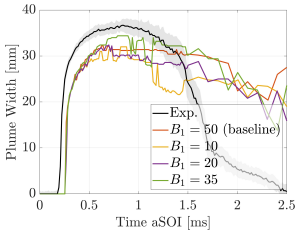

(b) KH Time Constant Sensitivity on Liquid Width at $z = 15$ mm axial cross-section from nozzle exit

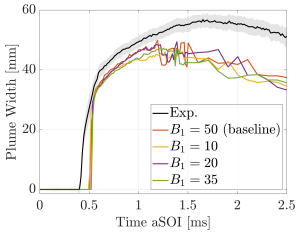

(c) KH Time Constant Sensitivity on Liquid Width at $z = 25$ mm axial cross-section from nozzle exit

Figure 4.7: Impact of KH Time Constant on Liquid Penetration & Width using the RANS modelling approach.

On the other hand, increasing the shed factor leads to higher mass fractions in the resulting child parcels after KH breakup occurrence. The influence of the shed factor in liquid penetration and width is shown in Figure 4.8. While the impact on liquid length is negligible, the shed factor 1.0 model captures better the spray width evolution until 1.5 ms after the start of injection (aSOI). The spray width remains constant in the later stages after the EOI, contrary to experimental observations, which note a decrease. This could possibly be attributed to accumulated droplets in the spray plume tips, which cause decreased evaporation (discussed in the following section). The difference in the qualitative comparison in the LVF distribution is negligible and, therefore, is not presented here. In conclusion, in the present RANS model, the global liquid penetration and width results are insensitive to alterations in B_1, while a shed factor of 1.0 yields a slightly improved prediction of the spray width.

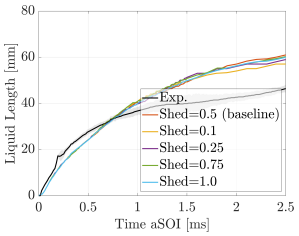

(a) KH Shed Factor Sensitivity on Liquid Penetration Length

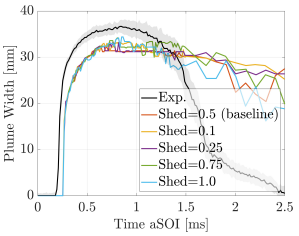

(b) KH Shed Factor Sensitivity on Liquid Width at $z = 15$ mm axial cross-section from nozzle exit

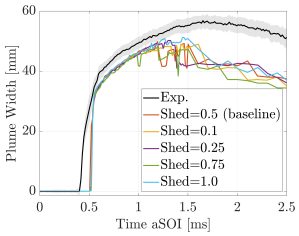

(c) KH Shed Factor Sensitivity on Liquid Width at $z = 25$ mm axial cross-section from nozzle exit

Figure 4.8: Impact of KH Shed Factor on Liquid Penetration & Width using the RANS modelling approach.

4

Influence of RT Size & Time Constant

The RT model constants were investigated based on their impact on the global spray results. Similarly with the KH model, the RT time constant C_τ determines the breakup time τ_{RT} and the RT breakup occurrence. Further, the RT size constant C_{RT} influences the size of the child parcels after the RT breakup. Increased values of the C_{RT} are expected to increase the spray momentum in the later stages after the EOI due to the delayed evaporation by the larger child parcels. Both of the investigated RT model constants ranged from 0.1 to 1.0, complying with recommended values [7]. This influence on liquid penetration and width is confirmed by Figure 4.9. For lower values of C_{RT}, the liquid length increases steeply until 1.7 ms, where the extremely small droplets evaporate abruptly, causing a massive decrease in liquid length. The initial increase in penetration can be attributed to the smaller drag force acting on the parcels due to their decreased diameter. Furthermore, the liquid width is massively under-predicted, which confirms the augmented evaporation occurring on the periphery of the spray plumes.

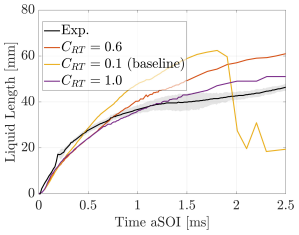

(a) RT Size Constant Sensitivity on Liquid Penetration Length

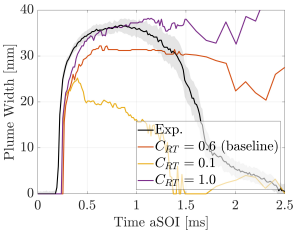

(b) RT Size Constant Sensitivity on Liquid Width at $z = 15$ mm axial cross-section from nozzle exit

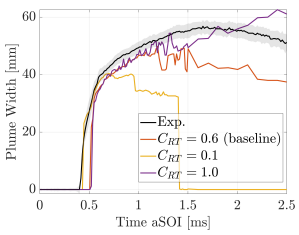

(c) RT Size Constant Sensitivity on Liquid Width at $z = 25$ mm axial cross-section from nozzle exit

Figure 4.9: Impact of RT Size Constant on Liquid Penetration & Width using the RANS modelling approach.

For the lower C_{RT} values, abrupt evaporation and narrower plume morphology are also highlighted by the comparison with the experimental liquid boundary in Figure 4.10. Increased C_{RT} values demonstrate a better agreement with the experimental liquid bound-

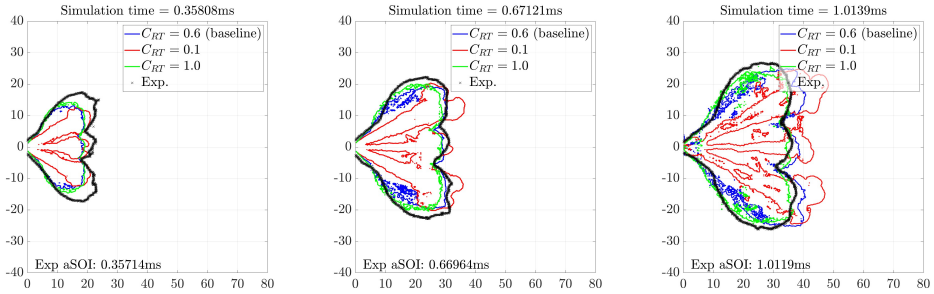

Figure 4.10: Liquid boundary derived by means of projected liquid volume (PLV) maps: Comparison for different C_{RT} values.

ary, liquid length and liquid width. Figure 4.11 depicts the plume-averaged LVF in the radial direction, which is perpendicular to the spray axis and at a distance of 15 mm downstream from the injector tip. The narrower plumes exhibit an accumulation of liquid in the centre of the plume, which causes an over-prediction of the LVF. Using a C_{RT} value of 1.0 creates a wider plume, which quantitatively adequately matches the experimental LVF during the spray formation stages before the EOI. During the later stages of the spray formation, the plume collapsing phenomenon, highlighted by the accumulation of LVF in the spray center-line axis, is not predicted adequately by the C_{RT} = 1.0 model. This reveals the weakness of the RANS model in capturing both the correct liquid length and the spray collapsing behavior of methanol.

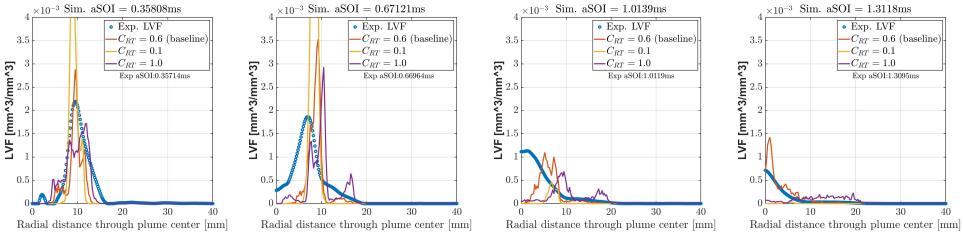

Figure 4.11: Quantitative plume-averaged Liquid Volume Fraction (LVF) at z = 15 mm axial cross-section from nozzle exit: Comparison for different C_{RT} values.

A similar trend is also observed in the parametric investigation of the RT time constant. Increasing the C_τ constant in Figure 4.12 leads to delayed RT breakup occurrence. Subsequently, the liquid length decreases, while the model captures more adequately the spray outward expansion. In Figure 4.13, despite the over-prediction in liquid length, the spray morphology and the liquid width is similar to the experimental plume morphology. The LVF in the radial direction is presented in Figure 4.14 for the tested range of C_τ constants. For a C_τ value of 1.0, spray collapsing is diminished, while the accumulation of liquid in the center of the plume decreases. This strongly indicates the significant influence of the RT model on spray penetration, spray morphology, and plume collapsing. Increasing both the RT size and time constants leads to a better agreement in the spray momentum (i.e.,

liquid length and liquid width) and the spray morphology. However, smaller values of the constants inflict a more pronounced spray collapsing, which is typical of the methanol injection ECN experiment. To more precisely tune these parameters, near-nozzle and Sauter Mean Diameter (SMD) measurements are required to accurately capture both the initial spray momentum and post-injection phenomena, including the plume collapsing and the subsequent outward spray sweeping.

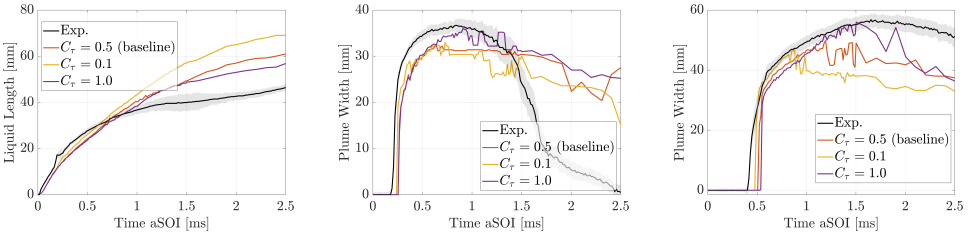

(a) RT Time Constant Sensitivity on Liquid Penetration Length

(b) RT Time Constant Sensitivity on Liquid Width at $z = 15$ mm axial cross-section from nozzle exit

(c) RT Time Constant Sensitivity on Liquid Width at $z = 25$ mm axial cross-section from nozzle exit

Figure 4.12: Impact of RT Time Constant on Liquid Penetration & Width using the RANS modelling approach.

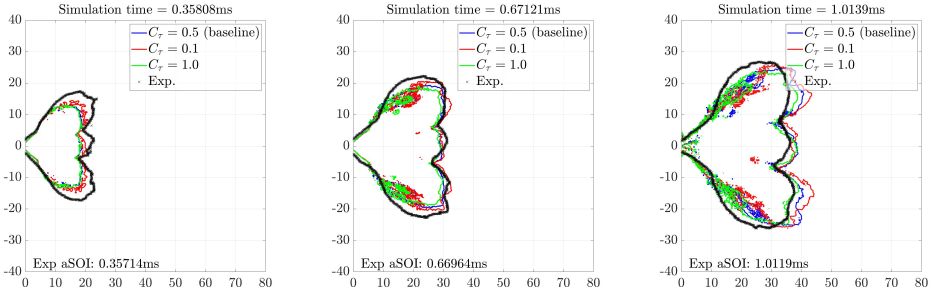

Figure 4.13: Liquid boundary derived by means of projected liquid volume (PLV) maps: Comparison for different C_τ values.

4.4.2 RANS Spray Model Calibration

Based on the evaluation of the KH-RT constants, we ran a calibrated RANS model combining the best performing parameters. For the KH constants, we maintained the same value for the time constant as it demonstrated minimal contribution to the spray results. Similarly, with the study of Bestel et al. [5], the shed factor was increased to 1.0 due to its potential to capture the spray morphology better. Furthermore, the tuning of the RT model was more impactful as both the size and time constants significantly affected the simulated methanol spray. Based on the available experimental LVF measurements, we determined a value of 1.0 for both of these constants, enabling accurate capture of liquid

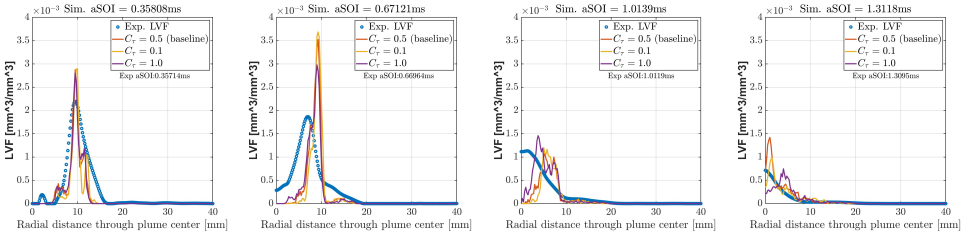

Figure 4.14: Quantitative plume-averaged Liquid Volume Fraction (LVF) at $z = 15$ mm axial cross-section from nozzle exit: Comparison for different C_τ values.

penetration, liquid width, and spray morphology. In Table 4.6, we present an overview of the baseline and the calibrated breakup constants. Interestingly, the optimal parameters closely align with the iso-octane and E30 study by Bestel et al. [5], indicating that Lagrangian breakup models are sufficiently versatile for methanol injection.

Table 4.6: Overview of baseline and calibrated KH-RT breakup constants

Constant	Baseline	Calibration
KH Time Constant B_1	50	50
KH Shed Factor s	0.5	1.0
RT Size constant C_{RT}	0.6	1.0
RT Time constant C_τ	0.5	1.0

Figure 4.15 illustrates the liquid penetration and liquid width of the calibrated RANS model, the initial baseline, and the experimental results. Compared to the baseline model, the calibrated case predicts liquid penetration more adequately with a smaller overshoot in the later stages after the EOI. In the initial injection stages, both models under-predicted liquid penetration, highlighting a disparity in the predicted spray momentum. Further reducing the discharge coefficient could aid in capturing the initial spray momentum and replicate potential in-nozzle methanol effects. However, to consistently improve the present model, additional experiments are required to determine the discharge and velocity coefficients. In-nozzle VoF simulations could also identify the methanol cavitation phenomena and enhance the predictive capabilities of the presented approach.

Concerning the liquid width, during the initial stages of the simulation, the calibrated model successfully recreated the experimental maximum spray width. The improved spray morphology is presented in Figure 4.16. The calibrated model finely captured the plume morphology and the outward expansion motion typical of a methanol multi-hole spray. Similar to liquid length, after 1.5 ms aSOI, the spray width is overpredicted for both RANS models. This behaviour indicates the presence of slowly evaporating droplets in the tip of the spray plumes, which locally increase the LVF of the simulations. This is confirmed by Figure 4.17, where the radial LVF is greater than zero in the outer regions of the spray, even for the $z = 15$ mm cross-section.

Figure 4.18 depicts the LVF distribution in the XY-plane at 15 mm distance from the injector tip. The presented RANS models adequately captured the qualitative and quanti-

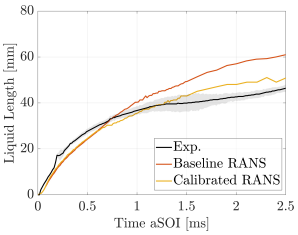

(a) Comparison between baseline & calibrated RANS models: Liquid Penetration Length

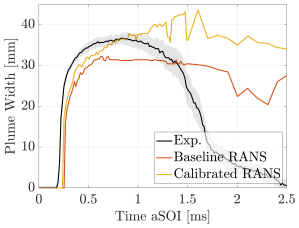

(b) Comparison between baseline & calibrated RANS models: Liquid Width at $z = 15$ mm axial cross-section from nozzle exit

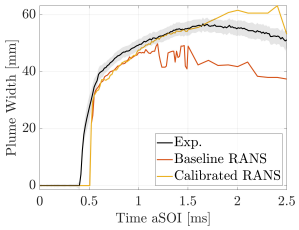

(c) Comparison between baseline & calibrated RANS models: Liquid Width at $z = 25$ mm axial cross-section from nozzle exit

Figure 4.15: Comparison between baseline & calibrated RANS models: Liquid Penetration & Width.

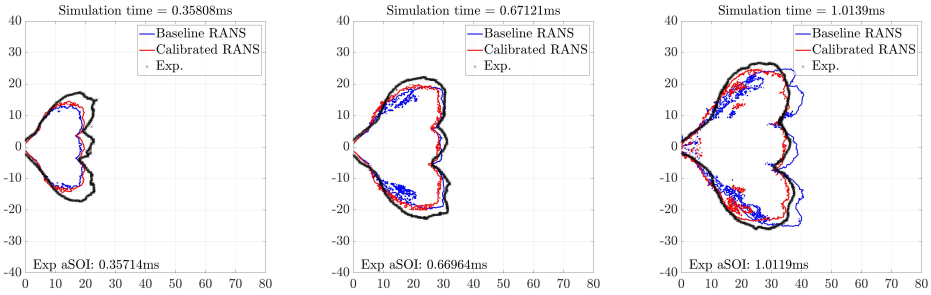

Figure 4.16: Liquid boundary derived by means of projected liquid volume (PLV) maps: Comparison between baseline & calibrated RANS models.

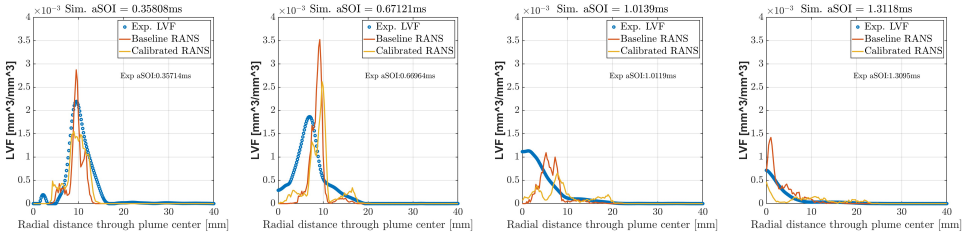

Figure 4.17: Quantitative plume-averaged Liquid Volume Fraction (LVF) at $z = 15$ mm axial cross-section from nozzle exit: Comparison between baseline & calibrated RANS models.

tative (Figure 4.17) distribution for the initial injection stages. However, during the later stages, methanol demonstrated a strong plume collapsing behaviour typical of flash-boiling gasoline sprays [13]. In the corresponding models, this tendency of the plumes to move towards the centre is severely under-predicted by all simulation cases. Furthermore, before the EOI, the calibrated RANS model exhibited a faster collapse and improved morphology compared to the baseline model. After the EOI, the baseline model showed improved plume collapsing and increased LVF values in the spray centre-line (1.0119 ms

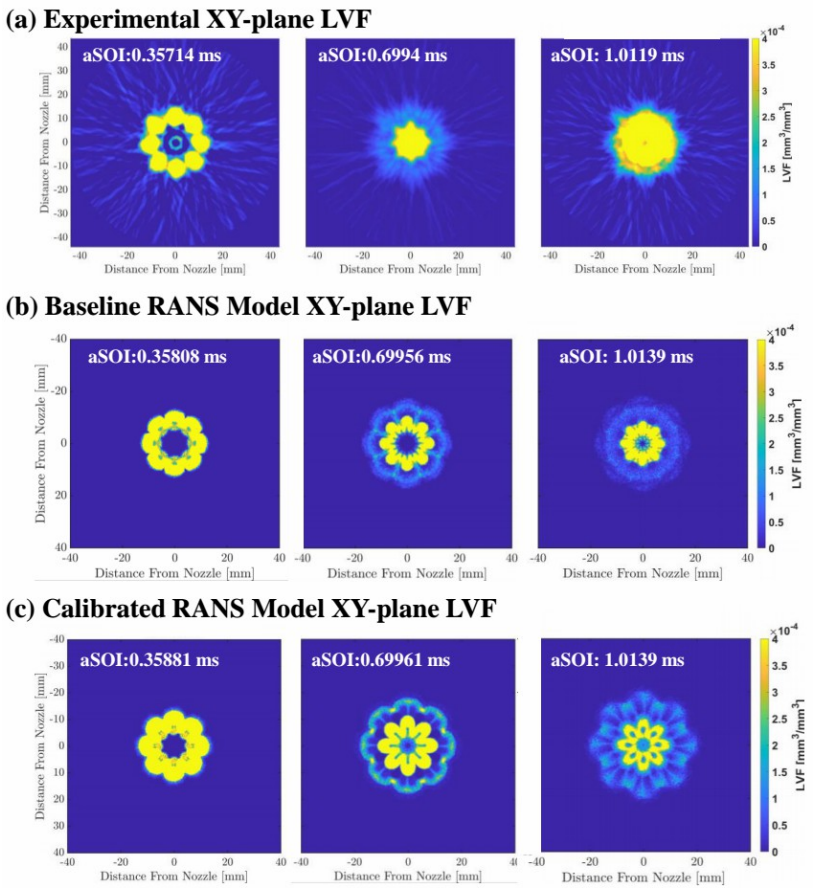

Figure 4.18: Qualitative Liquid Volume Fraction (LVF) distribution at $z = 15$ mm axial cross-section from nozzle exit: Comparison between experiment, baseline & calibrated RANS models

simulation time in Figure 4.17). Potentially, in the later stages after the EOI, this accumulation of liquid mass caused the over-prediction of the liquid penetration due to decreased evaporation rates. Despite having acceptable predictions of the liquid length and the morphology, these outlined discrepancies expose a weakness of the RANS approach in capturing the underlined physical phenomena. As a result, the spray plume collapsing, although partially replicated by the model, is weak compared to the experiments.

4.4.3 LES Model Results & Comparison with RANS Approach

A LES turbulence approach was implemented using the calibrated spray model settings from the RANS study to better capture post-injection phenomena. While RANS modelling is commonly preferred in CFD practices for automotive, heavy-duty and maritime engines, it is scientifically valuable to explore whether the observations would differ

when modelling the present spray using LES. Thus, the scope of the simulation was to capture the experimentally observed plume collapsing phenomenon while maintaining adequate predictions of the spray momentum and morphology. For comparison, we also ran an extra LES simulation using the baseline KH-RT constants. Figure 4.19 presents the liquid penetration and spray plume width results for the LES models. The calibrated LES model demonstrated slightly improved predictions for the liquid penetration compared to the RANS approach. In the 15 mm cross-section plume width, a major improvement was achieved by the LES model, which successfully recreated the declining plume width trend after 1.5 ms aSOI. This indicates that the LES model can effectively reproduce the designated methanol injection phenomena.

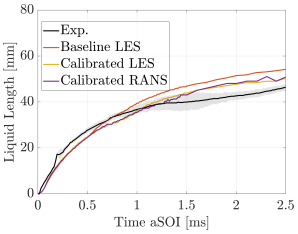

(a) Comparison between LES & RANS models: Liquid Penetration Length

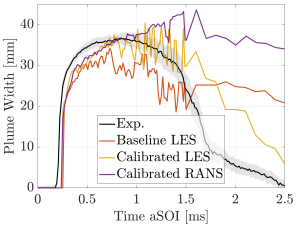

(b) Comparison between LES & RANS models: Liquid Width at z = 15 mm axial cross-section from nozzle exit

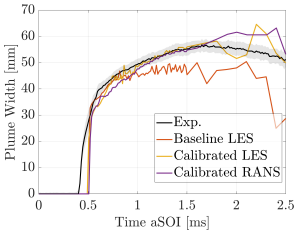

(c) Comparison between LES & RANS models: Liquid Width at z = 25 mm axial cross-section from nozzle exit

Figure 4.19: Comparison between LES & RANS models: Liquid Penetration & Width.

Figure 4.20 illustrates the plume-averaged LVF in the radial direction at 15 mm downstream distance from the injector tip. In the initial stages of injection, the calibrated LES model matches the experimental LVF distribution satisfactorily. During the EOI, at 0.669 64 ms time aSOI, all of the simulations fail to match the LVF due to the mismatch in the spray momentum. Following the end of injection, both LES models effectively capture the evolution of spray plume collapse and sweeping motion. In contrast, the RANS model underestimates the LVF accumulation along the spray centre-line, whereas the LES models successfully capture this phenomenon.

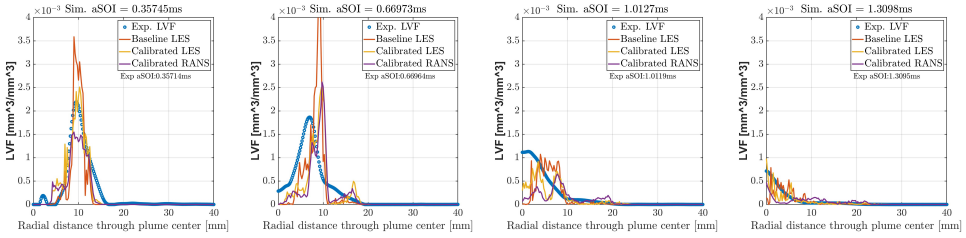

Figure 4.20: Quantitative plume-averaged Liquid Volume Fraction (LVF) at z = 15 mm axial cross-section from nozzle exit: Comparison between LES & RANS models.

Figure 4.21 compares the XY-plane LVF distribution between the LES models and the

experimental results. Both LES models present an improved prediction of the plume collapsing compared to the RANS models in Figure 4.18. Even in the baseline LES model, the plumes' tendency to move towards the center is more pronounced, suggesting that LES can provide accurate predictions without the need for extensive tuning. Utilizing the RANS-calibrated KH-RT model constants revealed that even more accurate predictions could be achieved in the final LES simulation.

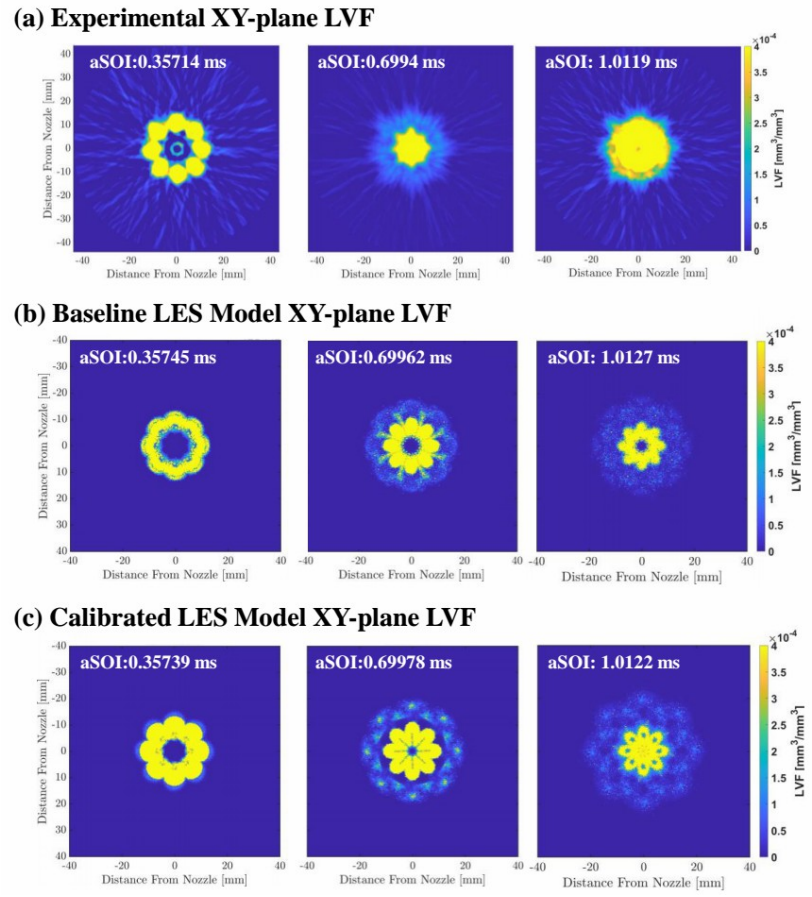

Figure 4.21: Qualitative Liquid Volume Fraction (LVF) distribution at $z = 15$ mm axial cross-section from nozzle exit: Comparison between experiment, baseline & calibrated LES models

Finally, Figure 4.22 presents the qualitative YZ-plane cross-section LVF distribution along the injection axis. This visualization allows for comparing plume geometry evolution between the calibrated RANS and LES models, as well as the experimental data. The LES model exhibits a more pronounced accumulation of liquid along the spray centreline, confirming the improved spray collapsing compared to the RANS model. Both approaches over-predict the liquid volume fraction (LVF) at the spray plume tips. This effect is more intense in the RANS model, while the LES model more accurately captures

the outward sweeping motion of the spray plumes (rotating and expanding motion of the spray tips). These discrepancies likely stem from the predicted droplet diameters at the plume tips, which are possibly larger than those in the experiment.

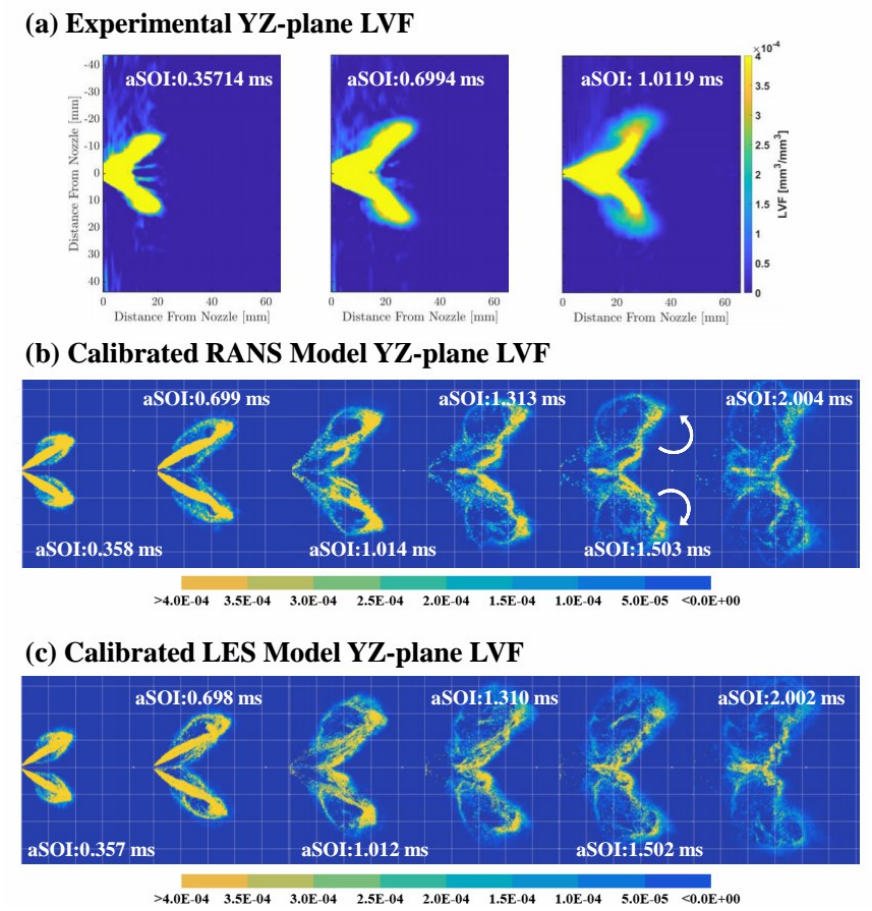

Figure 4.22: Qualitative YZ-plane Liquid Volume Fraction (LVF) : Comparison between experiment, RANS & LES models - In the CFD results each box represents a dimension of 10 mm.

4.5 Conclusions

In this chapter, we validated CFD models employing the Lagrangian-Eulerian framework for methanol sprays in a constant volume chamber environment. The simulated conditions replicated late-injection DI engine operation using the ECN spray M eight-hole counter-bore injector operating at 200 bar injection pressure. For model validation, we utilized the publicly available methanol Spray M1 data according to the new ECN guidelines using the PLV maps generated by the LVF results. The performance of various

modelling aspects (i.e., breakup model, turbulence approach, and plume cone angle) was investigated opting to recreate the experimental spray morphology and plume collapsing.

To obtain accurate numerical results, we conducted an extensive sensitivity analysis on the KH-RT breakup model constants using the RANS turbulence approach. By identifying the breakup constants contribution on the models, we calibrated the RANS model and obtained satisfying predictions of the spray morphology, liquid penetration, and liquid plume width. Despite the intensive tuning efforts, the experimentally observed methanol plume collapsing was weakly replicated by the RANS approach. This hindered post-injection methanol spray evolution, resulting in discrepancies in the LVF distribution and spray collapse behaviour. Based on the calibrated RANS model settings, we ran a high-fidelity LES model, which yielded adequate plume collapsing and spray sweeping.

In summary, the present chapter contributed a methodological investigation of spray modelling, which enabled a calibrated methanol injection model suitable for DI multi-hole injectors under late-injection conditions. Although the RANS model only partially captured the plume collapse and sweeping motions, it provided an adequate prediction of the overall spray morphology, rendering it suitable for engineering-level ICE simulations. Using computationally cheaper RANS models can provide a solid basis for calibrating more computationally intensive LES simulations. Furthermore, the inherent dissimilarities of the methanol sprays may cause delayed evaporation and increase the chances of wall wetting. This phenomena can potentially increase emissions and hinder engine stability. The proposed modelling approach can aid in optimizing these challenges by implementing split-injection strategies to minimize spray collapsing, or increasing the intake air temperature to enhance methanol evaporation.

Future studies could employ Volume-of-Fluid (VoF) methods to simulate in-nozzle flow conditions, providing insights into the complex phenomena of cavitation, evaporation, and turbulence during methanol injection. Additionally, precise estimation of nozzle coefficients could help reduce discrepancies in the spray momentum predictions. Further experimental work should focus on near-nozzle and droplet size measurements to support the development and calibration of more accurate RANS models. This will enable future CFD models to capture the cavitation-driven effects affecting methanol spray collapse. Our study provides valuable insights into modelling methanol spray behaviour in DI engines, potentially contributing to the advancement of sustainable methanol-powered engines.

Bibliography

[1] Avinash Kumar Agarwal et al. *Methanol and the alternate fuel economy*. Springer, 2019.

[2] Alex C Alkidas et al. "Contributors to the fuel economy advantage of DISI engines over PFI engines". In: *SAE Technical Paper*. 2003.

[3] Tawfik Badawy et al. "Macroscopic spray characteristics of iso-octane, ethanol, gasoline and methanol from a multi-hole injector under flash boiling conditions". en. In: *Fuel* 307 (Jan. 2022), p. 121820. DOI: 10.1016/j.fuel.2021.121820. (Visited on 11/02/2022).

[4] Jennifer C Beale et al. "Modeling spray atomization with the Kelvin-Helmholtz/Rayleigh-Taylor hybrid model". In: *Atomization and sprays* 9.6 (1999).

[5] Diego Bestel et al. "A comprehensive numerical investigation on spray models for Direct-Injection Spark-Ignition engines". In: *Fuel* 373 (2024), p. 132325.

[6] *CONVERGE CFD Software Website*. 2023. URL: https://convergecfd.com/.

[7] Convergent Science Inc. *CONVERGE MANUAL v3.0*. 2022.

[8] Scott Curran et al. "The future of ship engines: Renewable fuels and enabling technologies for decarbonization". In: *International Journal of Engine Research* (2023).

[9] A. Di Matteo et al. "Modeling Spray C and Spray D with FGM within the framework of RANS and LES". In: *Frontiers in Mechanical Engineering* 8 (2022), p. 1013138.

[10] J. Dierickx et al. "Retrofitting a high-speed marine engine to dual-fuel methanol-diesel operation: A comparison of multiple and single point methanol port injection". In: *Fuel Communications* 7 (2021), p. 10.

[11] Y. Dong et al. "High-pressure direct injection of methanol and pilot diesel: A non-premixed dual-fuel engine concept". In: *Fuel* 277 (Oct. 2020), p. 117932. DOI: 10.1016/j.fuel.2020.117932. (Visited on 05/30/2022).

[12] Francesco Duronio et al. "CFD unified approach under Eulerian–Lagrangian framework for methanol and gasoline direct injection sprays in evaporative and flash boiling conditions". In: *International Journal of Multiphase Flow* 182 (2025), p. 105048. DOI: https://doi.org/10.1016/j.ijmultiphaseflow.2024.105048.

[13] Francesco Duronio et al. “ECN Spray G injector: Numerical modelling of flash-boiling breakup and spray collapse”. In: *International Journal of Multiphase Flow* 145 (2021), p. 103817.

[14] Francesco Duronio et al. “Gasoline direct injection engines–A review of latest technologies and trends. Part 1: Spray breakup process”. In: *Fuel* 265 (2020), p. 116948.

[15] Francesco Duronio et al. “Gasoline direct injection engines–A review of latest technologies and trends. Part 2”. In: *Fuel* 265 (2020), p. 116947.

[16] *Engine Combustion Network*. 2023. URL: https://ecn.sandia.gov/.

[17] Joel H Ferziger et al. *Computational methods for fluid dynamics*. Vol. 3. Springer, 2002.

[18] ECN Spray G. *Engine Combustion Network Spray-G Conditions*. Accessed: 2023-10-07. URL: https://ecn.sandia.gov/gasoline-spray-combustion/target-condition/spray-g-operating-condition/.

[19] Zhiyu Han et al. “Turbulence modeling of internal combustion engines using RNG κ-ε models”. In: *Combustion science and technology* 106.4-6 (1995), pp. 267–295.

[20] AL Horvath. “Redlich-Kwong equation of state: review for chemical engineering calculations”. In: *Chemical Engineering Science* 29.5 (1974), pp. 1334–1340.

[21] Joonsik Hwang et al. “Spatio-temporal identification of plume dynamics by 3D computed tomography using engine combustion network spray G injector and various fuels”. In: *Fuel* 280 (2020), p. 118359.

[22] Raad I Issa. “Solution of the implicitly discretised fluid flow equations by operator-splitting”. In: *Journal of computational physics* 62.1 (1986), pp. 40–65.

[23] Gautam Kalghatgi. “Is it really the end of internal combustion engines and petroleum in transport?” In: *Applied energy* 225 (2018), pp. 965–974.

[24] Dagobert G Kessel. “Global warming—facts, assessment, countermeasures”. In: *Journal of Petroleum Science and Engineering* 26.1-4 (2000), pp. 157–168.

[25] Konstantinos I. Kiouranakis et al. “Methanol for heavy-duty internal combustion engines: Review of experimental studies and combustion strategies”. In: *Under Review in Renewable and Sustainable Energy Reviews* ().

[26] Aman Kumar et al. “Large-Eddy Simulation Study of Injector Geometry and Parcel Injection Location on Spray Simulation of the Engine Combustion Network Spray G Injector”. In: *Journal of Engineering for Gas Turbines and Power* 146 (2024), p. 081003. DOI: 10.1115/1.4063957.

[27] Aman Kumar et al. “Study of Injector Geometry and Parcel Injection Location on Spray Simulation of the Engine Combustion Network Spray G Injector”. In: *Journal of Engineering for Gas Turbines and Power* 145.7 (2023), p. 071012.

[28] Hao-Pin Lien et al. “Intake-injection Spray G and Spray M research using methanol and PACE-20 simulation”. In: *ECN9 Proceedings Presentation*. Engine Combustion Network. 2023. URL: https://ecn.sandia.gov/workshop/ECN9/ECN9_Spray_GM.pptx.

[29] Hao-Pin Lien et al. “Numerical studies of gasoline direct-injection sprays (ECN Spray G) under early-and late-injection conditions using Large Eddy Simulation and droplets-statistics-based Eulerian–Lagrangian framework”. In: *Fuel* 357 (2024), p. 129708.

[30] *Liquid Penetration Length*. 2024. URL: https://ecn.sandia.gov/diesel-spray-combustion/experimental-diagnostics/liquid-penetration-length/.

[31] Alex B Liu et al. “Modeling the effects of drop drag and breakup on fuel sprays”. In: *SAE Transactions* (1993), pp. 83–95.

[32] ECN Spray M. *Engine Combustion Network Spray-M Data*. Accessed: 2023-10-07. URL: https://ecn.sandia.gov/data/sandia-spray-m-data/.

[33] A. Matamis et al. “Optical characterization of methanol compression-ignition combustion in a heavy-duty engine”. In: *Proceedings of the Combustion Institute*. Vol. 38. Elsevier Ltd, 2021, pp. 5509–5517.

[34] Balaji Mohan et al. “Coupled in-nozzle flow and spray simulation of Engine Combustion Network Spray-G injector”. In: *International Journal of Engine Research* 22.9 (2021), pp. 2982–2996.

[35] K. Moreno Cabezas et al. “Characteristics of Methanol and Iso-Octane under Flashing and Non-Flashing Conditions in ECN-G Spray”. English. In: 2022. DOI: 10.4271/2022-01-0496.

[36] Peter J O’Rourke. “Statistical properties and numerical implementation of a model for droplet dispersion in a turbulent gas”. In: *Journal of Computational Physics* 83.2 (1989), pp. 345–360.

[37] Davide Paredi et al. “Validation of a comprehensive computational fluid dynamics methodology to predict the direct injection process of gasoline sprays using Spray G experimental data”. In: *International Journal of Engine Research* 21.1 (2020), pp. 199–216.

[38] Mark A Patterson et al. “Modeling the effects of fuel spray characteristics on diesel engine combustion and emission”. In: *SAE transactions* (1998), pp. 27–43.

[39] Eric Pomraning et al. “Dynamic one-equation nonviscosity large-eddy simulation model”. In: *AIAA journal* 40.4 (2002), pp. 689–701.

[40] Scott L Post et al. “Modeling the outcome of drop–drop collisions in Diesel sprays”. In: *International Journal of Multiphase Flow* 28.6 (2002), pp. 997–1019.

[41] R D Reitz et al. “IJER Editorial: The future of the internal combustion engine”. In: *International Journal of Engine Research* (2020). DOI: 10.1177/1468087419877990.

[42] Rolf D Reitz et al. “Structure of high-pressure fuel sprays”. In: *SAE transactions* (1987), pp. 492–509.

[43] David P Schmidt et al. “A new droplet collision algorithm”. In: *Journal of Computational Physics* 164.1 (2000), pp. 62–80.

[44] PK Senecal et al. “Grid-convergent spray models for internal combustion engine CFD simulations”. In: *Internal Combustion Engine Division Fall Technical Conference*. Vol. 55096. American Society of Mechanical Engineers. 2012, pp. 697–710.

[45] Sam Shamun et al. “Exhaust PM Emissions Analysis of Alcohol Fueled Heavy-Duty Engine Utilizing PPC”. In: *SAE International Journal of Engines* 9.4 (Oct. 2016), pp. 2142–2152. ISSN: 1946-3944. DOI: 10.4271/2016-01-2288.

[46] Shankar Subramaniam. “Lagrangian–Eulerian methods for multiphase flows”. In: *Progress in Energy and Combustion Science* 39.2-3 (2013), pp. 215–245.

[47] M. Svensson et al. “Low Load Ignitability of Methanol in a Heavy-Duty Compression Ignition Engine”. en. In: Aug. 2022, pp. 2022–01–1093. DOI: 10.4271/2022-01-1093. (Visited on 09/15/2022).

[48] A Tripathi et al. *Greener and Scalable E-Fuels for Decarbonization of Transport*. Energy, Environment, and Sustainability, Springer Nature, 2022.

[49] Martin Tuner. “Review and Benchmarking of Alternative Fuels in Conventional and Advanced Engine Concepts with Emphasis on Efficiency, CO2, and Regulated Emissions”. In: *SAE Technical Papers* (2016).

[50] Sebastian Verhelst et al. “Methanol as a fuel for internal combustion engines”. In: *Progress in Energy and Combustion Science* 70 (Jan. 2019), pp. 43–88. ISSN: 0360-1285. DOI: 10.1016/j.pecs.2018.10.001. URL: https://linkinghub.elsevier.com/retrieve/pii/S036012851830042X (visited on 09/16/2022).

[51] Xibin Wang et al. “Spray Characteristics of High-Pressure Swirl Injector Fueled with Methanol and Ethanol”. In: *Energy & Fuels* 19.6 (Nov. 2005), pp. 2394–2401. DOI: 10.1021/ef050135w. (Visited on 06/17/2022).

[52] Lukas Weiss et al. “Development of limited-view tomography for measurement of Spray G plume direction and liquid volume fraction”. In: *Experiments in Fluids* 61 (2020), pp. 1–17.

[53] Sameera Wijeyakulasuriya et al. “Enabling Powertrain Technologies for Euro 7/VII Vehicles with Computational Fluid Dynamics”. en. In: *Transportation Engineering* 9 (Sept. 2022), p. 100127. DOI: 10.1016/j.treng.2022.100127. (Visited on 09/20/2022).

[54] Christian Wouters et al. “Comprehensive assessment of methanol as an alternative fuel for spark-ignition engines”. In: *Fuel* 340 (2023), p. 127627.

[55] Wei Zeng et al. “Atomization and vaporization for flash-boiling multi-hole sprays with alcohol fuels”. In: *Fuel* 95 (May 2012), pp. 287–297. DOI: 10.1016/j.fuel.2011.08.048. (Visited on 06/17/2022).

[56] Wei Zeng et al. “Characterization of Methanol and Ethanol Sprays from Different DI Injectors by Using Mie-scattering and Laser Induced Fluorescence at Potential Engine Cold-start Conditions”. In: *SAE Technical Papers* (2010).

[57] Wei Zeng et al. “Macroscopic characteristics for direct-injection multi-hole sprays using dimensionless analysis”. In: *Experimental Thermal and Fluid Science* 40 (July 2012), pp. 81–92. DOI: 10.1016/j.expthermflusci.2012.02.003. (Visited on 06/17/2022).

[58] B. Zincir et al. “Investigation of effects of intake temperature on low load limitations of methanol partially premixed combustion”. In: *Energy and Fuels* 33.6 (June 2019), pp. 5695–5709. DOI: 10.1021/acs.energyfuels.9b00660. (Visited on 06/03/2022).

[59] Konstantinos Zoumpourlos et al. “CFD modeling approach for late-injection methanol sprays validated with ECN spray M”. In: *International Journal of Engine Research* (2025). DOI: 10.1177/14680874251323931.

[60] Konstantinos Zoumpourlos et al. “Evaluation of Methanol Sprays in Marine Internal Combustion Engines: a Case Study for Port Fuel Injection Systems”. In: *Modelling and Optimisation of Ship Energy Systems 2023* (Dec. 2023). DOI: 10.59490/moses.2023.655. URL: https://proceedings.open.tudelft.nl/moses2023/article/view/655.

[61] Konstantinos Zoumpourlos et al. “Methanol Operation in Heavy-Duty DICI Dual-Fuel Engines: Investigating Charge Cooling Effects using ECN Spray D Data”. In: *ASME ICEF 2024*. 2024.

Chapter 5

Methanol Operation in Heavy-Duty DICI Dual-Fuel Engines: Investigating Charge Cooling Effects using ECN Spray D Data

In medium and large bore marine engines, DF operation is achieved through either direct injection (DI) or port fuel injection (PFI) of methanol with diesel acting as a DI pilot fuel for ignition. However, the injection of methanol presents a significant challenge due to its high latent heat of vaporization and decreased lower heating value (LHV) compared to diesel. Therefore, for the same energy content, methanol requires around eight times the amount of heat to evaporate completely compared to diesel, resulting in lower in-cylinder temperatures. This charge cooling effect leads to a strong negative temperature gradient influencing ignition and flame propagation. This chapter aims to quantify the cooling effect of methanol in a heavy-duty dual-fuel DICI engine environment. The presented methodology utilises Computational Fluid Dynamics (CFD) simulations to model methanol sprays, with validation based on Engine Combustion Network (ECN) Spray D experimental data. Compared to diesel, injecting methanol with the same energy content resulted in up to 100 K *lower temperature within the mixture. Consequently, this cooled mixture may pose challenges to combustion stability due to the intense temperature gradients that it creates. Nonetheless, lower mixture temperature decreases NOx emissions, which can prove beneficial for high methanol energy fractions in dual-fuel DICI engines.*

This chapter was reproduced from [46]:
Zoumpourlos, K., Geertsma, R., Van De Ketterij, R., and Coraddu, A. (2025). Methanol Operation in Heavy-Duty DICI Dual-Fuel Engines: Investigating Charge Cooling Effects Using ECN Spray D Data. ASME. J. Eng. Gas Turbines Power. DOI: https://doi-org.tudelft.idm.oclc.org/10.1115/1.4067862

5.1 Introduction

IN the heavy-duty (HD) automotive and marine sector, power and propulsion is mainly realized by diesel compression ignition (CI) internal combustion engines (ICEs), which cause local (NO_x, SO_x, unburned hydrocarbons, and soot) and global CO_2 emissions [22, 15, 26]. Despite recent advances in the use of alternative energy sources, ICEs will remain at the forefront of power generation due to their power density, robustness, and cost advantages [33, 18]. To mitigate the combustion emissions issue, alternative fuels produced from biomass or captured CO_2 can assist in decarbonizing ICEs [40, 2]. Among the candidate alternative fuels, methanol is a promising contender owing to its advantageous properties (e.g., high burning velocity, low combustion temperature), scalable production, and lower hazardous emissions, such as NO_x, SO_x, and soot, compared to diesel [41, 31]. Contrary to ammonia and hydrogen, methanol is liquid at atmospheric conditions, which simplifies transportation and storage, while having adequate energy density [44]. For these reasons, methanol is considered the most cost-effective sustainable fuel option for the transportation sector [23].

Methanol combustion in CI HD engines is commonly achieved by either dual-fuel (DF) operation, which utilises a pilot fuel for ignition, or the addition of ignition improvers [20, 41]. In DF engines, methanol is premixed with the air, either through port fuel injection (PFI) or direct injection (DI), creating a low reactivity mixture. This premixed charge contains the main energy content and is ignited by a high-reactivity fuel, such as diesel, initiating the flame propagation [24, 21]. However, increasing diesel substitution in DF engines is limited due to methanol's high latent heat of vaporization and high auto-ignition temperature. Methanol's phase transition draws about eight times more energy from the in-cylinder air compared to diesel. Eventually, the air-fuel mixture will have a significantly decreased temperature prior to combustion initiation [37].

Previous studies on HD methanol-diesel engines have mainly focused on combustion performance and emissions [39, 43, 9, 28]. The reported conclusions in these studies implicitly indicated the strong impact of the methanol cooling effect on engine stability and NO_x emissions. Using an optical HD engine, Matamis et al. [28] demonstrated that the cooling effect impedes flame propagation while increasing the ignition delay. Moreover, other experimental studies suggested intake air heating as a way to maintain combustion stability [39, 8], especially under low load conditions [43]. Using PFI of methanol, Dierickx et al. [8] stated that the exacerbated cooling intensity even led to the condensation of methanol in the intake manifold. Despite this, lower NO_x emissions than in diesel operation were observed due to lower combustion temperature [8, 9, 39, 43].

Concerning previous methanol spray-dedicated studies, Wang et al. [42] experimentally compared methanol with diesel sprays in CI engine conditions. Their study demonstrated that at moderate ambient temperatures (600 K) and increased ambient pressures (ranging from 20 to 40 bar), methanol evaporates faster due to its lower boiling point. Their experiments highlighted many similarities in the macroscopic spray structure of methanol with that of diesel. Furthermore, Karimkashi et al. [21] conducted a Large Eddy Simulation (LES) study on DF ignition of methanol-air mixtures with n-dodecane acting as pilot fuel. Their simulated conditions showcased non-robust ignition of the methanol-air mixture and increased ignition delay. In addition, Kaario et al. [17] used

Engine Combustion Network (ECN) reacting Spray A data to validate their LES framework using n-dodecane under light-duty automotive injection quantities. Subsequently, the validated model was converted for methanol injection using a set of increased ambient temperatures to facilitate ignition. Compared to n-dodecane, the authors reported increased flame lift-off length under lower ambient temperatures. This increase is directly coupled to the reduced mixture temperature, which stems from the augmented latent heat.

5.1.1 Aim & Novelty

While previous research has investigated igniting diesel-methanol sprays with a focus on ignition delay and flame lift-off length [21, 17], a significant gap of knowledge exists on the charge cooling during the mixture formation process prior to combustion. To sufficiently understand methanol's impact on mixture formation, predictive computational fluid dynamics (CFD) models can assess the spray behaviour under CI engine conditions. This chapter aims to study the spray formation, evaporation, and mixing of methanol in a DICI engine environment in the context of HD-DF engines. The novelty of the present study constitutes of the quantification of the mixture cooling effect originating from methanol injection in comparison to diesel. For the present analysis, CFD modelling was used utilizing the Lagrangian-Eulerian (LE) coupling method to reproduce the multiphase flow phenomena. The model was developed using CONVERGE-CFD [4] following a Reynolds Averaged Navier Stokes (RANS) turbulence modelling approach in a constant volume chamber.

To validate our models, we used non-reacting data from the n-dodecane ECN Spray D experiments, which are representative of large-nozzle HD injection quantities [6]. Consequently, the validated model was converted for methanol simulation to facilitate near Top-dead-center (TDC) DI typical of DF engines. In the converted model, methanol was implemented through a set of varied properties and altered mass diffusivity constants used for evaporation modelling. The methanol spray model was used for different cases which represented equal quantity and equal energy injections as the baseline diesel model. To assess the mixture cooling effect, these methanol models were compared with diesel based on their liquid length, the evaporated mass fraction, and the mixture temperature distributions. The results demonstrated an excessive decrease in mixture temperature for the methanol cases. These findings indicate that methanol injection will eventually create cold spots in the cylinder, which impede flame propagation and influence combustion stability, confirming the experimental observations in HD-DF engines.

5.2 Background

METHANOL exhibits a significantly increased latent heat of vaporization, which is four times higher compared to diesel (Table 5.1). Considering also the reduced lower heating value, approximately eight times more thermal energy is required for the complete evaporation of methanol to achieve the same energy content as diesel [45]. Therefore, the extra heat required for the mixture formation leads to lower in-cylinder temperature highlighting an intensive charge cooling effect [37]. Subsequently, methanol

combusts differently than diesel, resulting in a longer ignition delay and local flame quenching due to its lower mixture temperature [28]. This phenomenon causes increased cycle-to-cycle variability and unstable operation over the working range of methanol engines.

Table 5.1: Fuel Properties [1]

Property	Diesel	Methanol
Lower Heating Value (LHV) [MJ/kg]	42.7	20.1
Density (at STP) [kg/m^3]	840	790
Heat of Vaporization (at 1 bar) [kJ/kg]	250	1089
Boiling Point (at 1 bar) [°C]	180-360	65
Surface Tension (at 20 °C) [mN/m]	27	23
Dynamic Viscosity (at 20 °C) [mPa·s]	2.1 - 2.52	0.57
Cetane Number [-]	38-53	<5
Octane Number [-]	15-25	109

5.2.1 Experimental Background

In the present chapter, we used the ECN Spray D to validate our computational models [10]. The Spray D is a Bosch single-hole injector characterized by a convergent channel to minimize cavitation (see Fig. 5.1). The nozzle diameter is 0.186 mm making it suitable for HD-DI conditions with large injection quantities. The Spray D experiments were conducted in a constant volume chamber under various ambient conditions reminiscent of CI diesel engines, using n-dodecane as the fuel. The ambient conditions were characterized by altered oxygen concentrations ranging from non-reacting to reacting conditions. Since we are investigating the mixture formation phenomena of methanol, we focus on the non-reacting condition with 0% oxygen. Table 5.2 summarizes the non-reacting Spray D conditions used in the present chapter.

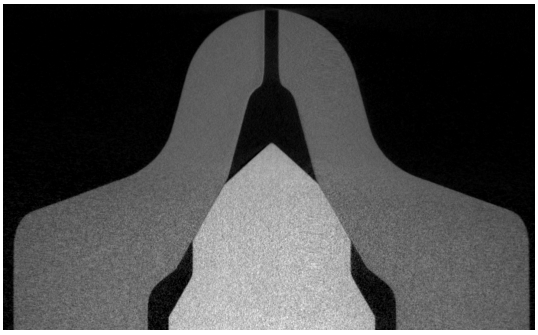

Figure 5.1: Spray D X-Ray Scan provided by Ref. [10]

Table 5.2: ECN Spray D non-reacting conditions

Item	Value
Test Fuel	N-dodecane
Ambient Pressure	60 bar
Ambient Temperature	900 K
Fuel Temperature	363 K
Injection Pressure	150 MPa
Injection Quantity	228 cc/min
Injection Duration	4.5 ms
Nozzle Diameter	0.186 mm
Ambient Gas Composition	O_2= 0%, N_2 = 89.71%, CO_2 = 6.52%, H_2O = 3.77%

5.3 Computational Methodology

In this study, we used the CONVERGE v3.0 CFD software [4, 36] to solve the compressible conservation equations of mass, momentum, and energy. To model turbulence, a RANS approach was followed using the RNG $k-\varepsilon$ model [12]. The conservation equations were solved using the density-based solver [5] along with the Pressure Implicit with Splitting of Operators (PISO) algorithm [16]. The numerical scheme is first order accurate in time and second order in space. Furthermore, the Courant-Friedrichs-Lewy (CFL) criterion [5, 11] was used to determine the time-step of the simulations. The thermodynamic properties of air, n-dodecane, and methanol were modelled based on the Redlich-Kwong equation of state [14].

5.3.1 Computational Domain & Mesh Grid

For the computational domain, we created a cylindrical geometry to conduct the numerical computations (Fig. 5.2) with a radius of 54 mm and a height of 108 mm. The dimensions of the geometry were chosen accordingly with similar ECN spray literature [7, 19]. All the cylinder boundary conditions were assigned as wall-type Dirichlet for the temperature and Neumann for the turbulent kinetic energy. The computational domain was discretized with a base cell size of 4 mm with additional manual and automatic refinements in the spray region. The spray cone region was treated with fixed embedding mesh refinement to increase resolution near the nozzle exit (Fig. 5.2). Moreover, finer mesh resolution was applied using Adaptive Mesh Refinement (AMR) based on velocity and species gradients. The max embedding level was set as 4 leading to a minimum cell size of 0.25 mm. The minimum cell size was selected as the most adequate in terms of computational cost and numerical accuracy [36]. Lastly, the sub-grid criterion was set to 0.1 m/s for velocity refinement and 0.001 for fuel mass fraction refinement.

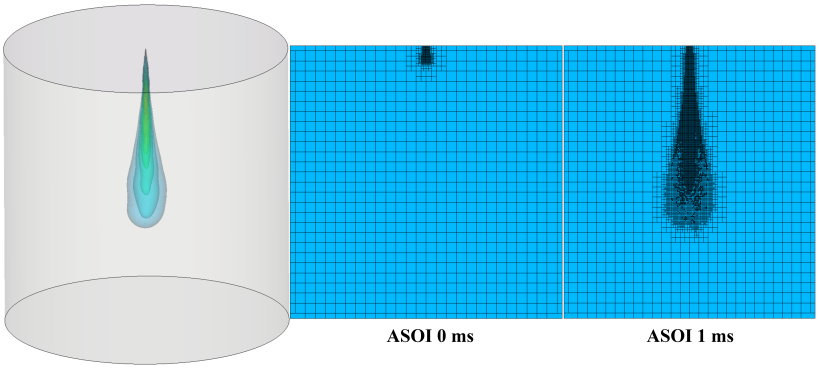

Figure 5.2: Simulation control volume and mesh grid at different simulation times

5.3.2 Spray Model

For multiphase flow modelling, we employed the Lagrangian-Eulerian (LE) coupling approach, which treats the liquid droplets as particles and the gas using an Eulerian representation. The same set of phenomenological spray models was applied to the particles to resolve sub-grid physical phenomena as in the previous chapters of this thesis. For the sake of completeness, a brief overview is provided in the present section. Moreover, the computational particles were injected using the Reitz and Diwakar [34] 'blob' model. To model breakup, we used the Kelvin Helmholtz - Rayleigh Taylor (KH-RT) model, which is based on fluid phenomena occurring during atomization and droplet breakup [3, 34].

Particle interactions were modeled by the No Time Counter (NTC) algorithm [35], estimating the collisions between droplets. The model of Post and Abraham [32] was used to predict the post-collision outcome, including bouncing, stretching, reflective separation, and coalescence. Furthermore, the drag forces were modelled using the dynamic drag model with altering drag coefficient according to the flow conditions [25]. The particle distortion was considered by Taylor Analogy Breakup (TAB) model calculations to ensure a consistent estimation of the drag coefficient. Turbulence effects on the particles were established through a turbulent dispersion model by O'Rourke [30]. Lastly, for evaporation modelling, the Frossling correlation was applied assuming uniform temperature distribution within each particle [29]. The summary of the adopted numerical models is shown in Table 5.3.

5.3.3 Numerical Setup

The details of the used model parameters are presented in Table 5.4. These modelling parameters were kept constant for both n-dodecane and methanol injection cases. To calculate the liquid and vapour penetration, a 95 % threshold for the liquid mass fraction and a threshold of 0.1 % of fuel vapour mass fraction were used, respectively. The rate-of-injection (ROI) profile was defined according to the measurements provided by ECN for the 150 MPa injection pressure case [38]. Moreover, Fig. 5.3 depicts the normalized

Table 5.3: Numerical models

Physical Phenomena	**Numerical Models**
Fluid Flow	Navier Stokes, density-based solver [5]
Turbulence	RNG $k-\varepsilon$ model [12]
Droplet Injection	Blob model [34]
Liquid Breakup	KH-RT model [3]
Droplet Drag Force	Dynamic Drag Model [25]
Droplet Collision	NTC model [35]
Droplet Coalescence	Post Collision Outcome model [32]
Droplet Turbulent Dispersion	O' Rourke model [30]
Droplet Evaporation	Frossling correlation-based model [29]

non-dimensional mass flow ROI profile that was used in the present study.

Table 5.4: Modelling Parameters

KH Model constants	$B_0 = 0.61, \quad B_1 = 10$
RT Model constants	$C_{RT} = 0.1, \quad C_\tau = 1$
RANS Constants	$C_\mu = 0.0845, \quad C_{\varepsilon 1} = 1.42,$ $C_{\varepsilon 2} = 1.68, \quad C_{\varepsilon 3} = -1.0$
Initial Turbulent Kinetic Energy (TKE)	$k_0 = 1\,\mathrm{m}^2/\mathrm{s}^2$
Initial TKE Dissipation Rate	$\varepsilon_0 = 90\,\mathrm{m}^2/\mathrm{s}^3$
Cone Angle	20°
Discharge Coefficient	$C_d = 0.86$
N-dodecane mass diffusivity constants	$D_0 = 4.16 \cdot 10^{-6}, \quad n_0 = 1.6$
Methanol mass diffusivity constants	$D_0 = 1.336 \cdot 10^{-5}, \quad n_0 = 1.8$

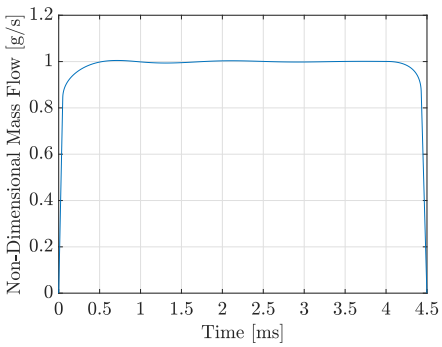

Figure 5.3: Spray D Rate of Injection (ROI) profile for 150 MPa injection pressure (provided by [38])

5.4 Results & Discussion

IN this section, we present the validation of our numerical model using the publicly available ECN Spray D data. Consequently, we convert our model for methanol operation and conduct an explicit comparison with the n-dodecane spray model. Since methanol exhibits nearly half the LHV of diesel, three extra models were run using increased injection quantities to account for equal energy content with diesel. By keeping the injection duration constant, these models utilized three different nozzle diameters to achieve the increased methanol quantity, which account for 100, 150, and 200 MPa injection pressure. Lastly, for the 150 MPa injection pressure simulation case, we investigated the effect of initial ambient temperature and evaluated the cooling effect.

5.4.1 Model Validation

We used the liquid and vapor penetration experimental data provided by ECN to validate our CFD setup. In Fig. 5.4, we compare the simulated liquid and vapor penetration with the experimental results. The model captures the liquid length accurately, while the vapor penetration is slightly overpredicted due to the employed mesh size. Moreover, Fig. 5.5

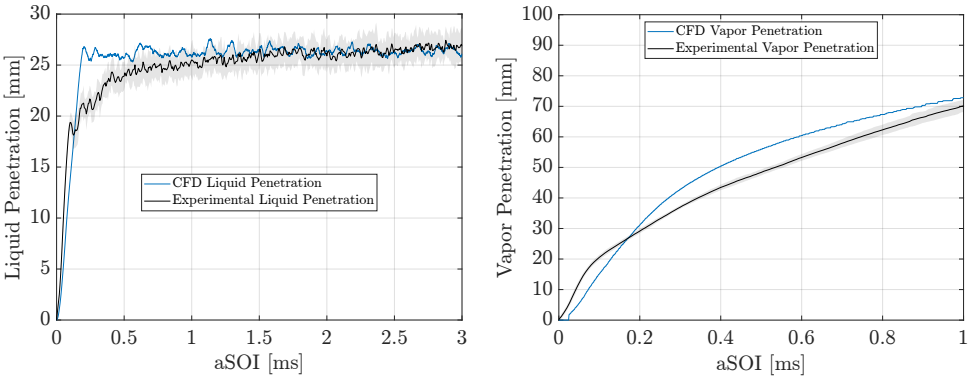

(a) Liquid Penetration

(b) Vapor Penetration

Figure 5.4: Validation for liquid and vapor penetration predictions for the diesel baseline model showing both CFD and ECN Spray D experimental results

depicts the spatial comparison of the spray morphology between the experiment and the simulation. For comparison, we used mass fraction contours along with Lagrangian particles to demonstrate the predictive capabilities of the presented model. The CFD spray morphology also reflects the slight overprediction in the vapor penetration. Despite the inability of the model to predict the initial flow dynamics, the predicted final liquid and vapour penetrations are within and near the experimental uncertainties presented in Fig. 5.4 as a grey shaded area. Based on the presented results, we consider the model validated for the scope of our study. Thus, the presented n-dodecane spray model is employed as the baseline model for the following methanol spray calculations.

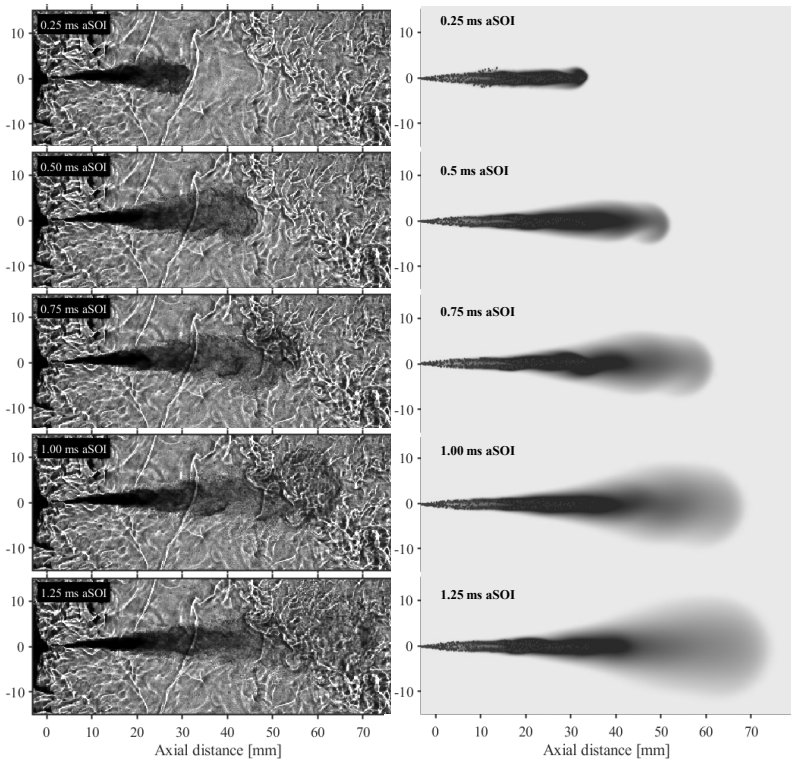

Figure 5.5: Comparison of spray morphology of ECN Spray D (left) and CFD n-dodecane mass fraction (right). Experimental results provided to ECN by Sandia National Laboratories [27, 10]

5.4.2 Spray D style Methanol Injection

Initially, we conducted an explicit comparison between the baseline diesel model and the methanol model. Fig. 5.6 compares the liquid and vapor penetration of the two fuels using the same injection quantity. Methanol exhibits slightly lower liquid length and similar vapor penetration compared to diesel. These outcomes align with the study of Wang et al. [42], which investigated light-duty CI engine conditions. Methanol injection facilitates increased evaporation rates originating from its lower boiling point. Hence, the model successfully captured the decreased liquid length under the designated HD conditions.

The increased evaporation of methanol is also observed in the fuel mass fraction contours (Fig. 5.7). Methanol's spray structure is similar to diesel's, but slightly increased mass fractions of evaporated fuel are observed in the vicinity of the spray. Furthermore, Fig. 5.8 depicts the mixture temperature during the initial stage of the injection. Due to intense evaporation conditions, a cooling effect is observed in the plotted contours, characterised by low temperatures in the vicinity of the spray.

Thus, methanol exhibits reduced temperature zones under 630 K, while temperature

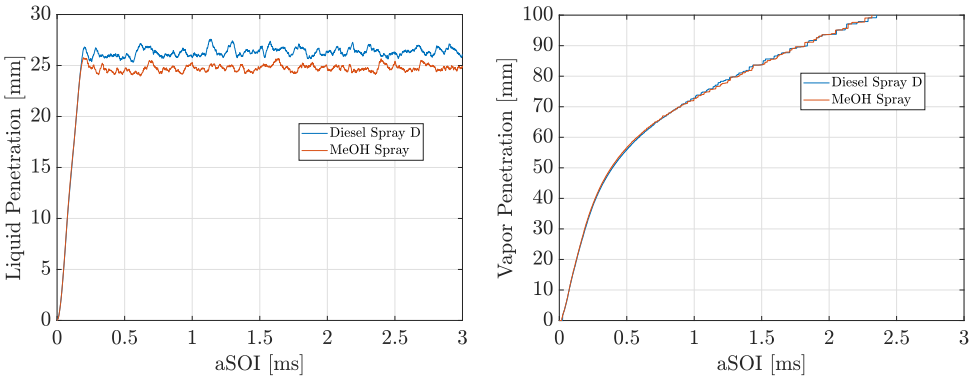

(a) Liquid Penetration

(b) Vapor Penetration

Figure 5.6: Comparison of liquid and vapor penetration between diesel and methanol using equal injection quantity

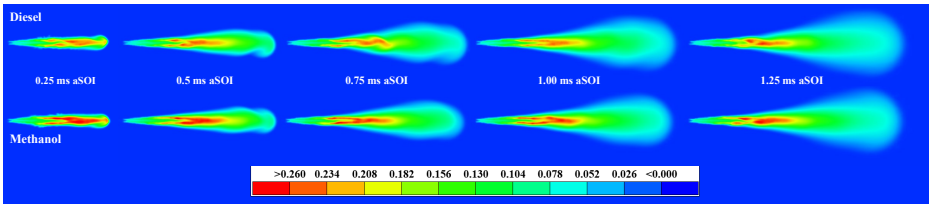

Figure 5.7: Mass fraction contours comparison between diesel Spray D baseline model and methanol for equal quantity injection

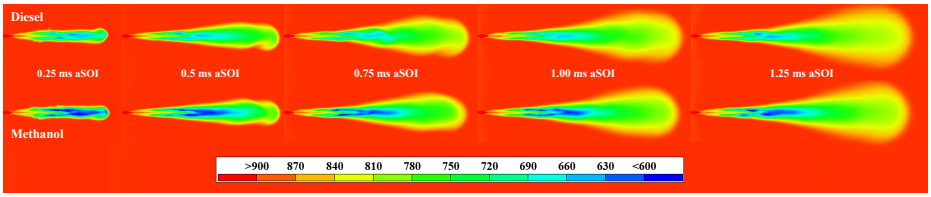

Figure 5.8: Mixture temperature for equal quantity diesel and methanol injection

at the same location in the diesel simulation is higher than 660 K. However, this difference may also be partially influenced by methanol's slightly higher evaporation rate.

5.4.3 Equal-Energy Methanol Injection

To accommodate equal energy injection quantities, we run three cases with increased fuel mass flow rates, accounting for 100, 150 and 200 MPa injection pressures, and altered nozzle diameters. The injection duration was maintained constant by altering the nozzle diameter to accommodate the required mass flow rate for the designated injection

pressure. The aim was to maintain the injection pressure at a predefined value to achieve similar initial bulk velocity of the spray jet as the initial simulation cases. Thus, by maintaining the velocity of the jet at a similar level, the effect of evaporation cooling due to methanol's properties can be isolated. Thus, the nozzle diameter for each case is the following:

- For 100 MPa injection pressure, $D_{noz} = 0.298$ mm.
- For 150 MPa injection pressure, $D_{noz} = 0.269$ mm.
- For 200 MPa injection pressure, $D_{noz} = 0.25$ mm.

Fig. 5.9 presents the liquid and vapor penetrations for the equal energy models and the baseline diesel and methanol cases. Particularly in the lower injection pressure

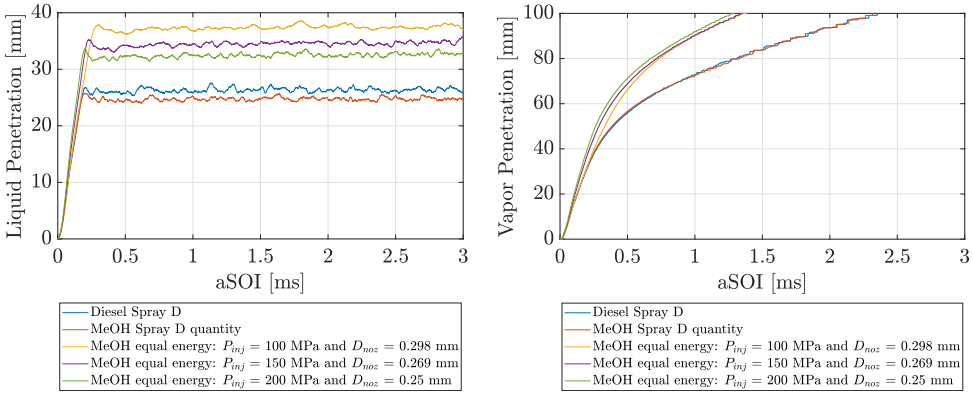

(a) Liquid Penetration (b) Vapor Penetration

Figure 5.9: Comparison of liquid and vapor penetration between diesel and methanol using equal quantity and equal energy injections

case of the equal energy methanol injection, the liquid length is substantially increased. This is justified by the lower injection pressure case, which produces larger droplets due to increased nozzle diameter which evaporate at a decreased rate. Moreover, the low injection pressure sprays have a decreased tendency for droplet breakup due to decreased jet velocity. This tendency is reflected by the spray Sauter Mean Diameter (SMD) for the initial stages of the injection (Fig. 5.10). Similar trends are also observed for the vapor penetration of the equal energy methanol cases. Contrary to the results for the liquid length, the higher injection pressure cases produced slightly higher vapor penetration lengths. Fig. 5.11 presents the mixture temperature for the equal energy methanol injection cases. For the increased injection quantities, the mixture temperature contours display enlarged cooled zones with temperatures lower than 600 K. These zones may significantly impact the combustion by forming zones of cooled mixture, which hinder the flame propagation phenomena.

In the case of methanol premixing, increased methanol substitution may induce increased cycle-to-cycle variability and unstable operation. A quantitative comparison

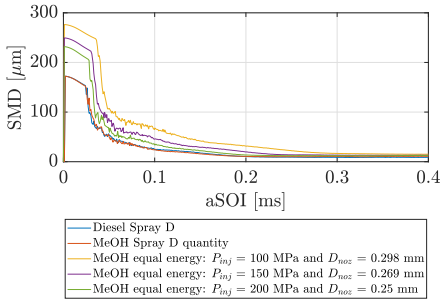

Figure 5.10: Comparison of Spray SMD between diesel and methanol using equal quantity and equal energy injections

of the mixture cooling in the vicinity of the spray is plotted in Fig. 5.12. For the equal energy cases, the temperature drop in the vicinity of the spray (40 mm axial location downstream) can reach up to 340 K. This decrease is significantly more intense than the diesel baseline case, with an average temperature drop of 200 K. Lastly, Table 5.5 shows the average temperature drop in the vicinity of the spray. In the equal energy cases, the different injection pressures lead to similar mixture cooling intensity, while diesel has a much less intense cooling effect, exhibiting up to 100 K increased mixture temperature.

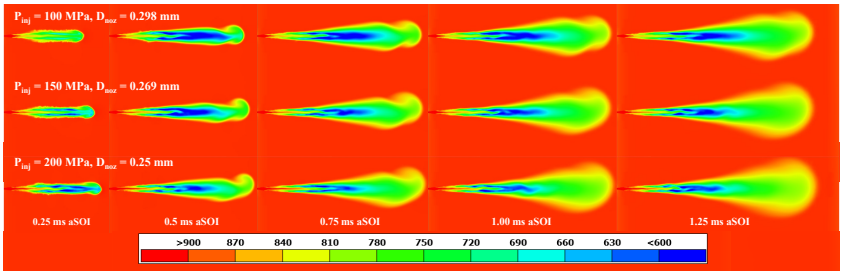

Figure 5.11: Mixture temperature for equal energy methanol injection for 100, 150, and 200 MPa injection pressure

Table 5.5: Average Temperature Drop at z = 40 mm axial location downstream

Case	**Average Temperature Drop (K)**
Diesel Spray D	198.3
Methanol Spray D Quantity	240.2
Methanol equal energy: P_{inj} = 100 MPa and D_{noz} = 0.298 mm	283.1
Methanol equal energy: P_{inj} = 150 MPa and D_{noz} = 0.269 mm	299.4
Methanol equal energy: P_{inj} = 200 MPa and D_{noz} = 0.25 mm	297.0

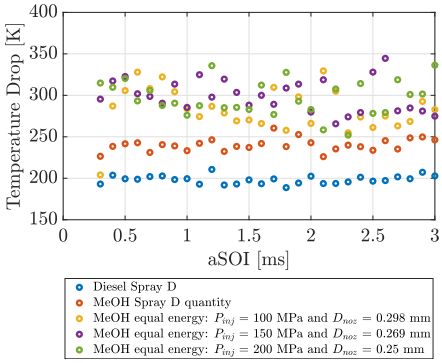

Figure 5.12: Temperature drop at z = 40 mm axial location downstream

5.4.4 Cooling Effect Sensitivity - Ambient Temperature Variation

In this section, we studied the mixture cooling under altered initial ambient temperatures using the equal energy methanol case with an injection pressure of 150 MPa. The tested range included ambient temperatures of 500, 700, 900, and 1100 K, while all the other parameters were kept constant. Here, the aim is to provide preliminary insights on varying methanol injection timings, which correspond to different levels of mixing ranging from premixed injection, during compression, to non-premixed injection near TDC. Fig. 5.13 illustrates the temperature contours for each reported ambient temperature case. Due to varying scales of mixture temperature, the color bar was varied accordingly to accommodate the initial assigned ambient temperature as the maximum value. For the higher initial ambient temperature cases, the cooling zones are significantly increased demonstrating a very intense cooling effect. The cooling intensity increases progressively and in proportion with the increase of initial ambient temperature.

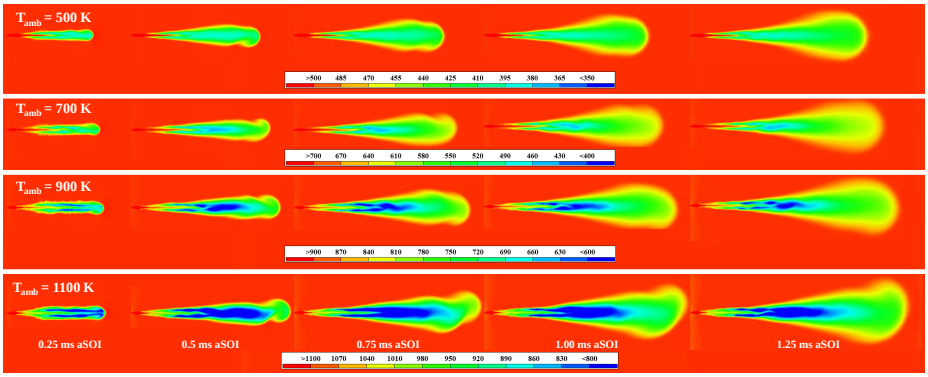

Figure 5.13: Mixture temperature for different ambient temperatures

Fig. 5.14 illustrates the temperature difference between the initial ambient temperature of each case and the point which is 40 mm downstream in the axial direction. In the

high ambient temperature cases (i.e., 900 and 1100 K), the rapid evaporation rate causes a significant temperature drop of 299.4 K and 351.3 K respectively (Table 5.6). However, these cases are related to near-TDC late injection conditions, when the piston has reached TDC. Considering compression to be an approximately adiabatic process [13], then the

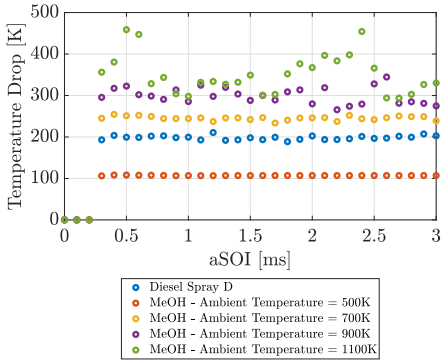

Figure 5.14: Temperature drop for 150 MPa equal energy methanol injection under different initial ambient temperatures at z = 40 mm axial location downstream

Table 5.6: Ambient Temperature Variation: Average Temperature Drop at z = 40 mm axial location downstream

Case	**Average Temperature Drop (K)**
Diesel Spray D	198.3
Methanol - Ambient Temperature = 500K	107.1
Methanol - Ambient Temperature = 700K	245.4
Methanol - Ambient Temperature = 900K	299.4
Methanol - Ambient Temperature = 1100K	351.3

cooled zones in the cylinder prior to combustion will be enlarged. Thus, after the mixture formation is completed, these cooled zones will inevitably act as an impediment to flame propagation and stable combustion. As a result, in early-like injection conditions, the mixture cooling is more impactful in the lower ambient temperature case (500 K), where the average temperature drop is around 100 K.

5.5 Conclusions

IN this chapter, we analysed the implications of methanol DI sprays on the mixture temperature in the context of HD-DF engines. The simulated conditions were characterized by a high ambient pressure and temperature environment, which resembles DICI near-TDC and, in the lower ambient temperature cases, early-stroke injection conditions. The presented approach used ECN non-reacting Spray D data with diesel as the baseline case to validate the CFD spray model. The validated model was then converted for methanol injection, with equal quantities and energy content as the diesel baseline.

Consequently, using the equal energy model, we performed a sensitivity analysis on the ambient temperature. By altering the initial temperature, we aimed to roughly recreate varying mixing levels during the compression stroke. The performance of each methanol model was compared with diesel based on the outcome mixture temperature and spray characteristics.

Our findings revealed a significant increase in the cooling intensity of methanol-air mixture formation, an effect mainly attributed to methanol's high latent heat of vaporization. Considering also methanol's decreased LHV, the average mixture temperature was significantly lower for injections under equal energy content as diesel. Specifically, our analysis demonstrated a drop in mixture temperatures of up to 300 K in the core of the spray plume, which was more than 100 K of temperature drop compared to diesel. Moreover, when methanol quantity was increased to facilitate equal energy injection as diesel, the liquid length was substantially increased due to slower evaporation rate, which could pose challenges with piston wall wetting. The mixture cooling was more pronounced for higher initial ambient temperatures due to rapid methanol evaporation. However, lower initial temperatures exhibited excessive mixture cooling of more than 100 K forming low temperature zones. These zones will eventually spread out in the cylinder in an uncertain way, and serve as the main cause of unstable combustion.

In conclusion, this chapter contributed an assessment of the charge cooling effect of methanol injection in DICI engines. By analyzing the spray and initial mixture formation prior to ignition, the impact of methanol's increased latent heat of vaporization on engines can be estimated. Future work could potentially apply the presented methodology and study the mixture formation in a full engine cylinder model. Thus, a link between the mixture formation and combustion with the methanol cooling effect can be established. Resolving the flow phenomena during the compression stroke prior to ignition is essential to improving methanol substitution while maintaining stable operation. In addition, potential measures to counteract the cooling effect could include increasing the air intake temperature and split injection of methanol. Furthermore, future methanol CFD models should incorporate methanol-dedicated spray experiments for proper validation. This step will ensure the accurate representation of the complex physics encompassing droplet breakup, evaporation, and mixing of methanol. The outcomes of this study could provide a roadmap for further investigation and the implementation of advanced methanol-diesel combustion modes, ultimately reducing the emissions and carbon footprint of HD and marine engines.

Bibliography

[1] A. K. Agarwal et al. *Methanol and the alternate fuel economy*. Springer, 2019.

[2] A. Ait Allal et al. "Toward an evaluation of marine fuels for a clean and efficient autonomous ship propulsion energy". In: *Materials Today: Proceedings* 13 (2019), pp. 486–495. DOI: 10.1016/j.matpr.2019.04.005. (Visited on 05/23/2022).

[3] J. C. Beale et al. "Modeling spray atomization with the Kelvin-Helmholtz/Rayleigh-Taylor hybrid model". In: *Atomization and sprays* 9.6 (1999).

[4] *CONVERGE CFD Software Website*. 2024. URL: https://convergecfd.com/.

[5] Convergent Science Inc. *CONVERGE MANUAL v3.0*. 2022.

[6] ECN Spray D. *Engine Combustion Network Spray-D Conditions*. Accessed: 2023-10-07. URL: https://ecn.sandia.gov/diesel-spray-combustion/target-condition/spray-d-nozzle-geometry/.

[7] A. Di Matteo et al. "Modeling Spray C and Spray D with FGM within the framework of RANS and LES". In: *Frontiers in Mechanical Engineering* 8 (2022), p. 1013138.

[8] J. Dierickx et al. "Retrofitting a high-speed marine engine to dual-fuel methanol-diesel operation: A comparison of multiple and single point methanol port injection". In: *Fuel Communications* 7 (2021), p. 10.

[9] Y. Dong et al. "High-pressure direct injection of methanol and pilot diesel: A non-premixed dual-fuel engine concept". In: *Fuel* 277 (Oct. 2020), p. 117932. DOI: 10.1016/j.fuel.2020.117932. (Visited on 05/30/2022).

[10] *Engine Combustion Network Spray-D Nozzle Geometry*. 2024. URL: https://ecn.sandia.gov/diesel-spray-combustion/target-condition/spray-d-nozzle-geometry/.

[11] J. H. Ferziger et al. *Computational methods for fluid dynamics*. Vol. 3. Springer, 2002.

[12] Z. Han et al. "Turbulence modeling of internal combustion engines using RNG κ-ε models". In: *Combustion science and technology* 106.4-6 (1995), pp. 267–295.

[13] J. B. Heywood. *Internal combustion engine fundamentals*. McGraw-Hill Education, 2018.

[14] A.L. Horvath. "Redlich-Kwong equation of state: review for chemical engineering calculations". In: *Chemical Engineering Science* 29.5 (1974), pp. 1334–1340.

[15] *International Maritime Organization: Fourth Greenhouse Gas Study 2020*. 2020. URL: https://www.imo.org/en/OurWork/Environment/Pages/Fourth-IMO-Greenhouse-Gas-Study-2020.aspx.

[16] R. I. Issa. "Solution of the implicitly discretised fluid flow equations by operator-splitting". In: *Journal of computational physics* 62.1 (1986), pp. 40–65.

[17] O. T. Kaario et al. "A comparative study on methanol and n-dodecane spray flames using Large-Eddy Simulation". In: *Combustion and Flame* 260 (2024), p. 113277.

[18] G. Kalghatgi. "Is it really the end of internal combustion engines and petroleum in transport?" In: *Applied energy* 225 (2018), pp. 965–974.

[19] A. Kalwar et al. "Gasohol sprays simulations of a multi-hole GDI injector in engine-like conditions". In: 2021.

[20] G. A. Karim. *Dual-fuel diesel engines*. CRC press, 2015.

[21] S. Karimkashi et al. "Large-eddy simulation of diesel pilot spray ignition in lean methane-air and methanol-air mixtures at different ambient temperatures". In: *International Journal of Engine Research* 24.3 (2023), pp. 965–981.

[22] D. G. Kessel. "Global warming—facts, assessment, countermeasures". In: *Journal of Petroleum Science and Engineering* 26.1-4 (2000), pp. 157–168.

[23] A. D. Korberg et al. "Techno-economic assessment of advanced fuels and propulsion systems in future fossil-free ships". In: *Renewable and Sustainable Energy Reviews* 142 (May 2021). DOI: 10.1016/j.rser.2021.110861. (Visited on 07/15/2022).

[24] A. Krishnasamy et al. "Prospective fuels for diesel low temperature combustion engine applications: A critical review". In: *International Journal of Engine Research* 22.7 (July 2021), pp. 2071–2106. DOI: 10.1177/1468087420960857. (Visited on 05/19/2022).

[25] A. B. Liu et al. "Modeling the effects of drop drag and breakup on fuel sprays". In: *SAE Transactions* (1993), pp. 83–95.

[26] N. Maes et al. "Heavy-duty diesel engine spray combustion processes: experiments and numerical simulations". In: *SAE technical paper* 2018 (2018), pp. 1–22.

[27] N. Maes et al. "Spray penetration, combustion, and soot formation characteristics of the ECN Spray C and Spray D injectors in multiple combustion facilities". In: *Applied Thermal Engineering* 172 (2020), p. 115136.

[28] A. Matamis et al. "Optical characterization of methanol compression-ignition combustion in a heavy-duty engine". In: *Proceedings of the Combustion Institute*. Vol. 38. Elsevier Ltd, 2021, pp. 5509–5517.

[29] R.S. Miller et al. "Evaluation of equilibrium and non-equilibrium evaporation models for many-droplet gas-liquid flow simulations". In: *International journal of multiphase flow* 24.6 (1998), pp. 1025–1055.

[30] P. J. O'Rourke. "Statistical properties and numerical implementation of a model for droplet dispersion in a turbulent gas". In: *Journal of Computational Physics* 83.2 (1989), pp. 345–360.

[31] M. Pipicelli et al. “Alcohol Fuels in Compression Ignition Engines”. In: *Energy, Environment, and Sustainability*. Springer Nature, 2022, pp. 9–31. DOI: 10.1007/978-981-16-8751-8_2.

[32] S. L. Post et al. “Modeling the outcome of drop–drop collisions in Diesel sprays”. In: *International Journal of Multiphase Flow* 28.6 (2002), pp. 997–1019.

[33] R. D. Reitz et al. “IJER Editorial: The future of the internal combustion engine”. In: *International Journal of Engine Research* (2020). DOI: 10.1177/1468087419877990.

[34] R. D. Reitz et al. “Structure of high-pressure fuel sprays”. In: *SAE transactions* (1987), pp. 492–509.

[35] D. P. Schmidt et al. “A new droplet collision algorithm”. In: *Journal of Computational Physics* 164.1 (2000), pp. 62–80.

[36] P.K. Senecal et al. “Grid-convergent spray models for internal combustion engine CFD simulations”. In: *Internal Combustion Engine Division Fall Technical Conference*. Vol. 55096. American Society of Mechanical Engineers. 2012, pp. 697–710.

[37] S. Shamun et al. “Quantification and analysis of the charge cooling effect of methanol in a compression ignition engine utilizing PPC strategy”. In: *Internal combustion engine division fall technical conference*. Vol. 51982. American Society of Mechanical Engineers. 2018, V001T02A007.

[38] *Spray C / D Rate of injection*. 2016. URL: https://www.cmt.upv.es/#/ecn/download/nozzlecharac/ncSprayCDRateOfInj.

[39] M. Svensson et al. “Low Load Ignitability of Methanol in a Heavy-Duty Compression Ignition Engine”. en. In: Aug. 2022, pp. 2022–01–1093. DOI: 10.4271/2022-01-1093. (Visited on 09/15/2022).

[40] M. Tuner. “Review and Benchmarking of Alternative Fuels in Conventional and Advanced Engine Concepts with Emphasis on Efficiency, CO2, and Regulated Emissions”. In: *SAE Technical Papers* (2016).

[41] S. Verhelst et al. “Methanol as a fuel for internal combustion engines”. In: *Progress in Energy and Combustion Science* 70 (Jan. 2019), pp. 43–88. DOI: 10.1016/j.pecs.2018.10.001.

[42] Y. Wang et al. “Characteristics of Evaporating Spray for Direct Injection Methanol Engine: Comparison between Methanol and Diesel Spray”. In: *Processes* 10.6 (June 2022), p. 1132. DOI: 10.3390/pr10061132. (Visited on 07/13/2022).

[43] B. Zincir et al. “Investigation of effects of intake temperature on low load limitations of methanol partially premixed combustion”. In: *Energy and Fuels* 33.6 (June 2019), pp. 5695–5709. DOI: 10.1021/acs.energyfuels.9b00660. (Visited on 06/03/2022).

[44] B. Zincir et al. “Methanol as a Fuel for Marine Diesel Engines”. In: *Energy, Environment, and Sustainability*. Springer Nature, 2021, pp. 45–85. DOI: 10.1007/978-981-16-0931-2_4. (Visited on 05/23/2022).

[45] K. Zoumpourlos et al. “Evaluation of Methanol Sprays in Marine Internal Combustion Engines: a Case Study for Port Fuel Injection Systems”. In: *Modelling and Optimisation of Ship Energy Systems 2023* (Dec. 2023). DOI: 10.59490/moses.2023.655. URL: https://proceedings.open.tudelft.nl/moses2023/article/view/655.

[46] Konstantinos Zoumpourlos et al. “Methanol Operation in Heavy-Duty DICI Dual-Fuel Engines: Investigating Charge Cooling Effects Using ECN Spray D Data”. In: *Journal of Engineering for Gas Turbines and Power* (2025), pp. 1–10. DOI: 10.1115/1.4067862.

Chapter 6

Conclusions & Recommendations

THIS chapter presents the concluding remarks of the thesis and provides future research recommendations. Section 6.1 revisits the initial problem statement and research questions presented in Chapter 1, and links them to the outcomes of the present dissertation. Following, Section 6.2 offers recommendations for future research. Lastly, we present a potential pathway for future multi-hole injector methanol direct injection (DI) research using the engine combustion network (ECN) experimental datasets, which expands the research outlined in Chapter 4.

6.1 Reflection & Discussion

IN this thesis, we investigated methanol sprays in marine engine-relevant conditions. These conditions included a PFI environment typical of an intake port manifold of premixed CI engines, a DI-CI partially premixed condition, and a DI-DF late-injection environment typical of large bore engines. The aim was to address the main problem statement, as presented in Section 1.2:

> *How do methanol sprays influence evaporation and mixture formation in marine ICEs? Can we develop a predictive simulation framework to aid in optimizing various methanol-fuelled marine engine injection strategies?*

The problem statement aimed to address the literature gap in methanol spray modelling using computational fluid dynamics (CFD) to better understand the influence of methanol sprays on mixture formation and evaporation. To identify the overarching knowledge gap, a literature review was conducted in Chapter 2, which identified the variety of methanol injection strategies and combustion modes. A structured classification framework was proposed to cover the ambiguous terminology found in the literature, encompassing heavy-duty and marine engines. Subsequently, through three interconnected studies, this research provided insights into methanol spray behaviour under both port fuel injection (PFI) and DI strategies. To validate the CFD models, Chapter 3 utilized experimental data specific for methanol in marine-style PFI conditions. The evaporation of methanol was studied in representative marine quantities, along with an assessment of its potential implications for engine performance. Chapter 4 used the recently published ECN spray methanol dataset to validate the state-of-the-art spray models in multi-hole DI conditions. Finally, Chapter 5 compared methanol and diesel sprays in ultra-high injection pressure conditions representative of dual-fuel diesel-methanol engines. The evaporation cooling effect was analysed for both fuels, highlighting methanol's intense air-fuel mixture temperature reduction.

Below, the key findings of the dissertation are synthesized in relation to the research questions:

1. ***How do PFI and DI methanol injection strategies compare in marine engine applications?***

   In Chapter 3, the first CFD spray study demonstrated that methanol PFI at low injection pressures (6–10 bar) suffers from poor atomisation and slow evaporation, increasing the risk of wall film formation in the intake manifold. In contrast, the second and third CFD studies (in Chapter 4 and Chapter 5 respectively) showed

that methanol DI under high injection pressures (200 bar and 1500 bar respectively) improves atomisation, and offers better control over the mixture formation. However, a strong charge cooling effect is introduced due to methanol's high latent heat of vaporization. While PFI is simpler to retrofit, DI offers better control over the mixture. In addition, careful DI optimisation (e.g., split injection, injector design avoiding spray collapsing etc.) is required to mitigate the excessive charge cooling that hinders combustion stability.

2. ***What is the atomization quality of methanol under low injection pressure in PFI systems, and how can it be improved to enhance mixture formation?***

   The PFI study revealed that low injection pressures (typical for marine retrofits) lead to large droplet sizes ($SMD > 100\,\mu m$) and minimal evaporation before wall impingement. We demonstrated that increasing the injection pressure (e.g., to 200 bar) significantly enhances atomisation by improving air entrainment and reducing droplet diameter. This suggests that high-pressure PFI systems could mitigate mixture formation challenges in marine engines. However, the impact of droplet size on wall film formation remains poorly understood, even for conventional fuels.

3. ***To what extent does PFI of methanol lead to fuel wall film formation on the intake manifold?***

   The PFI study highlighted that methanol's high latent heat and poor atomization exacerbates wall film formation, promotes mixture inhomogeneity, and increases cycle-to-cycle variability. This aligns with experimental observations from the literature, which also report condensation in the intake manifold. The CFD framework outlined in this thesis can become a valuable tool in mixture formation studies. In that extent, coupling these free-spray models with spray-wall interaction models can enable the optimization of injector position and injection timing to minimise film formation.

4. ***Can existing state-of-the-art spray modelling practices reliably predict methanol spray behaviour, or do they require significant adaptation?***

   Despite methanol's distinct properties (high vapour pressure and high latent heat), the CFD studies confirmed that existing Lagrangian-Eulerian (LE) spray models require moderate adaptation for methanol. The DI studies demonstrated that Reynolds-Averaged Navier-Stokes (RANS) models can predict global spray characteristics, such as liquid length, and spray collapsing. Additionally, computationally expensive large eddy simulation (LES) can capture complex physical phenomena, such as plume collapse and sweeping. Overall, the calibrated KH-RT breakup model constants provided in Chapter 3 and Chapter 4 improve methanol spray predictions for both PFI and DI applications.

5. ***How does methanol spray formation in DI systems differ from conventional fuels such as diesel and gasoline, particularly in terms of morphology and vaporization behaviour?***

   Compared to n-dodecane (diesel surrogate for the ECN Spray D case) and iso-octane (gasoline surrogate for the ECN Spray G case), methanol exhibits faster

initial evaporation due to its low boiling point but prolonged overall evaporation due to its high latent heat. In DI engines, this results in stronger charge cooling, with mixture temperatures up to 100 K lower than those of n-dodecane. This implicitly reduces NO_x emissions but may impede flame propagation. Moreover, under partially premixed conditions typical of marine engines, which are similar to late injection in DI spark-ignition automotive engines, the ECN Spray M1 study showed that methanol's high vapour pressure leads to spray collapse. This behaviour is not observed in iso-octane sprays under the same conditions, highlighting the unique spray structure of methanol. Thus, for methanol operation, this induced delay in overall evaporation causes improper mixture formation, ultimately leading to combustion issues and unburned methanol emissions.

6. ***How do methanol's distinct physical properties, such as high latent heat of vaporization and lower energy density, impact spray evolution and mixture preparation across injection strategies?***

   Methanol's high latent heat and lower energy density necessitate larger injection quantities for the same energy input, amplifying charge cooling effects. In PFI systems, this slows evaporation and increases the risk of wall wetting, while in DI, it creates steep temperature gradients that will affect ignition and combustion. To mitigate the intensified cooling effect, raising the intake air temperature can be an effective countermeasure. To capture these effects in CFD, the existing diesel/gasoline spray models, particularly the breakup sub-models, were calibrated using methanol experiments and were shown to be effective.

7. ***Is it feasible to develop a unified CFD-based spray modelling framework that accurately captures methanol behaviour in both PFI and DI configurations?***

   This thesis successfully developed a validated CFD framework applicable to both PFI and DI methanol sprays. The CFD framework was validated using DI experimental data from ECN Spray M and dedicated PFI experiments found in the literature. While RANS models are sufficient for engineering-level PFI and DI simulations, LES is recommended for multi-hole DI applications where capturing the plume collapsing and sweeping phenomena is critical.

8. ***What are the implications of methanol DI spray characteristics on marine engine operation?***

   For DI methanol-diesel dual-fuel engines, the primary concern is managing charge cooling to avoid combustion instability, potentially via split-injection strategies or optimised pilot diesel timing. Another important concern for DI methanol sprays is the increased liquid penetration observed in Chapter 4, which stems from the higher vapour pressure of methanol. This increased in-cylinder liquid presence amplifies the risk of liner or piston crown droplet impingement, leading to potential incomplete combustion and increased unburned hydrocarbons. These effects highlight the need for further optimisation of spray targeting, injection timing, and nozzle design in marine DI methanol engines. The predictive models developed in this thesis enable these optimisations, supporting the maritime industry's transition to methanol.

In summary, this thesis advances the understanding of methanol spray behaviour in marine engines, providing:

- Validated CFD frameworks for PFI and DI methanol injection.
- Calibrated spray models addressing methanol's unique properties.
- Practical insights for optimizing methanol engine operation.

6.2 Outlook for Future Research

IN this section, we highlight several critical areas for further investigation. The following recommendations aim to address existing knowledge gaps and guide future research:

- **Validation of spray wall interaction (SWI) CFD models in PFI systems.**

  Wall wetting models should be validated using methanol-specific experiments in optical access test setups. These experiments should measure wall film thickness and area, as well as evaporation rates, under intake manifold conditions representative of marine applications. Previous studies indicate that smaller droplets and higher jet velocities may improve mixture formation, underscoring the importance of further investigation into methanol spray dynamics. Given the unique characteristics of methanol injection in marine engines, isolating SWI effects—as demonstrated in Chapter 3 for free sprays—is crucial. Such decoupled analysis will support accurate CFD model calibration and enable the optimisation of PFI mixture formation.

- **Investigating the applicability of state-of-the-art spray models for large marine-engine quantities.**

  The available experimental data used in the present thesis represent automotive-style injection quantities. The CFD framework validation should be extended to large-bore marine engine experiments using larger constant volume chambers (CVCs). Under these conditions, injector nozzle geometries and flow regimes differ substantially from those in automotive-scale systems. Due to the scale differences, empirical models developed for smaller engines may not be directly applicable, highlighting the need for further investigation and possible re-calibration for marine contexts.

- **Expanding ECN methanol spray research for flash-boiling and split-injection conditions.**

  Figure 6.1 proposes a research framework aimed at advancing the understanding of multi-hole methanol injection within the Engine Combustion Network (ECN) context. Future research could utilize Volume-of-Fluid (VoF) methods to capture in-nozzle flow dynamics, offering detailed insights into cavitation, evaporation, and turbulence during methanol injection. Accurate determination of nozzle flow coefficients is also crucial for improving spray momentum predictions. Additional experimental efforts should focus on near-nozzle flow visualization and droplet size

distribution to better inform and calibrate RANS-based spray models. Advanced injection techniques, such as split injection and early injection inducing flash-boiling, should also be investigated and benchmarked against ECN data to enhance model accuracy, particularly in representing cavitation-induced spray collapse in methanol injection. Finally, expanding methanol spray validation under late-injection compression ignition conditions—characterized by ultra-high injection and ambient pressures—is essential for improving model accuracy in realistic engine environments.

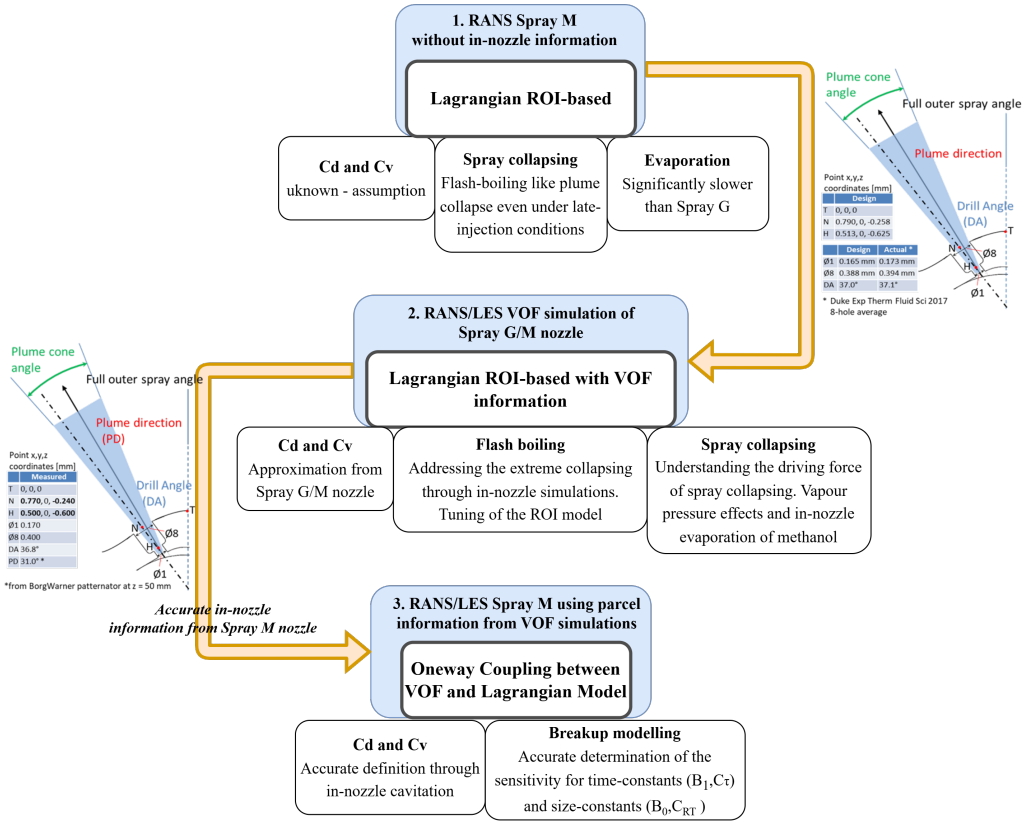

Figure 6.1: Future Research Direction for Multi-Hole ECN Spray M

- **Full-engine 3D-CFD simulations coupling spray, mixture formation, combustion, and emissions formation.**

  Although this thesis focused on validating spray models in isolation, future research should integrate these models into full-engine 3D-CFD simulations. This will enable the investigation of the interactions between methanol sprays, in-cylinder flow dynamics, and combustion behaviour. Moreover, future studies should model dual-fuel methanol-diesel combustion to evaluate ignition delay, flame propagation, and

emissions. To assess the impact of cooling effect and wall wetting, cycle-to-cycle variability should also be explored. Lastly, accurate emissions models—particularly for unburned hydrocarbons (UHC), formaldehyde, and NO_x—are essential for compliance with future regulatory standards.

Appendix A

Effect of plume cone angle on spray collapsing

In this appendix, we consider the influence of cone angle on spray characteristics as an additional calibration parameter for the work presented in Chapter 4. The cone angle strongly influences liquid penetration and spray jet morphology, and hence, appropriate tuning is compulsory. An increased cone angle negatively affects spray momentum due to higher air entrainment rate, enabling elevated mixing and evaporation. In addition, elevated cone angle values create a less dense spray liquid core and promote inter-plume interactions. To successfully recreate the experimental injection phenomena, increasing the inter-plume interactions can enhance spray collapsing and subsequently, spray sweeping phenomena.

In the RANS model, the effect of the cone angle was less intensive than expected and slightly affected spray plume collapsing. For both the RANS and LES cases, a cone angle value of 33° was selected as the most appropriate for obtaining an adequate prediction of the liquid length (Figure A.1 and Figure A.2). However, in the RANS case, the selected

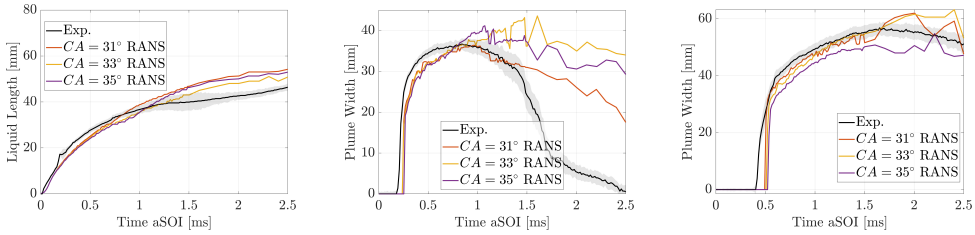

(a) RANS Model Cone Angle Influence: Liquid Penetration Length

(b) RANS Model Cone Angle Influence: Liquid Width at $z = 15$ mm axial cross-section from nozzle exit

(c) RANS Model Cone Angle Influence: Liquid Width at $z = 25$ mm axial cross-section from nozzle exit

Figure A.1: RANS Model Cone Angle Influence: Liquid Penetration & Width

cone angle did not represent well the spray liquid width due to the model's weakness in fully capturing spray collapsing and sweeping phenomena. Figure A.3 presents the RANS model insensitivity to cone angle perturbations using the LVF in the radial direction of the 15 mm downstream cross-section.

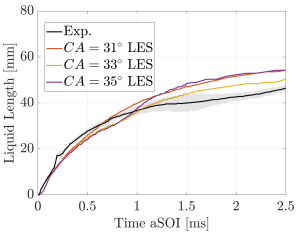

(a) LES Model Cone Angle Influence: Liquid Penetration Length

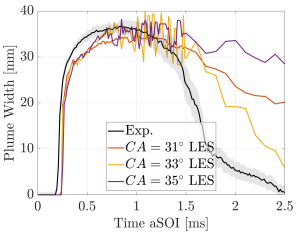

(b) LES Model Cone Angle Influence: Liquid Width at $z = 15$ mm axial cross-section from nozzle exit

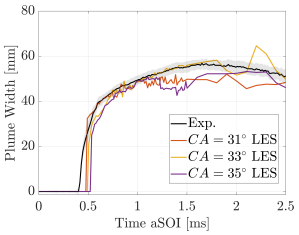

(c) LES Model Cone Angle Influence: Liquid Width at $z = 25$ mm axial cross-section from nozzle exit

Figure A.2: LES Model Cone Angle Influence: Liquid Penetration & Width

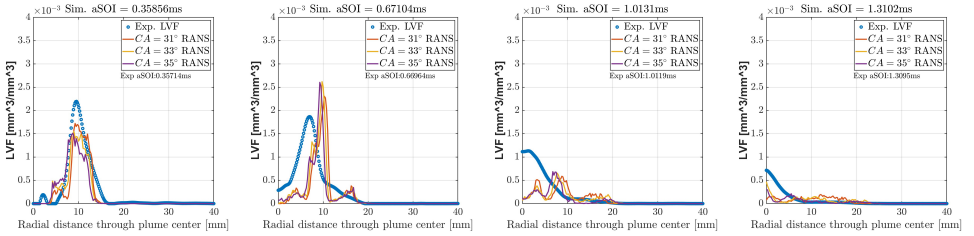

Figure A.3: Quantitative plume-averaged Liquid Volume Fraction (LVF) at $z = 15$ mm axial cross-section from nozzle exit: Impact of cone angle in RANS Model

On the contrary, the LVF of the LES model presents greater sensitivity to the cone angle (Figure A.4). Overall, the LES model performed better than RANS, and achieved better predictions of the experiment by accurately recreating the desired spray momentum and morphology. Interestingly, for the early stages of the spray formation prior to EOI, the

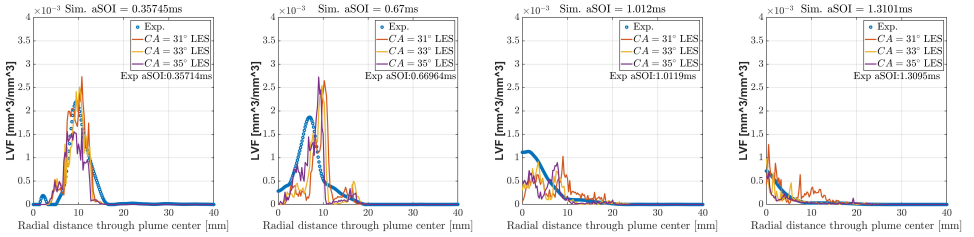

Figure A.4: Quantitative plume-averaged Liquid Volume Fraction (LVF) at $z = 15$ mm axial cross-section from nozzle exit: Impact of cone angle in LES Model

smaller cone angles exhibited the expected increased liquid penetration. After the EOI, especially the 35° cone angle model displays a more intense collapsing as highlighted by the elevated LVF values near the nozzle center-line at 0.67 ms. This spray collapsing phenomenon generates an excessive accumulation of liquid droplets in the center-line of the spray. Consequently, this bulk of liquid fuel merges and forms a single high-momentum plume, which eventually, increases liquid penetration.

Appendix B

Supplementary Data Availability

THE data of the present thesis are available in the following links from Table B.1 through the TU Delft repository. Using the data of this research is allowed for academic and research purposes. For future publishing, proper citation and attribution to the author of the present thesis must be ensured when referencing its content or findings.

Table B.1: Supplementary data access links

Data	DOI/URL
Chapter 3	https://doi.org/10.4121/3384b915-3c9c-4e45-90c8-6be0d07c7ed1
Chapter 4	https://doi.org/10.4121/fd5dc0c7-a17f-4c93-8309-fce712e2f9f9
Chapter 5	https://doi.org/10.4121/29e4a39f-b23d-4e77-bbc2-98cb79805311

Acknowledgements

This chapter marks the conclusion of a journey that started four years ago. These last four years have flown by incredibly fast. During this time, I have grown in ways I could never have imagined when I first stepped onto the airplane to move to the Netherlands. I have been fortunate to receive this remarkable opportunity to conduct research on a topic I am truly passionate about. Equally important, I have been lucky to meet people here who supported me throughout these years, many of whom I am grateful to call my friends. To all of them, I owe my sincere gratitude.

First and foremost, I would like to express my sincere gratitude to my supervisory team: Andrea Coraddu, Rinze Geertsma, and Robert van de Ketterij. To my promotor, Andrea, thank you for giving me this opportunity and for trusting and supporting me throughout the course of this research. To my co-promotor, Rinze, I am grateful for the constant motivation you provided and for pushing me to strengthen my analytical thinking and research skills. And to Robert, thank you for always being supportive and for taking the time to sit down and discuss science. I will truly miss our conversations.

Furthermore, I would like to express my sincere appreciation to my external committee for taking the time to review my dissertation and for providing valuable feedback. I look forward to meeting you during my defence and engaging in an interesting and constructive scientific debate. To my project partners from the MENENS project, I extend my gratitude to Cemil Bekdemir from TNO powertrains, who continuously supported me whenever I reached out, and who has been part of my scientific journey from the very beginning. To me, you have been my fourth unofficial supervisor, and I am sincerely grateful for that. I would also like to thank the Netherlands Defence Academy (NLDA) team in Den Helder for always being welcoming and for supporting us in our research, especially Marcel Roberscheuten.

To my dear colleagues, who made this journey truly interesting and colourful in my everyday office life over the past four years. Thank you to my office-mates, Annabel and Bojan, and to the engine team PhDs, Kostas and Jasper, with whom I shared an outstanding PhD trajectory from the very beginning. Thank you Adrien, Ana, Abhishek, Giang, Ahmed, Andrea, Charlotte, Kris, Manuel, Marcel, Matthis, Niek, Sara, Shaheen, Skirmantas, Hesam and many others... I am sorry if I have missed some names, but I am certain that the memories we have created together will stay with us for the rest of our lives. Lastly, I extend my warm regards to the Greek community, who made my PhD years feel like home: Nicole, Nikos[3], Apostolos, Foivos, Zacharias, and Vasilis.

To my bandmates—Giovanni, Rachele, Martijn, Leo, Zhonggang, and Costas—thank

you for providing a beautiful soundtrack alongside my PhD journey. To my friends outside the university, thank you for the enjoyable moments and for supporting me during challenging times. Thank you, Lefteris, Nikoleta, Silvestros, Johny, Giannis, George, Faidon, Penny, and Sofia. To my arts and music friends, especially Dimitris Groke, thank you for making this beautiful dissertation cover art possible and for giving me the space to pursue my artistic vision. I would also like to extend my gratitude to my dearest friends back in Greece—Dimitris, Theo, Nikolas, Thomas, Efthimis, and Kostis—who continued to support me in life and music from afar. I am looking forward to all the music that is yet to come. Finally, to Stelios, with whom I have shared an inseparable friendship for nearly twenty-three years, I wish you the very best in your own PhD trajectory in Antwerpen.

Following this, I would like to extend my regards to my family in the USA, who have always supported me and my family in Greece through all these difficult years. Without you, my life would probably have taken a different course, and I would not have found the inspiration to keep going. Thank you, Stergios and Marina, for being like second parents to me and for helping expand my spirituality beyond engineering. And to Arsenis, Eleni and Irene, thank you for being the wonderful cousins that you are. Thank you to my family in Canada-Costas, Maya, Leandro, and Amalia. Now that I have easier access to Toronto, I hope we can see each other more often. Finally, even if you joined the journey only in the last six months of my PhD, thank you, Olga-Eirini, for becoming part of my life. By completing this dissertation, a very special chapter comes to an end, and I am excited to see what the future holds.

I would like to conclude this acknowledgements section by expressing my deepest gratitude to my family. I am thankful for your unwavering support in everything I have achieved so far, for giving me the space to express myself, and for the countless sacrifices you have made along the way. I am forever grateful to my mother, Olga, for her endless love and emotional support, and to my father, Giorgos, for being one of my best friends and greatest motivators in life. You are both role models to me, and together truly a force of nature to be reckoned with. Next, I would like to thank my brother, Arsenis-Stefanos, for being one of my closest friends and for always being all ears when it comes to exchanging complaints about the good and bad sides of life. To my grandmother, Ioanna, thank you for all the wonderful conversations and for teaching me what it means to be a good and kind human being. And to the rest of my grandparents—Kostas, Arsenis, and Loula—who are no longer with us, I will always remember you. This book, together with the four years of effort behind it, is dedicated to your memory.

Konstantinos Zoumpourlos
Delft, April 2026

Curriculum Vitæ

Konstantinos ZOUMPOURLOS

29-04-1997 Born in Lamia, Greece.

Education

2012–2015 High School
1st High School of Lamia, Greece

2015–2020 Diploma in Mechanical & Aeronautics Engineering
University of Patras, Greece

2022–2026 PhD. Marine Engineering
Department of Maritime and Transport Technology
Faculty of Mechanical Engineering,
Delft University of Technology, Delft, the Netherlands
Thesis: Methanol Sprays in Marine Internal Combustion Engines: A Computational Fluid Dynamics Approach
Promotor: dr. A. Coraddu
Copromotor: dr. ir. R. D. Geertsma
Copromotor: prof. dr. ir. R. G. van de Ketterij

List of Publications

Journal Publications (Included in the Present Thesis)

4. **Zoumpourlos, K.**, Geertsma, R., Ketterij, R. V. D., and Coraddu, A. (March 18, 2025). *Methanol Operation in Heavy-Duty DICI Dual-Fuel Engines: Investigating Charge Cooling Effects Using Engine Combustion Network Spray D Data.* ASME. J. Eng. Gas Turbines Power. October 2025.

3. Kiouranakis, K. I., de Vos, P., **Zoumpourlos, K.**, Coraddu, A., and Geertsma, R. *Methanol for heavy-duty internal combustion engines: Review of experimental studies and combustion strategies.* Renewable and Sustainable Energy Reviews. 2025.

2. **Zoumpourlos, K.**, Bekdemir, C., Geertsma, R., van de Ketterij, R., and Coraddu, A. *CFD modeling approach for late-injection methanol sprays validated with ECN spray M.* International Journal of Engine Research. 2025.

1. **Zoumpourlos, K.**, Bekdemir, C., Geertsma, R., van de Ketterij, R., and Coraddu, A. *Methanol sprays in marine engines: CFD modelling of port fuel injection systems.* Journal of Marine Engineering & Technology. 2025.

Other Journal Publications

3. **Zoumpourlos, K.**, Bekdemir, C., Kiouranakis, K.I., Geertsma, R., van de Ketterij, R., Coraddu, A. *CFD modelling of methanol RCCI combustion in low load marine engine conditions - A comparative study with conventional dual-fuel combustion.* Under Preparation. 2026.

2. Bui, H.G., **Zoumpourlos, K.**, Bekdemir, C., Somers, L.M.T. *Numerical investigation of methanol-air mixture formation and combustion in a dual-fuel marine engine at low load.* Fuel. 2026.

1. Karvounis, P., Theotokatos, G., **Zoumpourlos, K.**, Coraddu, A. *Parametric optimisation of methanol combustion in marine dual-fuel engines at low loads.* Applied Thermal Engineering. 2025.

Conference Publications

2. **Zoumpourlos, K,** Geertsma, R, van de Ketterij, R, and Coraddu, A. *Methanol Operation in Heavy-Duty DICI Dual-Fuel Engines: Investigating Charge Cooling Effects Using ECN Spray D Data.* Proceedings of the ASME 2024 ICE Forward Conference. ASME 2024 ICE Forward Conference. San Antonio, Texas, USA. October 20–23, 2024.

1. **Zoumpourlos, K.**, Coraddu, A., Geertsma, R., and van de Ketterij, R. (2023). *Evaluation of Methanol Sprays in Marine Internal Combustion Engines: A Case Study for Port Fuel Injection Systems.* Modelling and Optimisation of Ship Energy Systems 2023.

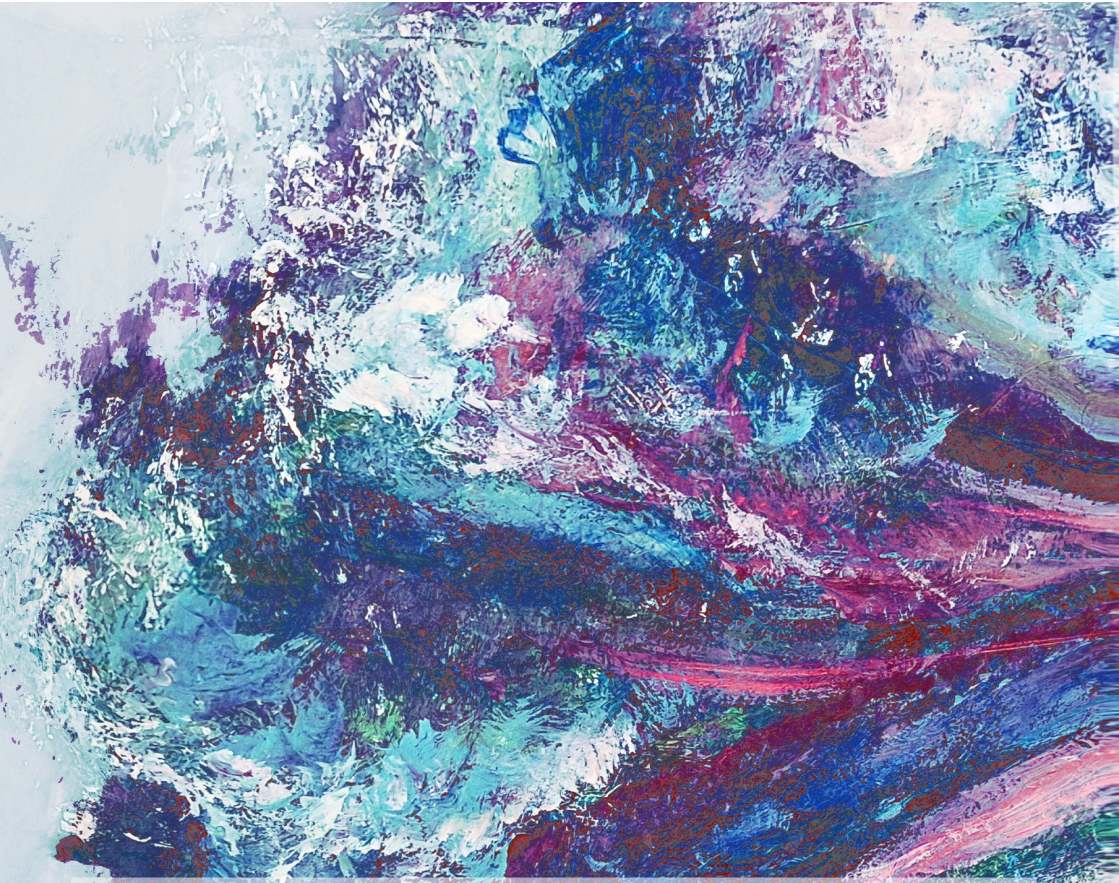

Summary

The adoption of methanol in contemporary marine engines presents unique challenges, particularly during injection and mixture formation. This thesis presents a validated computional fluid dynamics (CFD) spray framework, capable of simulating methanolsprays in marine engine environments. The framework is subsequently used to analyse methanol spray characteristics across operating conditions relevant to marine applications, covering both port fuel injection (PFI) and direct injection (DI) configurations.

About the author

Konstantinos Zoumpourlos earned his Diploma in Mechanical & Aeronautics Engineering from the University of Patras, Greece, in 2020. From 2022 to 2026, he conducted his PhD research in Sustainable Drive & Energy Systems (SDES) at the Maritime & Transport Technology Department of Delft University of Technology, in the Netherlands.

ISBN 978-94-6537-442-0